

**Modeling the exchange of water and
energy over natural land surfaces**

Modeling the exchange of water and
energy over natural land surfaces

Het modelleren van de uitwisseling van
water en energie over natuurlijke
landschappen.

Reinder Jan Ronda

Promotor:

Prof.dr. A.A.M. Holtslag

Hoogleraar in de meteorologie en luchtkwaliteit

Co-promotoren:

Dr. H.A.R. de Bruin

Universitair hoofddocent bij de leerstoelgroep
meteorologie en luchtkwaliteit

Dr.ir. B.J.J.M. van den Hurk

Senior onderzoeker Koninklijk Nederlands
Meteorologisch Instituut, De Bilt

Samenstelling promotiecommissie:

Prof.dr. A.J. Dolman – Vrije Universiteit Amsterdam

Dr.ir. A.C.M. Beljaars – European Centre for
Medium-ranged Weather Forecasts, Reading, UK

Prof.dr. P.A. Troch – Wageningen Universiteit

Prof.dr. M. Scheffer – Wageningen Universiteit

Dr. W. Bouten – Universiteit van Amsterdam

NNO8201, 3198

Modeling the exchange of water and energy over natural land surfaces

Reinder Jan Ronda

Proefschrift
ter verkrijging van de graad van doctor
op gezag van de rector magnificus
van Wageningen Universiteit,
prof.dr.ir. L. Speelman,
in het openbaar te verdedigen
op woensdag 15 mei 2002
des namiddags te vier uur in de aula

16 u 8785

ISBN 90-5808-617-8

Stellingen behorende bij het proefschrift 'Modeling the exchange of water and energy over natural land surfaces' van Reinder Jan Ronda

1. Voor het berekenen van de transpiratie van lage vegetaties in grootschalige atmosferische modellen zijn methoden die de gewasweerstand koppelen aan de fotosynthese geschikter dan empirisch-statistische methoden.

Dit proefschrift

2. Voor de correcte modellering van de seizoensvariatie van de latente warmtestroom en de specifieke vochtigheid op twee meter, is het van belang om rekening te houden met de variatie van het bodemvocht binnen roostercellen van grootschalige atmosferische modellen.

Dit proefschrift.

3. Voor gebieden met een sterk variërende topografie is een model dat de bodemkolom verdeelt in horizontale lagen een foute beschrijving van de werkelijkheid. Een model dat de bodemkolom als een emmer beschrijft, is een te simple beschrijving van de werkelijkheid.

Koster, R.D., M.J. Suarez, A. Ducharne, M. Stieglitz, and P. Kumar, 2000: A catchment based approach to modeling land surface processes in a general circulation model; 1. Model structure. *J. Geophys. Res.*, 105, 24809-24822

4. De methode van Monteith waarbij de gewasweerstand lineair afhangt van de transpiratie is van belang voor het begrip van de respons van de gewasweerstand op de vochtigheid van de atmosfeer. Om de gewasweerstand te schatten in grootschalige atmosferische modellen is deze methode echter minder geschikt.

Monteith, J.L., 1995: A re-interpretation of stomatal responses to humidity. *Plant, Cell Env.* 18, 357-364

Bosveld, F.C., 1999: Exchange processes between a coniferous forest and the atmosphere. Ph.D. thesis Wageningen University

5. De doorrekening van verkiezingsprogramma's door het Centraal Planbureau zou aan belang winnen als dezelfde berekeningen ook zouden worden gedaan door vergelijkbare bureaus in het buitenland.
6. Theocratieën worden niet door God bestuurd, maar door mensen die Hem het beste denken te kennen.
7. Het aantal opgenomen vluchtelingen is een goede indicator voor de kwaliteit van de sociale en economische structuur van een land.

*Ce qui est simple est toujours faux. Ce
qui ne l'est pas est inutilisable.*

Paul Valéry

Abstract

This thesis deals with the modeling of the surface energy balance and the atmospheric boundary layer over natural land surfaces, on scales of the grid cell of large-scale atmospheric models. In the first part, a model to calculate the canopy conductance as a function of environmental variables evaluated at leaf level is developed and validated. The parameter values of this approach are retained from plant-physiological theory. For a C_4 prairie grass in Kansas and a C_3 soybean crop in southern France, the plant-physiological approach gives better estimates of the canopy conductance, compared to a traditional Jarvis-Stewart approach which relates the canopy conductance to environmental variables at a reference level, using empirical-statistical functions. For a C_3 grass land in the Netherlands, both the plant-physiological approach and the Jarvis-Stewart approach give comparable estimates of the latent heat flux density. In the second part, two approaches to calculate the impact of soil moisture stress on the surface flux densities over natural, heterogeneous areas are compared: a bulk approach where the soil moisture content is assumed to be uniform in a grid cell, and a distributed approach which takes account of the spatial variation of the soil moisture content. In wet conditions, the bulk approach gives larger predictions of the latent heat flux density than the distributed approach. In dry conditions the bulk approach gives lower predictions than the distributed approach. Especially for dry climates the bulk approach predicts during the dry season a severe suppression of the latent heat flux density. In the third part, using three cases that occur frequently in nature it is shown that only a tiling approach can provide estimates of the averaged surface flux densities that are consistent with the averaged temperature difference over the surface layer, the layer of air adjacent to the surface, in all situations.

Voorwoord

Velen hebben bijgedragen aan het tot stand komen van dit proefschrift. Ik wil hen allen bedanken daarvoor. Een aantal mensen wil ik in het bijzonder noemen.

In de eerste plaats wil ik Henk de Bruin bedanken. Henk, dankzij jou was mijn overstap van de hydrologie naar de (micro)-meteorologie overbrugbaar. Vooral in het begin is jouw bijdrage aan mijn onderzoek erg groot geweest. Ook wil ik graag Bert Holtslag bedanken. Gekomen van het KNMI waar hij zich bezighield met grenslaagonderzoek, werd hij door mij gedwongen snel een specialist te worden in de uitwisselingsprocessen tussen planten en de atmosfeer. Bert, bedankt voor de stimulerende discussies, je kritische opmerkingen en je goede adviezen over het schrijven van artikelen. Leo Kroon mag ook niet onvermeld blijven. Vooral in het begin is jouw bijdrage van groot belang geweest. Je stimulant om mijn eerste resultaten gewoon te gaan presenteren op conferenties, is erg belangrijk geweest. Bart van den Hurk begon als collega binnen het project, maar kreeg in een later stadium steeds meer een rol als begeleider en co-promotor. Bart, bedankt voor je discussies en het snelle lezen van nieuwe versies van artikelen en hoofdstukken van dit proefschrift.

Ik wil ook graag de mensen bedanken van het NOP-project 'representatie van de hydrologische cyclus in klimaat- en weersverwachtingsmodellen in West-Europa. In de eerste plaats Margje Soet met wie ik in het begin intensief heb samengewerkt. Ook de andere leden van de projectgroep wil ik bedanken: Han Dolman, met wie ik nu nog intensiever hoop te gaan samenwerken op de Vrije Universiteit Amsterdam, Han Stricker, Pavel Kabat, Reinder Feddes, Anton Beljaars.

Verder wil ik de mensen op Duivendaal 2 bedanken. De sfeer op de vakgroep meteorologie en luchtkwaliteit is informeel en erg prettig. In het bijzonder wil ik Kees van

den Dries bedanken voor zijn ondersteuning bij het vele computerwerk dat nodig was voor het onderzoek zoals beschreven in dit proefschrift. Maar ook van de andere collega's kan hun bijdrage aan dit proefschrift alleen maar worden onderschat. Bedankt, Adrie, Jordi, Peter, Bert Heus., Arjan, Dirk, Wouter, Oscar, Arnold, Willy, Teun, Frits, Michaël, Gerrie, Bas, Job, Berenice, Miaou Junfeng, Joost, Floris, Wim and of course our colleagues from abroad: Michael, Dirk, Jeff and Alessandro.

Gedurende mijn promotietijd heb ik de kans gehad om ook op het KNMI rond te kijken. Ook daar heerst een goede sfeer en heb ik een fijne tijd gehad. Rein, Frank, Casper, Brigitta, Greet, Ruben, Wim, Hanneke, Daan, Nanne, Gerard, Michiel, Xueli, Theo en Erik bedankt.

Ik wil ook graag mijn (schoon)ouders, broer en schoonzus bedanken. Bovenal natuurlijk Ellen, mijn lief. Met jou deel ik al weer bijna vijf jaar lief en leed. Zonder jou was dit proefschrift er nooit gekomen. Bedankt daarvoor.

Reinder Ronda

Almere, 25 maart 2002

Contents

1	Introduction	1
1.1	Land surface and climate	2
1.2	Land surface and the overlying atmosphere	5
1.2.1	Diurnal time scale	5
1.2.2	Seasonal time Scale	7
1.3	Land surface schemes and atmospheric models	8
1.4	Context and motivation	11
1.5	Research question and outline of thesis	12
2	Representation of the canopy conductance in modeling the surface energy budget for low vegetation	15
2.1	Introduction	17
2.2	Descriptions of data sets	19
2.2.1	FIFE-KANSAS	19
2.2.2	HAPEX-MOBILHY	20
2.2.3	Cabauw	20
2.3	Surface energy budget and canopy conductance	21
2.3.1	Background	21
2.3.2	The Jarvis-Stewart approach	22
2.3.3	The plant physiological approach	23
2.4	Soil moisture stress	25
2.5	Results	27
2.5.1	FIFE-KANSAS	28
2.5.2	HAPEX-Mobilhy	32
2.5.3	Cabauw	35
2.6	Discussion and Conclusion	36

3 Spatial heterogeneity of the soil moisture content and its impact on the surface flux densities and near-surface meteorology	41
3.1 Introduction	43
3.2 Calculation of the surface flux densities	46
3.3 Distributed approach versus the bulk approach	49
3.3.1 Variability of the relative saturation	49
3.3.2 The distributed approach	51
3.3.3 The bulk approach	52
3.3.4 Sensitivity study using fixed forcings	53
3.4 Impact on the seasonal cycle	56
3.5 Coupling to the Convective Boundary Layer	59
3.6 Summary and Conclusion	64
4 The Concept of 'Effective' Bulk Exchange Coefficients for Determination of Surface Flux Densities	67
4.1 Introduction	69
4.2 Upscaling the Surface Energy Balance	70
4.3 Setup of evaluation study	73
4.4 Results	75
4.5 Conclusion	78
5 Conclusion and perspective	81
5.1 Summary	82
5.2 Perspective	86
A The plant physiological model.	89
B Scaling the $A_g - g_{c,w}$ approach up from leaf to canopy.	91
C The aerodynamic conductance	93
D The boundary layer model	95
Bibliography	97
Samenvatting	111
Curriculum vitae	115

CONTENTS

vii

List of publications by author

117

Chapter 1

Introduction

1.1 Land surface and climate

A quick look into a common atlas reveals the close connection between the climate and the land surface. Spatial and temporal variations in both the biomass of the vegetation and the land cover type reflect variations in the local climate (Köppen 1936). For natural vegetation the minimal winter temperature and the availability of water are especially important (Woodward 1987). These climatic variables are primarily correlated to the latitude and the altitude. For example when going from south to north on the northern hemisphere, one easily distinguishes: the tropical evergreen broadleaf rainforest in the warm, humid tropics, the vast deserts in the dry tropics, the deciduous broadleaf forests in the temperate zone and the pine forest, tundra vegetation and eventually land ice in the (sub-)polar regions. In addition, on the Eurasian continent the climate generally changes from a maritime climate in the coastal regions to a continental climate in the inland areas. As a result, on the Eurasian continent we find large forests in the coastal regions, whereas the inland areas are dominated by shrubs and grasses.

The land surface also influences the local and the global climate. The most direct impact of the land surface on the climate is through differences in albedo. This already becomes clear when the earth's surface temperature is calculated using a very simple model for the global surface energy balance where the globally averaged incoming solar radiation is used as input (see for instance Stull 2000). It appears that only small perturbations in the albedo yield significantly different global surface temperatures. The sensitivity of the climate to the albedo is confirmed by simulations using more realistic climate models (Charney 1975; Laval and Picon 1986; Garratt 1993). In areas where the albedo is large, most of the incoming short wave radiation is reflected. As a result, the surface temperature in these areas is low as compared to climatologically similar areas where the albedo is small.

The short wave radiation that is not reflected, is absorbed at the surface. In addition, the earth's surface receives long wave radiation from the overlying atmosphere. At the surface, the total absorbed radiation is then partitioned over the sensible heat flux

density, the outgoing longwave radiation flux density, the latent heat flux density and the ground heat flux density. A schematic picture of the energy transfer processes at the surface is given in Figure 1.1. The surface energy budget reads:

$$K^\downarrow - K^\uparrow + L^\downarrow - L^\uparrow = H + \lambda E + G, \quad (1.1)$$

where K^\downarrow is the incoming short wave radiation flux density, K^\uparrow is the reflected short

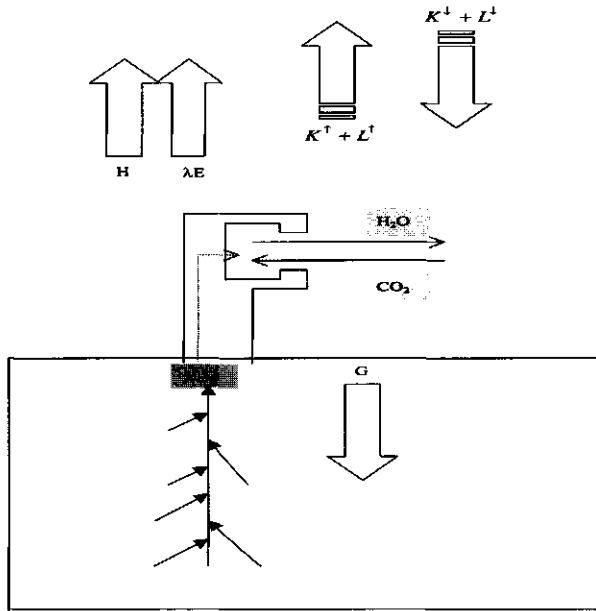


Figure 1.1: An illustration of the exchange of water and carbon dioxide at the land surface and the partitioning of the incoming radiation flux densities into the surface energy flux densities

wave radiation flux density, L^\downarrow is the incoming long wave radiation flux density, L^\uparrow is the flux density of the long wave radiation emitted at the surface, H is the sensible heat flux density, λE is the latent heat flux density and G is the ground heat flux density. On a local scale, the existing land cover strongly controls the partitioning of the available energy at the surface (Garratt 1992). At open water bodies, water availability is unlimited. As a result, the latent heat flux density is typically large in these areas; the Bowen ratio, the ratio of the sensible heat flux density over the latent heat flux density is very small (De Bruin and Keijman 1979). Examples of open water bodies are lakes and films of water intercepted on the ground or on leaves. A somewhat smaller latent heat flux density is observed over wet areas covered with short grass. In these areas, the sensible heat flux density is typically larger (Stricker and Brutsaert 1978), though the Bowen ratio is often still smaller than 0.5 in these areas (e.g. Beljaars and Bosveld 1997). In forests, the transpiration of the canopy is considerably smaller than over grass land areas (Stewart and Thom 1973; Shuttleworth 1989; Bosveld 1999; Ganzeveld 2001). Here, the Bowen ratio ranges from 1 to

2. However, over forests the evaporation of intercepted water contributes importantly to the annual evaporation (Rutter et al. 1972). In dry areas covered with grasses or shrubs or with a bare soil cover, the sensible heat flux density and the ground heat flux density are large (Braud et al. 1993; Van den Hurk 1995; Verhoef 1995). In these areas the latent heat flux density is much smaller or even absent; the Bowen ratio is very large in these areas.

The first numerical simulations performed to assess the effect of land cover on the regional climate were the deforestation experiments done by Henderson-Sellers and Gornitz (1984) and Dickinson and Henderson-Sellers (1988). They found that replacing the tropical rainforest by pasture led to a significant decrease of the annual evapotranspiration and the simulated precipitation, and an increase of the surface temperature. A detailed analysis revealed that these changes were mainly caused by the decrease of the roughness length. This reduction hampered the exchange of water and energy from the surface to the lower atmosphere (Garratt 1993). Similar climate impact studies were performed for the Sahelian (e.g. De Ridder 1998) and for the Boreal region (e.g. Bonan et al. 1992). These studies clearly found an impact of both the wetness of the soil and the land cover type on the regional climate. Often, in these simulations teleconnections have been observed: anomalies in climatic variables in one region affect the climate in other regions.

The role of the vegetation cover on the global climate was investigated recently by Fraedrich et al. (1999). In one simulation the entire world was covered by vegetation, whereas in another run all vegetation was replaced by bare soil. They found that the run with vegetation gave considerably larger values for the latent heat flux density. This resulted in a decrease of the surface temperature and because of an enhanced latent heat release in convective cells due to precipitation, an enhancement of the temperature of the upper troposphere.

The importance of the land surface for the hydrological budget of the continents also appears in an analysis of the global hydrological budget. Figure 1.2 shows the global hydrological budget of the ocean, the atmosphere over the ocean, the land surface and the atmosphere over land. From Figure 1.2 it appears that about 30 % of the precipitation over the continents originates from the ocean. The moisture evaporated from the land surface is a major source of precipitation. However, there appear to be pronounced regional differences in the impact of the land surface on the precipitation. Koster et al. (2000a) studied how land impacts the global precipitation patterns. They found that the land surface had a considerable impact on the precipitation pattern only in extra-tropical areas where sufficient energy and water was

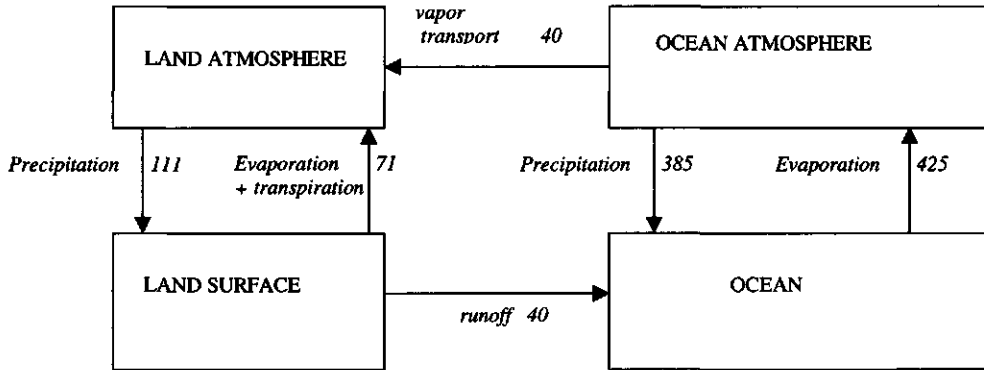


Figure 1.2: The average annual global hydrological budget: units of the fluxes are thousands of cubic kilometers per year (Values taken from La Rivière (1989))

available. In these regions, the land surface plays a role in the additional deepening of convective cells through additional moisture supply and resulting latent heat release.

From the studies listed above it appears that the land surface interacts with the overlying atmosphere on a variety of temporal and spatial scales. For vegetated surfaces the diurnal time scale and the seasonal time scale are most important. These will be discussed in the next section.

1.2 Land surface and the overlying atmosphere

1.2.1 Diurnal time scale

On a diurnal time scale the land surface and the overlying atmospheric boundary layer are closely connected. This is depicted in Figure 1.3 which shows the main interactions between the surface and the lower atmosphere during daytime. During daytime the surface of the earth is heated by the energy provided by the incoming solar radiation. This warming causes a buoyant forcing of the air near the surface. As a result, the boundary layer grows due to convection (Garratt 1992). Over most land surfaces the sensible heat flux density mainly determines this convection (Ball 1960; Tennekes 1973). As a result, the boundary layer growth varies as the sensible heat flux density varies. Over large water bodies and over wet grassy areas the sensible heat flux density is usually small. Here, the boundary layer is usually shallow, to

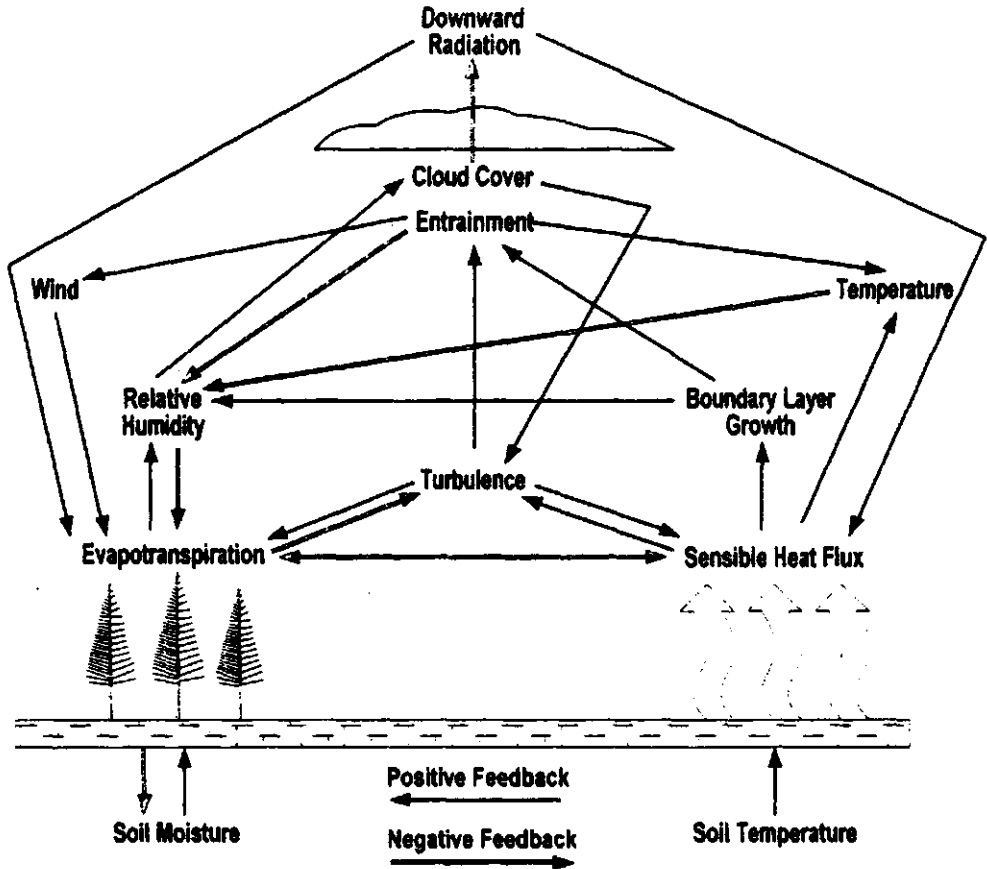


Figure 1.3: Interactions between the earth's land surface and the overlying atmospheric boundary layer (courtesy by M. Ek (see Ek and Mahrt 1991))

about 1600 m at the end of the afternoon (Holtslag and Ek 1996). In contrast, over dry areas the boundary layer is usually much deeper, to 3500 m at the end of the afternoon (Van den Hurk 1995).

The differences in boundary layer growth at their turn affect the meteorological conditions near the surface (Jacobs and De Bruin 1992; Holtslag and Ek 1996). A schematic picture of the feedback processes is given in Figure 1.3 (Ek and Mahrt 1991). As the boundary layer grows, warm and usually dry air is entrained into the boundary layer from the free tropospheric air aloft. Therefore, over areas with shallow boundary layers the specific humidity near the surface is relatively large compared to

similar areas where the boundary layer is much deeper. Also, the temperature near the surface in the former areas is relatively low compared to areas where the boundary layer is much deeper.

The differences in the surface flux densities also impact the predicted cloud cover (Ek and Mahrt 1991). In convective conditions, the thermals transport air parcels directly from the surface to the top of the boundary layer (Garratt 1992). While ascending, the absolute air temperature of the air parcel decreases. Often the temperature of the air parcel drops below the dew point temperature. As a result, the moisture in the parcel condensates and clouds are formed. Using a model applied at Cabauw in the Netherlands Ek and Holtslag (2002a, 2002b) found that the predicted cloud cover closely depends on the soil moisture content. These clouds affect the surface by decreasing the incoming short wave radiation, partly compensated by an enhancement of the incoming long wave radiation (Figure 1.3).

1.2.2 Seasonal time Scale

On a seasonal time scale, the land cover exerts a strong control on the hydrological budget over continents through (Dolman et al 2002):

1. the water stored in the soil moisture reservoir,
2. the rooting depth of plants,
3. the seasonal cycle in the vegetation characteristics.

During the wet season in the dry tropics or the winter season in temperate regions, large-scale synoptic systems transport water from the oceans to the continents. A major part of the resulting precipitation infiltrates into the soil. As the precipitation usually exceeds the evapotranspiration, the infiltrated water is able to percolate towards deeper layers, where it is stored. In the dry season in the dry tropics or the summer season in the temperate regions, the evapotranspiration increases and eventually exceeds the precipitation. During this period, the surface and the upper layers of the soil are very dry. However, plants extract the stored water using their roots and often succeed to maintain a considerable transpiration during the dry season.

For many areas in the world this transpired water is the major source of moisture for the atmosphere during the dry season. The resulting water condensates higher in the convective boundary layer or in convection cells in the troposphere (see subsection 1.2.1) which makes the transpired water important for the formation of clouds during the dry season. These clouds reduce the incoming short wave radiation at the surface.

As a result, via the seasonal cycle of the hydrological budget the land cover indirectly impacts the global radiation balance. Also, the water released from the soil through transpiration is a major source of precipitation during the dry season. Using a general circulation model, Milly and Dunne (1994) found that predictions of the cloud cover and the precipitation were sensitive to initial conditions in the soil moisture content and the ability of roots to extract water from a larger depth in the soil.

The percolated water is an important source of water during the dry season. This highlights the importance of vegetation and its roots for the simulated climate. In contrast to a bare soil surface, plants extract water from deeper soil layers. However, the rooting depth depends strongly on the species type of vegetation. Shrubs in the Sahelian savannah are adapted to the severe drought conditions during the dry season. Roots are found till a depth of a few meters (Verhoef 1995).

Also important for the seasonal cycle of the hydrological budget is the seasonal cycle of vegetation parameters, like the leaf area index and the fraction of the area covered by vegetation. For example, Van den Hurk et al. (2001a) incorporated a seasonal cycle of the vegetation coverage fraction into a regional climate model. They compared results obtained using this run with results obtained using a model with fixed vegetation parameters during the growing season. In the Northwestern area of Europe, they found that the run with the time-varying vegetation cover gave much higher estimates of the transpiration and the precipitation during the dry season. This was caused by a reduction of the vegetation coverage in the dry season. During this period, the vegetation cover of the time-varying run was considerably lower than the vegetation cover in the fixed run. This resulted in a larger canopy conductance and smaller estimates of the evapotranspiration during this period. Hence, more water was available for transpiration during the dry season. In contrast, in the Southeastern region of Europe, the transpiration during the dry season was reduced. This was caused by the vegetation cover which was in the fixed run much smaller than in the time-varying run in the early dry season. Thus, it appears that the seasonal cycle of the vegetation parameters have an important impact on the regional hydrological budget.

1.3 Land surface schemes and atmospheric models

Land surface models provide the lower boundary condition of atmospheric models. As apparent in the previous sections, the land surface has an important impact on both the global and regional climate. Therefore, land surface models are an impor-

tant part of climate models and numerical weather prediction models (Viterbo and Beljaars 1995; Henderson-Sellers et al. 1996).

In the first generation of land surface models the soil column was simply represented as a bucket. The bucket was filled by the precipitation minus the interception. It was emptied by the runoff and the evapotranspiration (Manabe 1969). The effect of soil moisture stress on the latent heat flux density was described very simple. The atmospherically controlled latent heat flux density was multiplied with a factor that was a function of the water level in the bucket.

An important focus of land surface scheme development has been the representation of the transpiration by vegetation canopies. Over vegetated surfaces, the leaf exchanges water vapor with the atmosphere through molecular diffusion through the stomata. This diffusion could effectively be described by introduction of a stomatal conductance (Monteith 1965). This conductance acts in series with the aerodynamic conductance that describes the effectiveness of turbulent diffusion in the surface layer, the layer of air adjacent to the surface. Upscaling the individual leaf conductances is then applied to obtain one canopy conductance. As such, the canopy is considered as one big leaf having only one big stomatum (see Figure 1.1). Plants control their water loss by consecutively opening and closing of their stomata. Jarvis (1976) found that this control is empirically related to environmental conditions like the incoming amount of photosynthetically active radiation, the temperature of the canopy and the air humidity. Usually, these dependencies are calculated by using observed statistical relationships between the canopy conductance and the environmental variables evaluated at a reference level in the surface layer (Jarvis 1976; Stewart 1988). Recently, these statistical relations have been replaced by more physiologically-oriented models which take account of the physical processes inside a plant. Moreover, these describe the canopy conductance as a function of the absorbed photosynthetically active radiation, the leaf temperature, the vapor pressure deficit difference between the leaf interior and exterior rather than on environmental variables evaluated at a reference level (Jacobs 1994; Sellers et al. 1996). As a result, these formulations are more suitable for climate impact studies, as compared to the previous statistical-empirical functions.

Another development in land surface modeling was the replacement of the bucket scheme for the soil moisture reservoir into more advanced schemes. Often, modellers now divide the soil column into multiple soil layers. These models allow infiltrated water to percolate towards deeper layers, where the root density is usually less. This leads to a reduction of the latent heat flux density at the beginning of a dry-down pe-

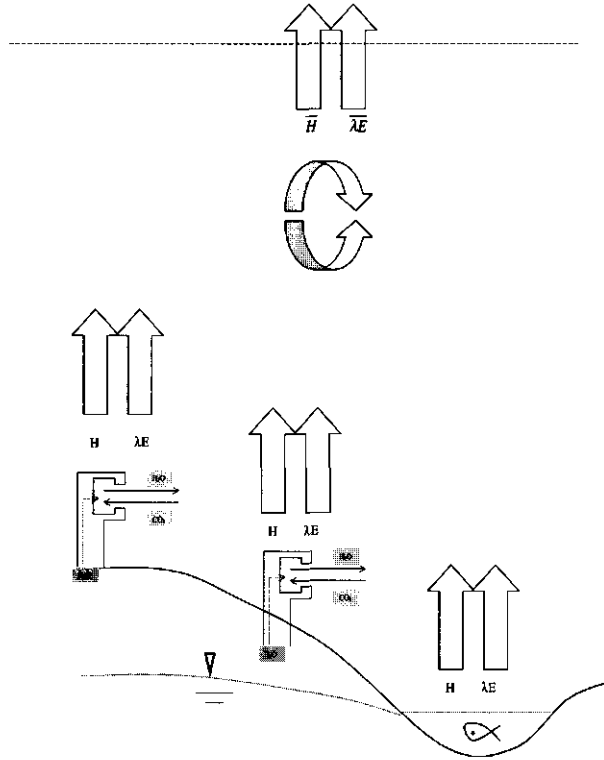


Figure 1.4: Cartoon representing geography of a grid cell of an atmospheric model. In this Figure the dotted line represents the ground water level and the water level within the stream and the dashed line represents the top of the atmospheric boundary layer.

riod (Kim 1995). As a result, more water is available for the transpiration during the dry season. Roots can extract water from these deeper layers (see previous section). Especially in dry Sahelian climates, this appeared to be very important for a correct simulation of the seasonal cycle of the evapotranspiration (Soet et al. 2000).

Another important issue in land surface modeling is the parameterization of the runoff which is very important for the seasonal hydrological budget. Biases in runoff lead to significant biases in the estimated soil moisture content later in the season. Koster and Milly (1997) found that even when the latent heat flux density was known exactly as a function of the soil moisture content, differences in the runoff could give considerable biases in the estimated evapotranspiration during the dry season. In the

bucket model, runoff simply occurred only when the bucket overflowed (Manabe 1969). Later, Dümenil and Todini (1992) extended the bucket approach and introduced a parameterization for the slow runoff due to ground water discharge. Furthermore, they assumed that the soil moisture component over an area is distributed. Thus, they define areas where runoff is small and areas where runoff is larger. At higher elevation the soil is dry and almost all precipitated water infiltrates. In contrast, in lower elevation areas, the soil is wetter. Here, most precipitated water runs off (Figure 1.4). In schemes where the soil is divided into multiple soil layers, runoff usually occurs when the precipitation minus the interception exceeds the infiltration capacity of the upper soil layer (Viterbo and Beljaars 1995). Deep drainage in these schemes is usually calculated as free drainage from the lower soil layer due to gravity.

1.4 Context and motivation

Progress in hydrology, (micro)-meteorology and plant science all have contributed to a better understanding of the transfer of heat, water vapor and mass fluxed through the soil-vegetation-atmosphere system. This led to a variety of land surface models which have been thoroughly validated for local experimental sites (Henderson-Sellers et al. 1996). However, despite the major progress made in land surface modeling, large-scale atmospheric models still tend to overestimate the evapotranspiration in early summer or early in the dry season (Viterbo 1994; Delage and Verseghy 1995). As a result, the infiltrated water is released to the atmosphere too quickly and the evapotranspiration is underestimated later in the summer or in the dry season. In many conditions, this leads to an underestimation of the humidity of the lower atmosphere and a suppression of the precipitation during the dry season (Viterbo 1994; Rowntree 1995; Dolman 2001a). For example Viterbo and Courtier (1995) reported a severe dry bias over the European continent during summer in forecasts obtained using the Numerical Weather Prediction Model (NWPM) of the European Centre for Medium-Range Weather Forecasting (ECMWF). They resolved the observed dry bias by including the soil moisture content in a data-assimilation cycle.

The problems in correctly representing the seasonal hydrological cycle within large-scale models warranted investigations of errors in current parameterizations. Therefore, the Dutch National Research Programme on Global Air Pollution and Climate Change initiated a project under number 951246 entitled 'Representation of the seasonal hydrological cycle in climate and weather prediction models in West Europe' (Dolman et al. 2002; Van den Hurk et al. 2001a). Within this framework, Soet et

al. (2000) investigated the parameterization of the water transfer below the surface. Using observations obtained at three sites which differed with respect to climate and soil, Soet et al. (2000) compared simulations of the seasonal hydrological budget obtained using the state-of-the-art land surface model SWAPS with different versions of the land surface model used in the NWPM of ECMWF (Viterbo and Beljaars 1995). Their main result was that the use of local soil characteristics gave a better representation of the infiltration and the percolation than using the global soil characteristics adopted by Viterbo and Beljaars (1995).

Unfortunately, for most areas in the world no detailed local information is available. Therefore, for use in large-scale models the soil characteristics have to be obtained from crude maps. For Europe, such a classification was made by Wošten et al. (1998). The resulting data base is called the Hydraulic Properties of European soils (HYPRES) data base and defines five textural classes: a very fine textured soil, a fine-textured soil, a medium-fine textured soil and a coarse-textured soil. To assess the usefulness of this classification to get good predictions of the seasonal cycle, Soet et al. (2000) compared the annual cycle of the hydrological budget simulated using the soil characteristics from the HYPRES data base with a simulation where the local soil characteristics are used. For a medium-textured soil it was found that the 'a priori' estimated parameters predicted a considerable different annual cycle of the hydrological budget. In contrast, for a coarse-textured sand soil, they found that using the 'a priori' estimated parameters gave a similar annual cycle of the hydrological budget.

1.5 Research question and outline of thesis

In this study we concentrate on the exchange of water and energy between the earth's surface and the lower troposphere. Its central aim is to elucidate how to describe this exchange in large-scale atmospheric models appreciating that the parameter values of these models should be obtained from coarse land surface maps and that the grid cells of such models are usually heterogeneous. The goals of this thesis are:

1. develop and validate a plant-physiologically based model for the canopy conductance that can effectively be implemented in large-scale atmospheric models,
2. to study the impact of the soil moisture heterogeneity on the estimated surface flux densities and near-surface meteorology on spatial scales typical of large-scale atmospheric models, and

3. to study the impact of the surface temperature on the estimated surface flux densities and near-surface meteorology on scales typical of large-scale atmospheric models.

These goals are dealt with in four chapters.

In chapter 2 of this thesis we will study the representation of the canopy conductance in large-scale atmospheric models. In this chapter we develop and validate a model that is based on the physics of plant functioning. The parameter values used in the approach are not optimized locally. For most areas in the world, no detailed local information is available. Therefore, the parameters of a land surface model should be obtained from crude maps. Usually, these maps divide the range of parameter values into a limited number of classes. It is, therefore, useful to study whether the parameters estimated from those crude maps lead to useful estimates of the water and heat transfer at the surface.

Chapter 3 and chapter 4 deal with scaling up land surface models developed for homogeneous areas to large areas which usually are heterogeneous. In Figure 1.4 we depict an example of a grid cell of an atmospheric model. Usually, the grid cell consists of dry areas at the higher elevations, and wetter areas located at the lower elevations

In chapter 3 we study the impact of the heterogeneity of the soil moisture content on the surface energy flux densities and near-surface meteorology. Using a distribution which has successfully been used to describe the effect of soil moisture heterogeneity on the runoff, we assess the impact of subgrid variations of the soil moisture content on the grid cell averaged surface flux densities. Furthermore, we evaluate the impact of spatial variations of the soil moisture content on the seasonal hydrological budget (see section 1.2.2). Finally, in this chapter we study the impact of spatial variations in the soil moisture content on the development of the convective boundary layer. Thus, we study how the boundary layer feeds back on the surface flux densities over an area where the soil moisture content is spatially heterogeneous (see section 1.2.1).

Chapter 4 deals with the heterogeneity of the surface temperature. For three surfaces that occur frequently in nature, we study how the averaged sensible heat flux density is related to the averaged temperature difference over the surface layer. In this chapter, we show that the averaged temperature difference over the surface layer cannot be used to obtain the average sensible heat flux densities in all situations.

In chapter 5 we provide a summary. Furthermore, in this chapter we give an overview of results obtained by others who used the ideas presented in this thesis for further research. In addition, in this chapter we give a concise discussion of possible

routes for further research.

Chapter 2

Representation of the canopy conductance in modeling the surface energy budget for low vegetation

This chapter is published as Ronda, R.J., H.A.R. de Bruin, and A.A.M. Holtslag, 2001: Representation of the canopy conductance in modeling the surface energy budget of low vegetation. *J. Appl. Meteor.*, **40**, 1431-1444

©Copyright 2000 by AMS

abstract

In this study, the authors develop and validate an approach to calculate a canopy conductance that can successfully be implemented in an atmospheric model. The approach is based on plant physiology approaches that have been developed recently. However, it includes a new analytic formulation to scale the conductance up from leaf to canopy. Furthermore, a new expression that accounts for the effect of soil moisture on the canopy conductance is proposed. The parameters are not optimized locally; rather, values are assigned to them as a function of vegetation type. This approach is validated for three experimental sites: the First International Satellite Land Surface Climatology Project Field Experiment (FIFE)-KANSAS area, the Hydrological Atmospheric Pilot Experiment-Modélisation du Bilan Hydrique (HAPEX-Mobilhy) site, and the Cabauw area. The vegetation at these sites is representative for large areas with low vegetation in the world. The results of the plant physiological approach are based on a distinction in C_3 and C_4 plant types, and these results are found to be better (FIFE-KANSAS) and more consistent (HAPEX-Mobilhy) than estimates obtained by a traditional Jarvis-Stewart approach. The parameters of the latter are also obtained from a vegetation classification. For the Cabauw area, both approaches give comparable estimates of the surface flux densities. Furthermore, the new soil moisture content response function is found to work well, as compared with previous formulations.

2.1 Introduction

As shown in various studies (e.g. Viterbo and Beljaars 1995; Dickinson et al. 1991; Garratt 1993), the performance of atmospheric models depends on a proper representation of the surface processes. The surface conductance is especially important. For vegetative surfaces, the surface conductance equals the canopy conductance. This conductance is the stomatal conductance scaled up from leaf to canopy. A large percentage of surfaces in the world is vegetated. Therefore, the representation of this conductance is a key component in modeling the surface energy budget.

The canopy conductance critically determines the partitioning of the available energy (net radiation minus the soil heat flux density) over the sensible and latent heat flux density. This is illustrated in Figure 2.1 for observations taken at a site in Kansas, USA. In this figure the latent and sensible heat flux densities are plotted as a function of the derived surface conductance (see section 2.3 for details). Most notably for low values of the conductance, it appears that the partitioning of the available energy into sensible and latent heat flux densities depends critically on the surface conductance.

In most current atmospheric models, the canopy conductance is calculated with functions relating the canopy conductance diagnostically to environmental variables at an atmospheric reference height (Jarvis 1976; Stewart 1988). This approach is usually referred to as Jarvis-Stewart (henceforth JS) approach. The empirical relations are based on statistical relationships between the canopy conductance and the environmental variables. The most appropriate application of the JS approach is, therefore, in hydrological models and land surface models. Typically, these models use the values at the reference height as input. The JS method is less appropriate for atmospheric models. In such models the environmental variables are fields that evolve among others as a function of the canopy conductance itself. Moreover, the method cannot be used in climate impact studies, since it is uncertain whether either the empirical functions or the function parameters still hold in future climates, when carbon dioxide concentrations and other environmental conditions are expected to be different.

In laboratory experiments performed under different climatic conditions, the canopy conductance was found to be linearly related to the gross assimilation rate. Furthermore, it was found to be inversely proportional to the carbon dioxide concentration (Goudriaan and Van Laar 1978; Ball et al. 1987; Leuning 1990, 1995; Jacobs 1994). To estimate the plant assimilation rate, robust models are available. Parameter values

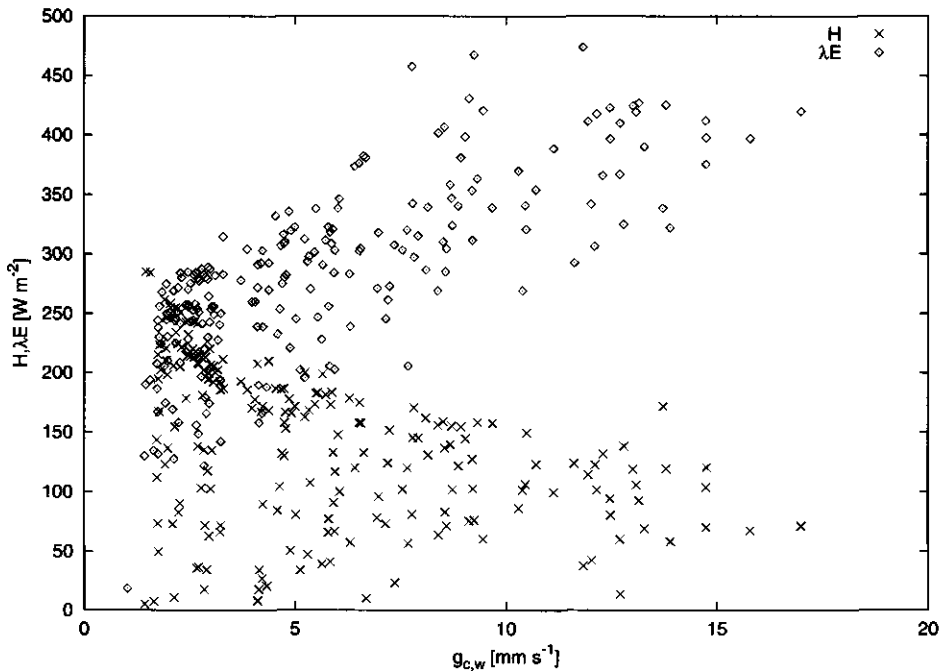


Figure 2.1: The dependence of the sensible heat flux density (H) and the latent heat flux density (λE) on $g_{c,w}$ for the FIFE-KANSAS area. Crosses refer to H , whereas diamonds refer to λE .

are generally based on a distinction in C_3 and C_4 plants (Collatz et al. 1991, 1992). The relations are based on plant physiology theory. As such the canopy conductance is an indirect function of the environmental variables evaluated at leaf level. Therefore, this method is more appropriate for prognostic atmospheric models and climate impact studies. Hereafter, this method will be referred to as the $A_g - g_{c,w}$ approach.

The objective of this study is to develop and validate a plant physiological approach for low vegetation that can successfully be implemented in an atmospheric model. For that purpose, we simplify the method of Jacobs (1994). Furthermore, we develop a new analytic formulation to scale the conductance up from leaf to canopy. In addition, we propose a function that accounts for the effect of the soil moisture content on the conductance. Because for most areas in the world no detailed, local information is known, the parameters of the approach should be rather robust. The

parameters have to be estimated from crude land surface maps in which only a limited number of vegetative classes or biomes are distinguished.

The resulting $A_g - g_{c,w}$ method is validated with measurements. Moreover, we compare its output with results obtained using a traditional JS approach. The parameters of both approaches are not optimized locally. Rather, they are set a priori as a function of vegetation type or biome (Dorman and Sellers 1989; Van den Hurk et al. 2000). Previous detailed intercomparison studies (e.g. Cox et al. 1999a) revealed that if the parameters are optimized locally, both methods give good and comparable approximations of the canopy conductance. Finally, we validate our soil moisture response function. Its results are compared with results obtained using functions provided in the literature.

The JS approach and the developed plant physiology approach are implemented in a land surface model. Results are shown for the First International Satellite Land Surface Climatology Project Field Experiment (FIFE)-KANSAS site, a prairie grass land in KANSAS; the Hydrological Atmospheric Pilot Experiment-Modélisation du Bilan Hydrique (HAPEX-Mobilhy) site, a soybean field in southern France; and the Cabauw site, a grass land in the Netherlands. The vegetation types at these sites are representative for large areas of low vegetation in the world.

Section 2.2 describes the datasets. Section 2.3 gives the background of modeling the surface energy budget and describes the JS approach and the physiologically based approach. Section 2.4 focuses on the effect of soil moisture stress on the canopy conductance. Section 2.5 provides the results. In section 2.6 a discussion and a conclusion are given.

2.2 Descriptions of data sets

2.2.1 FIFE-KANSAS

The data of the FIFE-KANSAS area (39.03 °N, -96.97 °E) were measured between May and October 1987, during the FIFE 1987 experiment (Sellers et al. 1988). They were collected from different sites and then areally averaged (Betts and Ball 1992). The set consists of half-hourly averages of the downward short wave and longwave radiation, the surface skin temperature, the temperature and specific humidity at 2 m and the windspeed at 5.4 m. Moreover, it contains 30-minute averages of the net radiation, the sensible heat flux density, the latent heat flux density and the soil heat flux density. During the intensive field campaigns, the sensible heat flux density was

measured with eddy-correlation devices. Outside these campaigns, the Bowen ratio method was used. However, the directly measured net radiation does not always match the residual of the radiation balance. Since the Bowen ratio method is not applicable in such situations, data for which the difference exceeds 5%, are excluded from the set.

The soil moisture content was measured weekly at different sites. Probes were inserted every 0.1 m to a depth of 2 m. The weekly data were interpolated to daily values. The resulting daily values were finally areally averaged (Betts and Ball 1992).

2.2.2 HAPEX-MOBILHY

The data used here, were measured at the Caumont Soybean site (43.68 °N, -0.1 °E) during the HAPEX-MOBILHY experiment in 1986 (Goutorbe 1991). Note that this data set was used in the PILPS study also (Shao and Henderson-Sellers 1996). It consists of half-hourly values of the incoming short- and longwave radiation and the temperature, specific humidity and wind speed at screen level (2 m). For the 37-day intensive observation period, measurements of the net radiation and the soil, sensible and latent heat flux densities are available in 30-minute intervals. The sensible heat flux density was calculated using flux-profile relationships. The latent heat flux density was derived as a residual of the surface energy budget. On day 174 and day 175 the derived latent heat flux density exceeds 90% of the net radiation. This is unrealistic for a canopy. Therefore, data obtained on these days are excluded from the set. Furthermore, soil moisture contents were measured every 0.1 cm to a depth of 1.6 m. The data were collected and then were interpolated to daily values.

2.2.3 Cabauw

The data used in this analysis were collected during 1987 in Cabauw (51.97 °N, 4.93 °E), in the Netherlands (Beljaars and Bosveld 1997). The set contains half-hourly values of the incoming short- and longwave radiation, the temperature, specific humidity and wind speed at screen level (20 m). Furthermore, measurements of the net radiation and the soil, sensible and latent heat flux densities are available. The sensible heat flux density was calculated using flux-profile relationships. The latent heat flux density was obtained as a residual of the surface energy budget. On the days 67, 68 and 130 errors were found in the measured net radiation. Therefore, data obtained on these days are excluded.

Soil moisture contents have not been measured. However, the soil moisture content

was above field capacity on most days. Between yeardays 180 and 200, the soil moisture content is suspected to be below field capacity. Consequently, these days are removed from the analysis.

2.3 Surface energy budget and canopy conductance

2.3.1 Background

The surface energy budget (SEB) reads:

$$(1 - a)K^\downarrow + \epsilon L^\downarrow - \epsilon\sigma T_{sk}^4 = H + \lambda E + G, \quad (2.1)$$

where K^\downarrow is the incoming short wave radiation flux density, L^\downarrow is the incoming long-wave radiation flux density, H is the sensible heat flux density, λE is the latent heat flux density, and G is the soil heat flux density; ϵ is the emissivity of the earth's surface, a is the albedo and σ is the Stephan-Boltzmann's constant. T_{sk} is the surface skin temperature.

Usually, the sensible heat flux density and latent heat flux density are calculated by means of bulk exchange relations. Typically, these relate the flux density to profiles in the surface layer (e.g. Beljaars and Holtslag 1991):

$$H = \rho_a c_p g_a (T_{sk} - T_a), \quad (2.2)$$

$$\lambda E = \rho_a \lambda g_a \frac{q^*(T_{sk}) - q_a}{1 + g_a/g_{c,w}}, \quad (2.3)$$

where ρ_a is the air density, c_p is the isobaric specific heat, g_a is the aerodynamic conductance, $g_{c,w}$ is the canopy conductance to water vapor flow, T_a is the air temperature at the reference level z_r , $q^*(T_{sk})$ is the saturated specific humidity at the surface and q_a is the specific humidity at the reference level.

In atmospheric models g_a is, generally, calculated using Monin-Obukhov similarity theory. As such, it is a function of $|u|$, the horizontal wind velocity, the roughness length for heat, z_h , the roughness length for momentum, z_{0m} , z_r and $(T_{sk} - T_a)$ (Beljaars and Holtslag 1991). Recall that Figure 2.1 illustrates the dependence of the sensible and latent heat flux densities on $g_{c,w}$. The latter have been derived by first inverting Eq.(2.2) to obtain g_a from observations of H , T_{sk} and T_a . Subsequently, the values for $g_{c,w}$ are derived by using Eq.(2.3) and the observations of λE , q_a and the estimates of g_a .

In the next two subsections we present two methods to calculate the canopy conductance. Because water vapor and carbon dioxide are exchanged through the same

stomata, the water vapor and carbon dioxide conductance are closely related:

$$g_{l,c} = \frac{g_{l,w}}{1.6} \Rightarrow g_{c,c} = \frac{g_{c,w}}{1.6}. \quad (2.4)$$

In these relations $g_{l,c}$ and $g_{l,w}$ are the leaf conductance (l) to carbon dioxide (c) and water vapor (w) respectively, while $g_{c,c}$ is the canopy (c) conductance to carbon dioxide flow. The factor 1.6 results from the ratio of the molecular diffusivities of water vapor and carbon dioxide in air.

2.3.2 The Jarvis-Stewart approach

The Jarvis-Stewart approach is based on statistical relationships between the canopy conductance and the downward short wave radiation, the leaf area index, the humidity, temperature and carbon dioxide concentration at screen level and the soil moisture content. Heuristically, Jarvis (1976) proposed the following functional:

$$g_{c,w} = g_{\max,w} \left(f_1(K^\downarrow) f_2(D_a) f_3(T_a) f_4(C_a) f_5(\bar{w}) + \frac{g_{\min,w}}{g_{\max,w}} \right) \text{LAI}. \quad (2.5)$$

In this equation $g_{\max,w}$ is a maximal stomatal conductance, $g_{\min,w}$ is a minimal conductance, LAI is the leaf area index, D_a the vapor pressure deficit at screen level, $q^*(T_a) - q_a$, C_a the CO_2 concentration at the screen level and \bar{w} the root zone soil moisture content.

The functions f_1 to f_5 are assumed independent and typically take on values between 1 and 0. For the functions various representations have been proposed. Here, we adopt the following formulations:

$$f_1(K^\downarrow) = \frac{K^\downarrow}{K^\downarrow + a_1}, \quad (2.6)$$

$$f_2(D_a) = e^{-a_2 D_a}, \quad (2.7)$$

$$f_3(T_a) = \max\left(0, 1 - a_3(298 - T_a)^2\right), \quad (2.8)$$

where f_1 and f_2 can be shown to be equivalent to the expressions used by Van den Hurk et al. (2000) in the European Centre for Medium-Range Weather Forecasts ERA40 surface scheme. Here, f_3 is taken from Noilhan and Planton (1989), and C_a is assumed not to vary during the experiments. Therefore, $f_4(C_a)$ is equal to 1. Also, $f_5(\bar{w})$ is in common with the $A_g - g_{c,w}$ approach and will be discussed in section 2.4.

The parameters $g_{\max,w}$, $g_{\min,w}$ and a_1 to a_3 are tunable and generally have to be optimized locally. However, for large areas in the world, no detailed local information is available and parameters have to be taken from crude vegetation maps (Van den Hurk et al. 2000).

2.3.3 The plant physiological approach

In analogy to water vapor flow, the flow density of carbon dioxide, which results from the difference between the gross assimilation rate and the dark respiration, is given by

$$A_n = g_{l,c}(C_s - C_i) = A_g - R_d, \quad (2.9)$$

where A_n is the net flow of carbon dioxide into the plant, C_s is the CO_2 concentration at the leaf surface, C_i is the CO_2 concentration in the plant interior, A_g is the gross assimilation rate and R_d is the dark respiration rate. Here, A_g and R_d result from photochemical reactions. As such they are functions of the photosynthetically active radiation, the leaf skin temperature and the internal CO_2 concentration. Note that PAR is typically 50% of the absorbed (non-reflected) incoming short wave radiation. Plant physiological models for A_g and R_d are well-established (Collatz et al. 1991, 1992). Representations for the reactions involved are given in Appendix A.

In laboratory experiments the internal CO_2 concentration, C_i , is often found to be a fraction of the external CO_2 concentration. When sufficient amounts of radiation density are coming in, it appeared that the ratio of the internal and external concentration is only a function of the water vapor deficit (Jacobs 1994; Zhang and Nobel 1996):

$$\frac{C_i - \Gamma}{C_s - \Gamma} = f_0 \left(1 - \frac{D_s}{D_0} \right) + f_{\min} \frac{D_s}{D_0}, \quad (2.10)$$

where D_s is the vapor pressure deficit at plant level, f_0 is the maximum value of $(C_i - \Gamma)/(C_s - \Gamma)$, D_0 is the value of D_s at which the stomata close and f_{\min} is a minimal value of $(C_i - \Gamma)/(C_s - \Gamma)$. Eqs. (2.9) and (2.10) can be solved for $g_{l,c}$:

$$g_{l,c} = g_{\min,c} + \frac{a_1 A_g}{(C_s - \Gamma) \left(1 + \frac{D_s}{D_*} \right)}, \quad (2.11)$$

where $g_{\min,c}$ is the cuticular conductance, D_* is $\frac{1}{a_1 - 1} D_0$ and a_1 is equal to $\frac{1}{1 - f_0}$. An expression for f_{\min} is given in Appendix A. The linear dependence implies that, in dry conditions, the photosynthesis is more efficient. Larger photosynthesis rates are maintained at lower values of the conductance.

We adopt a hyperbolic dependence of the canopy conductance on D_s . Ball et al. (1987) assumed that $g_{l,c}$ decreases linearly as a function of decreasing relative humidity. This approach was followed by Collatz et al. (1991, 1992) and Sellers et al. (1996). Unfortunately, there is no exclusive evidence for either approach (Leuning 1995). Intercomparison studies (Niyogi and Gifford 1997, Cox et al. 1999a) showed that the performance of both approaches is comparable. We adopt the hyperbolic

Table 2.1: Parameter values of the biochemical module in the plant physiological approach

plant type	parameter	$X(T_{sk} = 298)$	Q_{10}	$T_1[K]$	$T_2[K]$
C_3	$f_0[-]$	0.89			
	$a_d[kPa^{-1}]$	0.07			
	$\mu_0[mg J^{-1}]$	0.017			
	$\Gamma[mg m^{-3}]$	$68.5\rho_a$	1.5		
	$g_m[mm s^{-1}]$	7.0	2.0	278	301
	$A_{m,max}[mg m^{-2} s^{-1}]$	2.2	2.0	281	311
C_4	$f_0[-]$	0.85			
	$a_d[kPa^{-1}]$	0.15			
	$\mu_0[mg J^{-1}]$	0.014			
	$\Gamma[mg m^{-3}]$	$4.3\rho_a$	1.5		
	$g_m[mm s^{-1}]$	17.5	2.0	286	309
	$A_{m,max}[mg m^{-2} s^{-1}]$	1.7	2.0	286	311

function since the parameter can be more easily valued for C_3 and C_4 plants.

In the approach proposed by Jacobs (1994) expression (2.9) is also applied for low light conditions. This leads to erroneous values of the conductance in such cases. To correct this, Jacobs (1994) introduced a complicated interpolation formula. We adopt a much simpler approach and use relation (2.11) directly to calculate the canopy conductance. C_i is then only used as input for the plant physiological approach. Fortunately, under low light conditions A_g becomes independent on C_i (see appendix A).

Jacobs (1994) found values for the parameter of equations (2.10) and (2.11) by evaluating laboratory experiments. However, his results appear to underestimate $(C_i - \Gamma)/(C_s - \Gamma)$ at low values of D_s . Recently, Zhang and Nobel (1996) evaluated the linear expression given by (2.10) for several C_3 plants (*Encelia farinosa*, *Larrea tridentata*, *Nicotiana glauca*, *Oryza sativa*, *Phalaris aquatica* and *Phaseolus vulgaris*) and C_4 plants (*Pleuraphis rigida*, *Paspalum plicatulum* and *Zea mays*):

$$\frac{C_i - \Gamma}{C_s - \Gamma} = f_0 - a_d D_s, \quad (2.12)$$

where f_0 and a_d are empirically found as regression coefficients. They found that f_0 is 0.89 for C_3 plants and 0.85 for C_4 plants (P. Nobel 1999, personal communication). For a_d they obtained values of $0.07[kPa^{-1}]$ and $0.15[kPa^{-1}]$ for C_3 and C_4 plants

respectively. So, D_0 is then found by stating that equation (2.10) the regression of the parameters given in eq. (2.12) at low values of D_s :

$$D_0 = \frac{f_0 - f_{\min}}{a_d}. \quad (2.13)$$

To scale up from leaf to canopy, we adopt a simple big leaf approach. It is assumed that D_s , T_{sk} and C_s adopt a constant value in the whole canopy interior. However, PAR is assumed to decay exponentially as a function of leaf area index. Integrating the plant physiological model over the canopy leads then to an expression for the canopy conductance (Appendix B).

When the environmental variables are known, the internal CO_2 concentration can be calculated with equation (2.10). A_g is then calculated with the plant physiological model. Subsequently, $g_{c,w}$ is found using expression (2.11) as scaled up from leaf to canopy (see Appendix B). The parameter values of our model are listed in Table 2.1.

2.4 Soil moisture stress

Most vegetative canopies suffer from soil moisture stress during dry spells. The influence of this stress on the canopy conductance is very complex, and a full discussion is beyond the scope of this study. However, it appears that the sum of all effects reduces the gross assimilation rate (J. Goudriaan 1999, personal communication). This can be formulated as:

$$A_g = A_g^* f(\bar{w}). \quad (2.14)$$

Here, A_g^* denotes the unstressed gross assimilation rate; $f(\bar{w})$ is a function of \bar{w} ranging from 1 (for plants not suffering from moisture stress) to 0 (for wilting plants).

Cox et al. (1999a) assume that A_g reduces linearly with decreasing soil moisture content:

$$A_g = A_g^* \beta(\bar{w}), \quad (2.15)$$

with $\beta(\bar{w})$ given by:

$$\beta(\bar{w}) = \max \left(0, \min \left(1, \frac{\bar{w} - WP}{FC - WP} \right) \right). \quad (2.16)$$

Here, FC and WP are the soil moisture content at field capacity and at permanent wilting point, respectively. However, if \bar{w} is close to field capacity plants generally do not react linearly to soil moisture stress (Feddes et al. 1978). Using a linear function would then lead to an underestimation of the photosynthetic rate. Consequently, the

latent heat flux density is underestimated (Wang and Leuning 1998).

Calvet et al. (1998) used another approach. They modified the mesophyll conductance (see Appendix A) with a linear soil moisture content response function:

$$g_m = g_m^* \beta(\bar{w}). \quad (2.17)$$

where g_m^* is the unstressed mesophyll conductance and g_m is the stressed conductance. The modified value of g_m is then used to calculate A_g and hence $g_{c,w}$. This formulation behaves properly when \bar{w} is near field capacity. However, g_m^* is, typically, larger for C_4 than for C_3 plants. Therefore, this procedure implies that C_4 plant conductances are less reduced than C_3 plant conductances. This is not confirmed by measurements (Cox et al. 1999a).

To get an expression that behaves properly in wet conditions and is equivalent for both C_3 and C_4 plants, we adopt a quadratic for $f(\bar{w})$:

$$A_g = A_g^* (2\beta(\bar{w}) - \beta^2(\bar{w})). \quad (2.18)$$

Here, $\beta(\bar{w})$ given by relation (2.16). This function describes a smooth transition of A_g for values of \bar{w} larger than FC for which $f(\bar{w}) = 1$.

In analogy with the formulation found for the physiological-based approach, $f_5(\bar{w})$ in the empirical-statistical approach is also given by relation (2.18). Hence,

$$f_5(\bar{w}) = 2\beta(\bar{w}) - \beta^2(\bar{w}). \quad (2.19)$$

This expression completes the set of expressions given in section 2.3.2.

Stewart and Verma (1992) and Cox et al. (1999a) assume that the canopy conductance is an exponential function of \bar{w} . This function is similar to f_5 given above, but requires one extra parameter to be specified. Some modellers (Mahfouf et al. 1995) assume that f_5 decreases linearly as a function of the soil matrix potential. However, experiments show that plants react on soil moisture content rather than on matrix potential (Gollan et al. 1986).

To obtain $f(\bar{w})$ a root zone averaged soil moisture content is needed: $\langle \bar{w} \rangle$. In this study we follow Van den Hurk et al. (2000) and calculate it as:

$$\bar{w} = R_1 w_1 + R_2 w_2 + R_3 w_3 + R_4 w_4.$$

Here, w_1 is the mean soil moisture content in the upper 0.07 m of the soil, w_2 is the mean soil moisture content in the next 0.21 m, w_3 is the mean soil moisture content in the next 0.72 m whereas w_4 refers to the mean soil water content below 1 m. R_1 - R_4 specify the fraction of roots in each layer.

Table 2.2: Parameter values of the surface energy budget model

parameter	FIFE-KANSAS	HAPEX-Mobilhy	Cabauw
a [-]	0.18	0.20	0.25
<i>vegetation fraction</i> [-]	0.85	0.9	0.86
LAI [-]	2.	3.	2.
ϵ	0.98	0.98	0.98
z_r [m]	2.	2.	20.
z_{0m} [m]	0.1	0.07	0.15
z_h [m]	0.0001	0.007	0.0001
$g_{min,w}$ [mm s ⁻¹]	0.25	0.25	0.25
FC [-]	0.38	0.32	-
WP [-]	0.17	0.15	-
R_1 [-]	0.27	0.24	-
R_2 [-]	0.37	0.41	-
R_3 [-]	0.27	0.31	-
R_4 [-]	0.09	0.04	-

2.5 Results

When the incoming short wave and longwave radiation densities and soil heat flux density are known, the surface energy budget can be solved to obtain the skin temperature. An explicit expression for the surface skin temperature can be obtained. Therefore, $g_{c,w}$ and g_a are evaluated at the surface skin temperature of the previous time step, while $q^*(T_{sk})$ and $\epsilon\sigma T_{sk}^4$ are linearised by means of a Taylor series' expansion around their values at the previous time step. The resulting skin temperature is then used to estimate the latent and sensible heat flux density. In this study we are primarily interested in the canopy latent heat flux density. Therefore, rainy days and two days following a rainy day are excluded from the analysis. Furthermore, we only use data obtained between 10h00 and 18h00 local time (i.e. 16h00 to 24h00 UTC for FIFE-KANSAS and 9h00 to 17h00 UTC for HAPEX-Mobilhy and Cabauw). For the considered experiments the bare soil fraction is 0.15 or smaller. Thus, flux densities from this fraction constitute only a very small part of the total flux densities. The bare soil evaporation is, therefore, neglected.

Table 2.3: Parameter values of the Jarvis-Stewart approach

experiment	$g_{\max,w}$ [mm s ⁻¹]	a_1 [W m ⁻²]	a_2 (-)	a_3 [K ⁻²]
FIFE-KANSAS (<i>a priori</i>)	12.3	263	0	0
HAPEX-Mobilhy (<i>a priori</i>)	6.9	263	0	0
Cabauw (<i>a priori</i>)	11.2	263	0	0

2.5.1 FIFE-KANSAS

At the FIFE-KANSAS site the vegetation consists primarily (about 80%) of tall, C₄ prairie grass (Stewart and Verma 1992). By comparing incoming and outgoing short wave radiation we find that $a = 0.18$ between May and October 1987. The effective roughness length for momentum was approximated as 0.19 m by Betts and Beljaars (1993). The latter found a value of 0.01 m for z_h . However, they derived this value from the whole data set, including wet vegetation situations. We find that a value of 0.0001 m (0.1 mm) works much better in our calculations for either approach (De Rooy and Holtslag 1999). This value is surprisingly low, but is consistent with other studies (Beljaars and Holtslag 1991; Holtslag and Ek 1996). Famiglietti et al. (1992) investigated the soil in the FIFE-KANSAS area. From their results we find that FC is 0.32, while WP is set to a value of 0.15 (Table 2.2).

The former parameters are site-specific. For the parameters R_1 to R_4 and the LAI we adopt the values of the ECMWF ERA40 global database (Van den Hurk et al. 2000). Thus, for tall grass the LAI is set to 2 and R_1 is 0.27, R_2 is 0.37, R_3 is 0.27 and R_4 is 0.09. As estimates for the JS approach parameters values for tall grass are adopted, (Table 2.3, see also Table 2 in Van den Hurk et al. 2000). For the $A_g - g_{c,w}$ approach parameters we take the default values for C₄ plants (Table 2.1).

In Table 2.4 results are given for both approaches. It can be seen that the JS approach severely overestimates the latent heat flux density (Table 2.4, upper line). The $A_g - g_{c,w}$ approach performs better (Table 2.4, second line). A detailed study reveals that the canopy conductance response to radiation density appears to be well represented by both approaches (not shown). In Figure 2.2a to Figure 2.2c, the canopy conductance is given as a function of the vapor pressure deficit for the JS approach, an updated JS approach and for the approach based on plant physiology. It can be seen that the JS approach overestimates the canopy conductance in dry conditions. As shown in Figure 2.2b, the data suggest a value of 0.35 [kPa⁻¹] for a_2 . From Figure

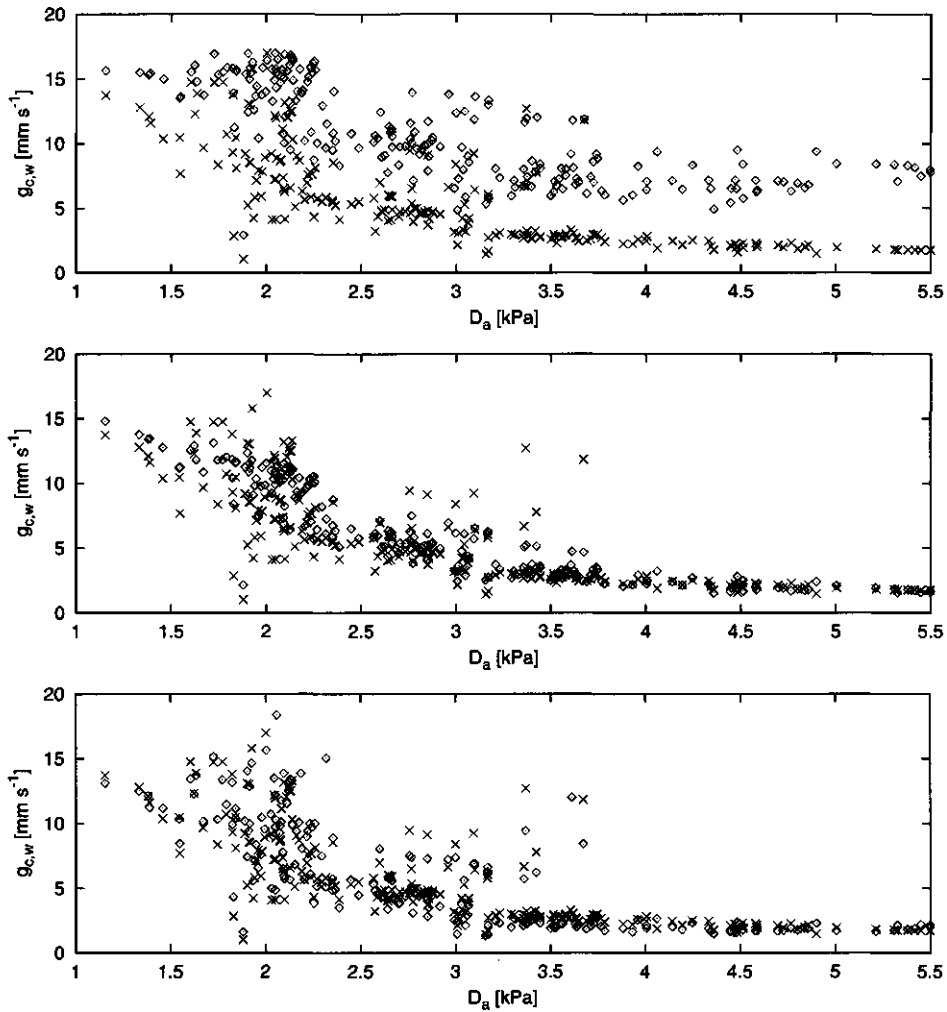


Figure 2.2: Measured (crosses) and modelled (diamonds) canopy conductance values as a function of the vapor pressure deficit at screen level for the FIFE-KANSAS area: canopy conductance calculated with the JS approach with *a priori* chosen parameters (upper panel), with the JS approach with $a_2 = 0.35$ kPa⁻¹ (middle panel) and the $A_g - g_{c,w}$ approach (lower panel).

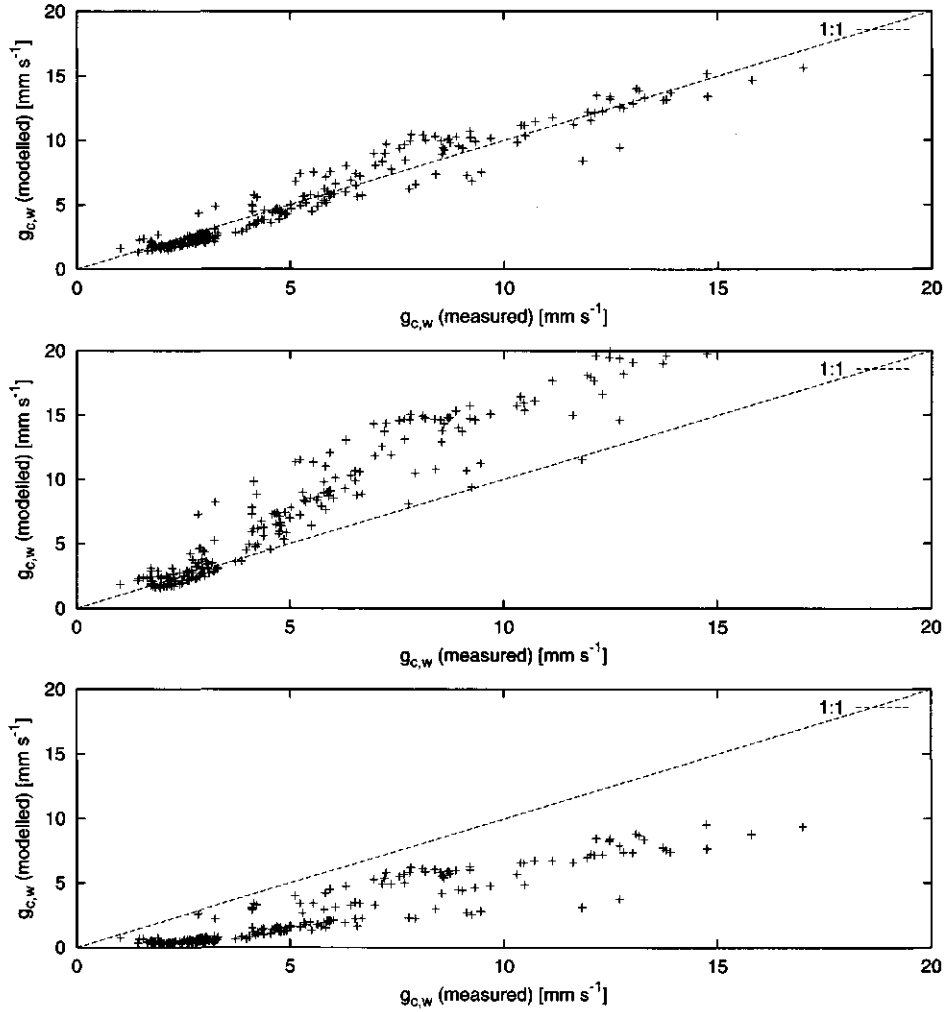


Figure 2.3: Modelled versus measured canopy conductance for the standard $A_g - g_{c,w}$ approach (upper panel), the $A_g - g_{c,w}$ approach with PAR assumed to be absorbed uniformly through the canopy (middle panel) and the standard $A_g - g_{c,w}$ with soil moisture assumed to affect the canopy conductance linearly (lower panel).

Table 2.4: Statistics for the observations obtained during the FIFE-KANSAS campaign

model	bias $_{\lambda E}$ [W m $^{-2}$]	bias $_{R_n}$ [W m $^{-2}$]	bias $_H$ [W m $^{-2}$]	SD $_{\lambda E}$ [W m $^{-2}$]	SD $_{R_n}$ [W m $^{-2}$]	SD $_H$ [W m $^{-2}$]
JS	102.8	47.0	-53.3	64.2	40.5	61.3
$A_g - g_{c,w}$	-8.3	21.2	31.5	58.0	44.6	43.9
$A_g - g_{c,w}$ (big leaf)	42.9	32.2	-8.7	77.9	46.2	57.2
$A_g - g_{c,w}$ (lsm)	-65.0	8.8	76.0	57.6	44.3	48.0
$A_g - g_{c,w}$ (csm)	26.0	29.0	4.8	58.4	42.9	48.7

2.2c is appears that the $A_g - g_{c,w}$ approach gives a better response of the stomata to dry conditions, though the canopy conductance is slightly underestimated in very dry conditions.

Assuming that the canopy absorbs the incoming short wave radiation uniformly, would simplify the plant physiological model. However, as shown in Figure 2.3a and Figure 2.3b, the resulting 'big leaf' approach overestimates the canopy conductance, in comparison with the original approach. Hence, the latent heat flux density is also overestimated with the 'big leaf' approach (Table 2.4, third line). Note that the 'big leaf' approach predicts the sensible heat flux density well. The bias is small. This is caused by compensating errors. The positive bias in the net radiation is relatively insensitive to the canopy conductance. Hence, estimating a too large latent heat flux density, can then lead to low biases in the sensible heat flux density. However, the latent heat flux density is most sensitive to the canopy conductance and therefore, the latent heat flux density is most appropriate to evaluate the performance of the different methods. Here, K_x is the extinction coefficient of the photosynthetically active radiation as a function of LAI. For realistic values of this parameter the $A_g - g_{c,w}$ approach appears to be rather insensitive to the exact value of K_x . A value of 0.6 is found to be optimal.

We also study the soil moisture response. Using the popular linear soil moisture (lsm) response [by Cox et al. (1999a)] introduced for the $A_g - g_{c,w}$ leads to underestimations of the canopy conductance (Figure 2.3c) and consequently of the latent heat flux density (Table 2.4, fourth line). With Calvet's soil moisture (csm) response function the approach slightly overestimates the latent heat flux density (Table 2.4, last line). Note that the sensible heat flux density (Table 2.4, last line) is predicted

best with Calvet's soil moisture response. As with the 'big leaf' approach, this is caused by compensating errors.

2.5.2 HAPEX-Mobilhy

The vegetation at the HAPEX-Mobilhy site consists of soybean, an agricultural crop. The parameters used to solve the SEB are listed in Table 2.2. Here, a is estimated as 0.2 during the whole year. z_{0m} is approximated as 0.06 m in June (Shao and Henderson-Sellers 1996). For z_h we adopt a value of 0.006 m, in accordance with Shao and Henderson-Sellers (1996). Following Mahfouf et al. (1995) FC is set to 0.32, while for WP we adopt a value of 0.15. These values seem to be reasonable for a loamy soil (Soet et al. 2000).

The LAI and R_1 to R_4 are taken from the ECMWF ERA40 global database (Van den Hurk et al. 2000). For an agricultural crop the LAI is 3, R_1 is 0.24, R_2 is 0.41, R_3 is 0.31 and R_4 is 0.04. The parameters of JS approach are taken from Van den Hurk et al. (2000). They are given in Table 2.3. Soybean is a C_3 plant. The $A - g_{c,w}$ approach parameters are valued accordingly.

From the bias given in Table 2.5 (upper two lines) it can be seen that the JS approach underestimates the latent heat flux density. On the other hand, the $A_g - g_{c,w}$ approach overestimates the latent heat flux density. The $SD_{\lambda E}$ of the JS approach is, however, smaller. It appears (see Figure 2.4a) that the large $SD_{\lambda E}$ of the $A_g - g_{c,w}$ approach results from an overestimation of the latent heat flux density at the end of the afternoon. Note that this overestimation coincides with an overestimation of the net radiation (Figure 2.4b). This overestimation is apparent for both approaches. An analysis of the incoming longwave radiation density revealed that it is unrealistically large in the end of the afternoon. The results suggest that the $A_g - g_{c,w}$ approach is more consistent.

The consistency of both approaches is investigated further. Therefore, in Figure 2.5 the evaporative fraction (the fraction of the available energy used for the latent heat flux density) is plotted during the day. It can be seen that the JS approach underestimates the evaporative fraction during the entire day. The $A_g - g_{c,w}$ approach slightly underestimates the morning evaporative fraction. It overestimates the evaporative fraction at the end of the afternoon. The $A_g - g_{c,w}$ is, indeed, more consistent. Furthermore, it provides the partitioning of available energy into sensible and latent heat flux densities better. The underestimation of the latent heat flux density by the JS approach leads to large overestimations of the sensible heat flux density (Table 2.5,

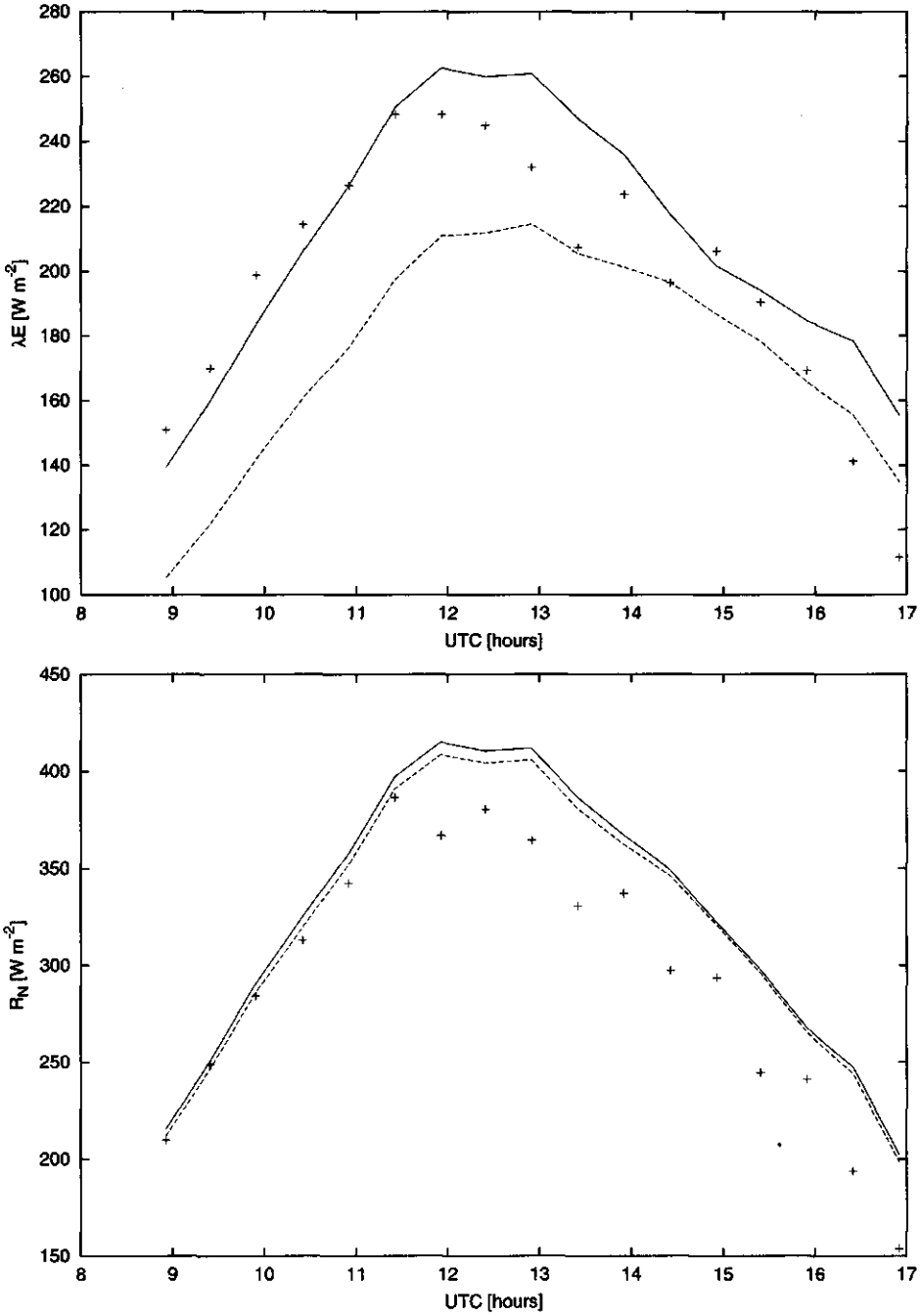


Figure 2.4: The mean of the latent heat flux density (upper panel) and the net radiation (lower panel) during the day for the HAPEX-Mobilhy experimental site: measurements (pluses), modelled with $A_g - g_{c,w}$ model (solid lines) and modelled with JS approach with *a priori* chosen parameter values (dashed lines).

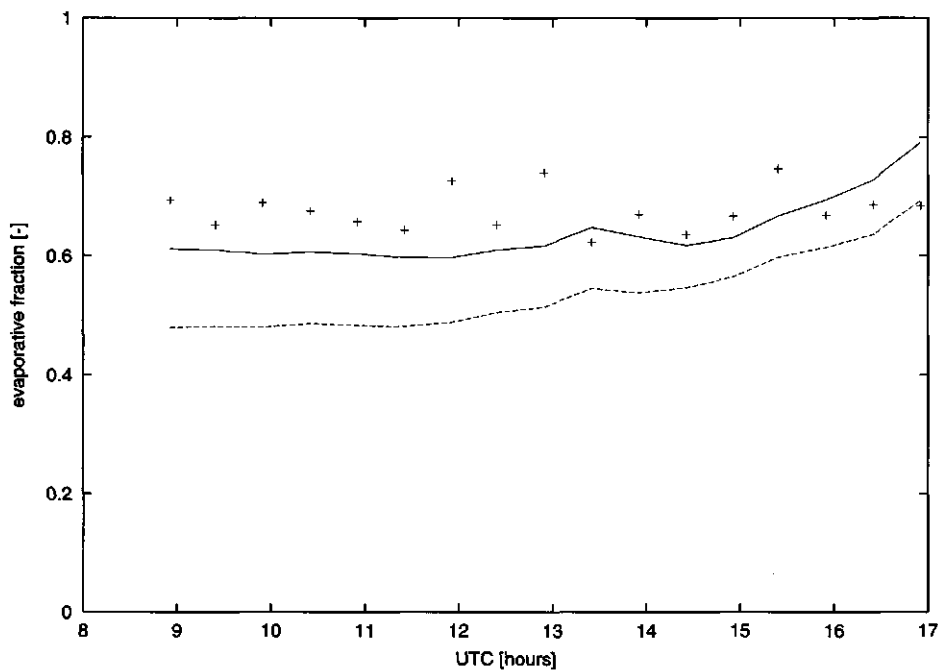


Figure 2.5: Evolution of the mean evaporative fraction during the day at the HAPEX-Mobilhy site: measurements (pluses), modelled with $A_g - g_{c,w}$ approach (solid lines) and the JS approach with *a priori* chosen parameter values (dashed lines).

Table 2.5: Statistics for the observations obtained at the Caumont Soybean site during the HAPEX-Mobilhy experiment in 1986

model	bias $_{\lambda E}$ [W m $^{-2}$]	bias $_{R_n}$ [W m $^{-2}$]	bias $_H$ [W m $^{-2}$]	SD $_{\lambda E}$ [W m $^{-2}$]	SD $_{R_n}$ [W m $^{-2}$]	SD $_H$ [W m $^{-2}$]
JS	-24.7	24.0	49.2	61.6	42.6	43.5
$A_g - g_{c,w}$	10.4	28.4	18.5	76.5	43.9	52.1
$A_g - g_{c,w}$ (big leaf)	57.6	35.2	-21.8	84.2	45.2	54.7
$A_g - g_{c,w}$ (lsm)	-32.0	22.5	54.8	87.0	43.0	70.4
$A_g - g_{c,w}$ (csm)	6.1	27.6	22.0	89.3	44.0	66.7

Table 2.6: Statistics for the observations obtained at the Cabauw site in 1987

model	bias $_{\lambda E}$ [W m $^{-2}$]	bias $_{R_n}$ [W m $^{-2}$]	bias $_H$ [W m $^{-2}$]	SD $_{\lambda E}$ [W m $^{-2}$]	SD $_{R_n}$ [W m $^{-2}$]	SD $_H$ [W m $^{-2}$]
JS	7.6	21.6	13.8	24.4	30.8	17.1
$A_g - g_{c,w}$	11.3	22.7	11.1	29.8	31.9	17.9
$A_g - g_{c,w}$ (big leaf)	16.7	24.1	7.2	33.3	32.8	18.4

first line), especially during the morning hours. Convective boundary layer growth depends critically on the sensible heat flux density and using the JS approach in an atmospheric model could lead to too deep and probably too dry convective boundary layers (see e.g. Holtslag and Ek 1996).

The $A_g - g_{c,w}$ approach with linear response to soil moisture underestimates the latent heat flux density (Table 2.5, fourth line). Furthermore, the standard deviation is larger. Calvet's soil moisture response function performs much better (Table 2.5, last line). However, the standard deviation is much larger using Calvet's soil moisture scheme (Table 2.5, last line). As such, the variation of the conductance as a function of soil moisture content is better described by the proposed quadratic response function.

Furthermore, we study whether a 'big leaf' approach leads to good results. However, from the third line in Table 2.5, it becomes clear that using such an approach leads to overestimations of the latent heat flux density. Here, we find that a value of 0.6 is optimal for K_x (defined in Appendix A).

2.5.3 Cabauw

The site at Cabauw consists of a C₃ grass land. The parameters used to solve the SEB are listed in Table 2.2. The albedo is estimated as 0.25 during the whole year. The roughness length for momentum, z_{0m} , is taken as 0.15 m, while for z_h we find a value of 0.0001 m. This value was also used by Viterbo and Beljaars (1995) for this data set.

The LAI is valued 2, in accordance with Van den Hurk et al. (2000). The parameters of JS approach are set a priori and have been taken from Van den Hurk et al. (2000). They are given in Table 2.3. The $A - g_{c,w}$ approach parameters we adopt the default values for C₃ plants (Table 2.1).

The $A_g - g_{c,w}$ approach overestimates the latent heat flux density (Figure 2.6b and Table 2.6, second line). The JS approach performs slightly better (Figure 2.6a and Table 2.6, first line). Both approaches overestimate the net radiation (Table 2.6, upper two lines) and the sensible heat flux density (Table 2.6, upper two lines). The slightly better performance of the JS approach is also reflected in the $SD_{\lambda E}$. It is smaller for the JS approach than for the $A_g - g_{c,w}$ approach (Table 2.6, upper two lines).

The $A_g - g_{c,w}$ approach in which the PAR is assumed to be uniformly absorbed by the canopy provides the best estimates of the sensible heat flux density (Table 2.6, third line). This is caused by the overestimation of the latent heat flux density (Figure 2.6c): the net radiation overestimation is only slightly larger. The big leaf approach, however, does not predict the variation in the sensible heat flux density well. The SD_H is largest for this approach (Table 2.6, third line).

2.6 Discussion and Conclusion

This study deals with the calculation of the canopy conductance for low vegetation in atmospheric models. We focus on an approach that is based on the theory of plant physiology. As such, we simplified the method proposed by Jacobs (1994) and developed a new analytic formulation for scaling up the conductance from leaf to canopy. Moreover, we proposed a function that describes the effect of the soil moisture content on the canopy conductance. For large areas in the world, no detailed information is available. Therefore, parameters were taken from global vegetation maps. Our approach was validated for three observational sites. The vegetation types at these sites are representative for large areas with low vegetation in the world. Furthermore, the proposed approach was compared with the classical Jarvis-Stewart (JS) approach. The parameters of the latter were also estimated from a global vegetation classification.

For the low vegetation sites considered, the parameters of the $A_g - g_{c,w}$ appeared to be robust and general formulations for biomes could be obtained. In fact, a distinction in C_3 and C_4 was sufficient for the involved parameters. However, distinct values had to be specified for the leaf area index and for the root distribution in the soil. Therefore, using the $A_g - g_{c,w}$ does not lead to a reduction of the number of vegetation classes, with respect to the JS approach as suggested by Sellers et al. (1996).

For tall, prairie grass the $A_g - g_{c,w}$ approach performed better than the JS ap-

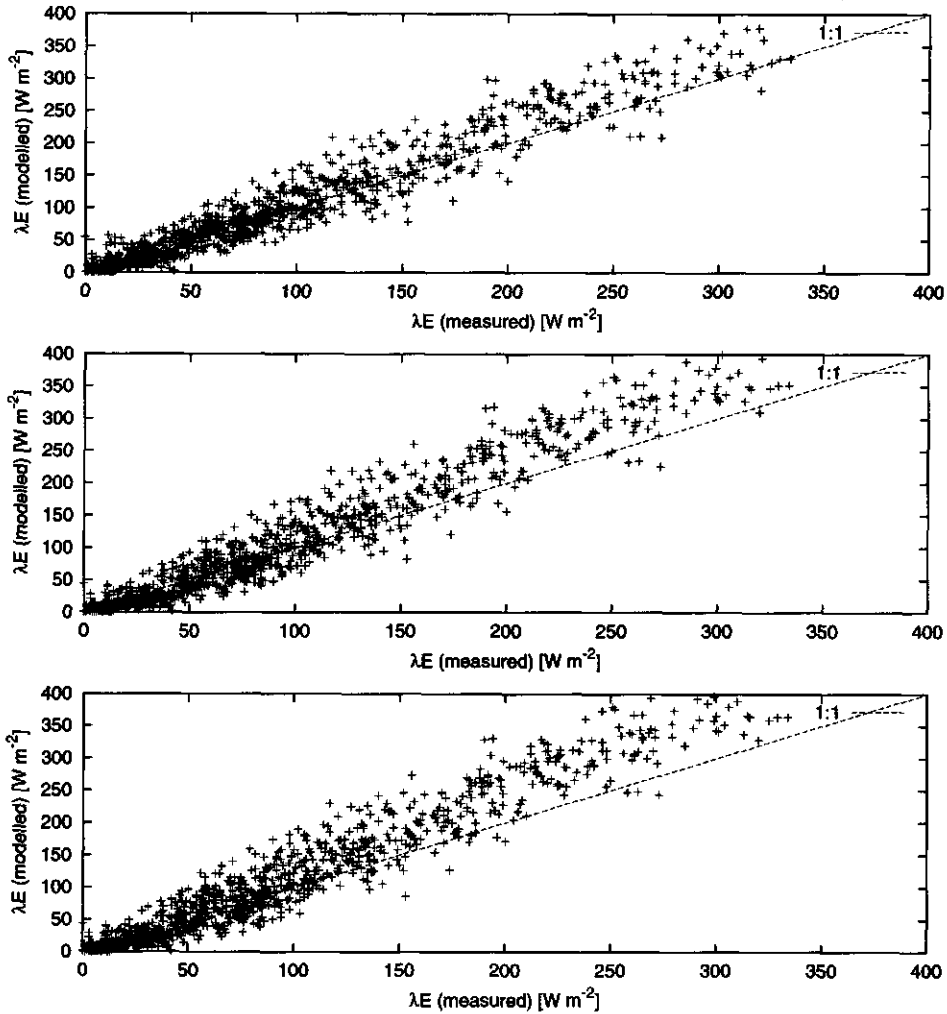


Figure 2.6: Modelled and measured latent heat flux density for the JS approach with *a priori* chosen parameters (upper panel), the $A_g - g_{c,w}$ approach (middle panel) and the $A_g - g_{c,w}$ approach with PAR assumed to be absorbed uniformly in the canopy (lower panel). Results are shown for the Cabauw observational site.

proach. Especially in dry conditions, the physiologically based approach appeared to represent the behaviour of the canopy conductance better. For a soybean crop, both approaches give comparable results. A detailed analysis revealed that the $A_g - g_{c,w}$ approach performs more consistently. It appeared that overestimations of the latent heat flux density coincide with overestimations of the net radiation. As a result, the evaporative fraction was found to be better approximated by the $A_g - g_{c,w}$ approach. Furthermore, the JS approach severely overestimated the sensible heat flux density in the morning. This could lead to too deep and probably too dry boundary layers. For the Cabauw site no large differences were found. Both approaches appeared to work well, though the JS approach provided somewhat better estimates of the latent heat flux density.

Assuming that the photosynthetically active radiation is absorbed uniformly by the canopy (big leaf approach), led to overestimations of the latent heat flux density. In this study it was assumed that PAR decays exponentially as a function of LAI. As such, it was possible to obtain an analytic expression for the canopy conductance. Note that some authors distinguished between direct and diffuse radiation. Here a simpler approach has been adopted, since the approach developed is intended for large scale atmospheric models which radiation schemes do not readily give separate values for direct and diffuse radiation flux densities at the surface.

The quadratic stress function for soil moisture as presented in Section 2.4 led to good estimates for the surface energy flux densities. The popular linear response function gave underestimations of the latent heat flux density. The method proposed by Calvet et al. (1998) gave a low bias for the C₃ soybean crop. However, it gave larger values of the standard deviation. It, therefore, represents the variation of the canopy conductance as a function of the soil moisture worse. Note that Calvet's soil moisture response predicted the latent heat flux density for the FIFE-KANSAS site relatively well. The bias and the standard deviation of the latent heat flux density were only slightly larger than for the quadratic response function.

It should be noted that improvements in the latent heat flux density do not necessarily lead to better results for the net radiation and the sensible heat flux density. Because of compensating errors, frequently a method that performs best for the latent heat flux density, gives worse results for the net radiation and the sensible heat flux density. However, it appeared that the latent heat flux density is most sensitive to the canopy conductance. Therefore, this flux density was primarily used to evaluate the performance of the methods.

Overall, the proposed plant physiological approach with the new soil moisture

content response function, provides satisfactory estimates of the surface energy flux densities. Because this approach is physically based, we recommend to apply this approach for prognostic atmospheric models and for climate impact studies.

Chapter 3

Spatial heterogeneity of the soil moisture content and its impact on the surface flux densities and near-surface meteorology

Material in this chapter is accepted for publication in the *J. Hydrometeor.* with B.J.J.M. van den Hurk and A.A.M. Holtslag as co-authors.

abstract

In this study, it is investigated how lateral variations in the soil moisture content impact the daily and seasonal cycle of the surface flux densities and near-surface meteorology. In agreement with earlier studies, which used less detailed model to describe locally the impact of soil moisture stress on the latent heat flux density, it is found that in wet conditions the use of one uniform volumetric soil moisture content, referred to as bulk approach, gives larger estimates of the latent heat flux density than a distributed approach where the lateral variation in the volumetric soil moisture content is taken into account. In contrast, in dry conditions the bulk approach gives lower estimates of the latent heat flux density. In this study the differences between flux density estimates obtained by both approaches appear even when the developing convective boundary is allowed to feed back on the surface. These differences have important consequences for the seasonal hydrological balance. Especially, for dry climates, the distributed approach predicts a more gradual decrease of the evapotranspiration during the dry season, resulting in a larger cumulative evapotranspiration over the dry season. In this study it is also shown that differences in the estimated surface flux densities lead to differences between the predicted atmospheric specific humidity and the predicted near-surface temperature. Thus, taking account of the spatial heterogeneity of the soil moisture content is a prerequisite for a proper representation of the seasonal hydrological cycle within large-scale atmospheric models.

3.1 Introduction

Because of its importance for a correct simulation of the climate system, the parameterization of the land surface has been a focus of recent research (Viterbo and Beljaars 1995; Henderson-Sellers et al. 1996). In the first generation of land surface models, the soil column was represented as a both horizontally and vertically homogeneous bucket that was filled by precipitation and emptied by runoff and evapotranspiration (Manabe 1969). Later, this model has been replaced by more complex models. Modelers now divide the soil column into multiple soil layers (Viterbo and Beljaars 1995; Soet et al. 2000) and calculate the impact of environmental variables on the latent heat flux density using physically based parameterizations for the canopy conductance. However, despite the improvements in their land surface schemes, large-scale atmospheric models still tend to overestimate the evapotranspiration in the early dry season (Viterbo 1994; Delage and Versegny 1995). As a result, the infiltrated water is released to the atmosphere too quickly and the evapotranspiration is underestimated later in the dry season. In many conditions this leads to a suppression of the humidity of the atmosphere and the precipitation during the dry season (Viterbo 1994; Rowntree 1995).

A next step in the development of land surface models is the introduction of schemes that take account of the spatial heterogeneity of the soil moisture content within the grid cell of a large-scale atmospheric model. Both observations (Owe et al. 1982; Entekhabi and Eagleson 1989) and modeling experiments (Wood 1997; Koster et al. 2000) indicate that on the scale of atmospheric model grid cells, about 50^2 km² or larger, the soil moisture content shows a considerable spatial variation. Often the lateral variation of the soil moisture content is associated with lateral variations in the topography. As a result, they often resist over long time scales, in contrast to lateral variations in the air temperature and specific humidity which mix rapidly due to buoyancy- and shear-driven turbulence (Raupach and Finnigan 1995).

For typical conditions in a moderate climate the latent heat flux density varies with the relative saturation at a point as given schematically in Figure 3.1 (Wetzel and Chang 1987). The relative saturation is here defined as the actual volume of water that is stored in the soil column scaled with the maximal volume of water that can be stored. For values of the soil moisture content lower than the wilting point (WP), the latent heat flux density is minimal. For larger values, the latent heat flux density increases till it reaches its maximum, atmospherically controlled value as the relative saturation gets above the field capacity (FC).

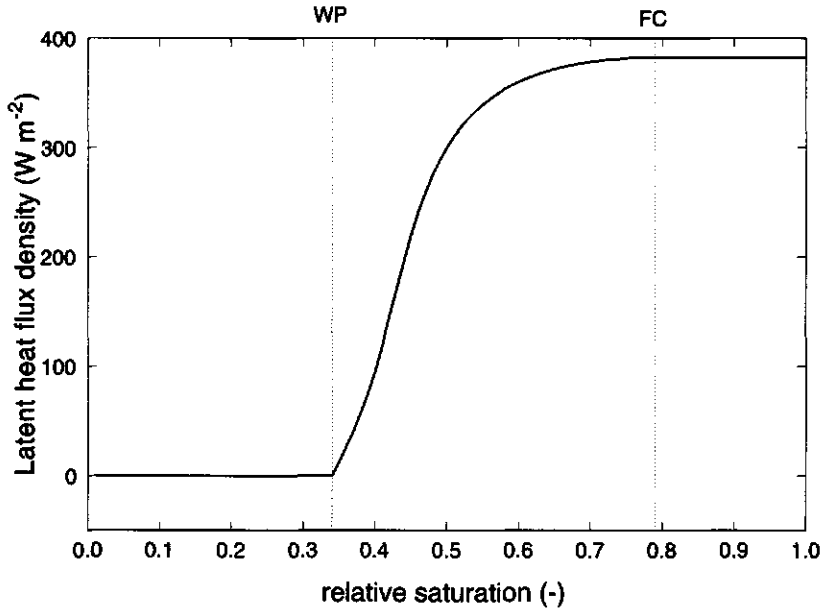


Figure 3.1: Schematic of the local latent heat flux density as a function of the relative saturation.

Wetzel and Chang (1987, 1988) studied the impact of the spatial heterogeneity of the soil moisture content on the horizontally averaged flux densities for grid cells containing subareas which local values of the relative saturation differ from the horizontally averaged relative saturation of the grid cell. Using a normal distribution for the soil moisture content they found that during the wet season, when most of the subareas within the grid cell are above field capacity (Ducharne et al. 2000), the horizontally averaged relative saturation predicts a large grid cell latent heat flux density. However, in the driest subareas the latent heat flux density may still be suppressed. Because the latent heat flux density in the wettest subareas is bound by the maximal value, this suppression in the drier areas leads to a reduction of the average evapotranspiration. In the bulk approach one uniform soil moisture content is used to compute the areally averaged surface flux densities. As a result, in wet conditions a bulk approach gives a larger prediction of the evapotranspiration than a distributed approach which takes account of the horizontal variation in the soil moisture content. During dry conditions the average relative saturation is often near or even below the wilting point and the average soil moisture content suggests a very low grid cell latent

heat flux density. However, in the wetter subareas, the latent heat flux density may still be considerable. As a result, use of the average relative saturation leads to lower estimates of the evapotranspiration in dry conditions, as compared to an approach where the lateral distribution of the soil moisture content is taken into account (Wetzel and Chang 1987, 1988).

Entekhabi and Eagleson (1989), Sivapalan and Woods (1995), and Wood (1997) assumed that for values of the local soil moisture content between WP and FC the actual latent heat flux density at a point in the grid cell could be calculated by multiplying an unstressed, potential, latent heat flux density with a function that depends on the point soil moisture content. To describe the variation of the soil moisture content within the grid cell, they adopted prescribed distributions. By integrating the actual latent heat flux density over all possible values of the soil moisture content within the grid cell, they could successfully obtain expressions relating the horizontally averaged latent heat flux density to the mean soil moisture content of the grid cell. Through variation of the prescribed variance, these authors found that, in accordance with the results of Wetzel and Chang (1987, 1988), an increase of the prescribed horizontal variation in the soil moisture content leads to a decrease of the latent heat flux density when the averaged soil moisture content is below a critical value and a decrease of the latent heat flux density when the soil moisture content is above a critical value.

The main aim of this paper is to show that introduction of prescribed lateral variations in the soil moisture content might lead to better predictions of the surface flux densities and the near-surface temperature and specific humidity in large-scale atmospheric models. Following Sivapalan and Woods (1995) we prescribe the horizontal variation or the relative saturation using the Variable Infiltration Capacity (VIC) model (Wood et al. 1992). This model assumes that at a point within the grid cell the soil column can be described as a bucket. However, it allows for a variable bucket depth throughout the grid cell.

First, we study the impact of the spatial heterogeneity of the soil moisture content using forcings at a reference level near the surface. In contrast to the previous sensitivity studies, we use in this study a detailed model for this exchange including an approach for calculating the canopy conductance which is based in plant physiology. Also, we test whether the discrepancy between the estimates of the latent heat flux density obtained using the distributed and the bulk approach can be addressed by lowering the wilting point and enhancing the field capacity within the bulk approach as suggested by Wetzel and Chang (1987). In addition, we extend the previous stud-

ies by showing that the spatial heterogeneity of the soil moisture content leads to a weaker seasonal cycle of the latent heat flux density. In this study, we use forcings obtained in a wet, moderate climate and a dry Sahelian climate.

Second, we use flux densities obtained by both approaches to force a simple model of the convective boundary layer. We show that even when boundary layer feedbacks are included (Jacobs and De Bruin 1992; Holtslag and Ek 1996), the bulk approach gives considerably different estimates of the surface flux densities, as compared to a distributed approach. In this study, we force the convective boundary layer with flux densities which result from the grid cell flux densities calculated using either the bulk approach and the distributed approach. As such, we extend the studies of Raupach (1993, 1995) and Silberstein and Sivapalan (1995) who studied the extreme case where a dry subarea was located adjacent to a wet area or a crop field next to grass field. Also, we extend the studies by Raupach (1993, 1995) and Sivapalan and Woods (1995) by showing that both in dry and in wet conditions, the soil moisture heterogeneity has an impact on the temperature and the specific humidity in the boundary layer and at 2 m, the height where most synoptic observations are obtained. These are important variables to validate large-scale atmospheric models (Viterbo 1994).

In section 3.2 we describe how the flux densities are calculated for a homogeneous area. In section 3.3 we describe both the distributed and the bulk approach. In section 3.4 both approaches are compared using forcings at a reference height in the surface layer. In section 3.5 we show the implication of allowing spatial variations in the soil moisture content for the seasonal hydrological cycle. Section 3.6 gives the results of the study where the model for the surface energy budget is coupled to a model for the atmospheric boundary layer. Section 3.7 provides a summary and conclusion.

3.2 Calculation of the surface flux densities

For a homogeneous area, the surface energy budget (SEB) reads:

$$(1 - a)K^\downarrow + \epsilon L^\downarrow - \epsilon\sigma T_{sk}^4 = H + \lambda E + G. \quad (3.1)$$

Here, a is the albedo, K^\downarrow is the incoming short wave radiation, ϵ is the emissivity, L^\downarrow is the downwelling long wave radiation, σ is the Stefan-Boltzman constant, T_{sk} is the surface skin temperature, H is the sensible heat flux density, λE is the latent heat flux density and G is the ground heat flux density. λ is the latent heat of vaporization.

In this study, we describe the latent heat flux density, the sensible heat flux density and the ground heat flux density of the canopy using a conductance scheme (Beljaars

and Holtslag 1991; Viterbo and Beljaars 1995):

$$\lambda E = \rho_a \lambda g_a \frac{(q^*(T_{sk}) - q_a)}{1 + g_a/g_{c,w}}, \quad (3.2)$$

$$H = \rho_a c_p g_a (T_{sk} - T_a), \quad (3.3)$$

$$G = \Lambda (T_{sk} - T_1) \quad (3.4)$$

where ρ_a is the air density, g_a is the aerodynamic conductance, z_a is a reference level in the surface layer, T_a is the temperature at z_a , $q^*(T_{sk})$ is the saturated specific humidity at the surface, q_a is the specific humidity at the reference level, $g_{c,w}$ is the canopy conductance to water vapor flow, c_p is the specific heat at constant pressure, Λ is the skin conductivity and T_1 is the temperature of the upper soil. Generally, the aerodynamic conductance is calculated using Monin-Obukhov similarity theory. It is a function of u , the horizontal wind velocity at the reference level, the roughness length for heat, z_h , the roughness length for momentum, z_{om} , the height of the reference level and the stability of the surface layer (Beljaars and Holtslag 1991).

When soil moisture is not limited, the canopy conductance is a function of the incoming short wave radiation, the temperature of the canopy and the specific humidity difference between the leaf interior and the leaf exterior. To model these dependencies, well-validated and robust biophysical models are available. Generally, these models take the canopy conductance to be linearly proportional to the photosynthetic assimilation rate. In this study we use the relations given in the previous chapter, which appear to work well for various sites with low vegetation. The canopy conductance is thus calculated as:

$$g_{c,w} = g_{min,w} LAI + \frac{1.6 (A_m + R_d)}{(1 - f_0) (C_s - \Gamma) \left(1 + \frac{D_s}{\left(\frac{1}{f_0} - 1 \right) \frac{f_0 - f_{min}}{a_d}} \right)} \times \left[LAI - \frac{1}{K_x} \left(E_1 \left(\frac{\mu K_x PAR_t}{A_m + R_d} e^{-K_x LAI} \right) - E_1 \left(\frac{\mu K_x PAR_t}{A_m + R_d} \right) \right) \right],$$

where $g_{min,w}$ is the minimal canopy conductance, LAI is the leaf area index, f_0 is an empirical constant, A_m is the primary production rate, R_d is the dark respiration rate, C_s is the carbon dioxide concentration at the leaf exterior, Γ is the carbon dioxide compensation point, D_s is the difference between the specific humidity inside the plant and the specific humidity at the leaf exterior, f_{min} , and a_d are empirical constants, K_x is the extinction coefficient of the photosynthetically active radiation (PAR) within the canopy, $E_1(x)$ is an exponential integral with argument x , μ is the light use efficiency, and PAR_t is the incoming flux density of PAR at the top of the

canopy. Γ , and f_{\min} are calculated using respectively Eq. A.4 and Aq A.5. A_m , and R_d result from biochemical models and calculated using Eq. A.3 and A.6. The latter vary as a function of temperature. For temperature lower than the optimum temperature, about 298 K, they increase with increasing temperature, whereas for temperatures above the optimum temperature they decrease with increasing temperature.

Vegetative canopies suffer from soil moisture stress during dry spells. Most modelers adopt a traditional linear response function to describe the soil moisture stress experienced by plants when the soil moisture content is below its value at field capacity and above its value at wilting point (Viterbo and Beljaars 1995). This simple function reads:

$$g_{c,w} = g_{c,w}^* f(w), \quad (3.5)$$

with $f(w)$ is the vegetation moisture status, defined by:

$$f(w) = \max \left(0, \min \left(1, \frac{w - WP}{FC - WP} \right) \right) \quad (3.6)$$

Here, $g_{c,w}^*$ is the unstressed canopy conductance, w is the local soil moisture content, FC is the field capacity and WP is the wilting point.

Various authors (see previous chapter) argued that Eq. 3.5 overestimates the moisture stress for values of the relative saturation which are slightly below the field capacity. In the previous chapter we show that for homogeneous areas this stress can be well described assuming that the canopy conductance decreases quadratically as a function of decreasing soil moisture content, when the soil moisture content is below its value at field capacity and above its value at wilting point:

$$g_{c,w} = g_{c,w}^* [2f(w) - f(w)^2], \quad (3.7)$$

where $f(w)$ is given by relation 3.6. The value of the soil moisture content at wilting point and at field capacity depend on soil type (Soet et al. 2000). The soil type varies from a coarse-textured sand soil for which FC and WP are small, to a very fine-textured clay soil for which FC and WP are large. In the following section, the soil moisture content used in relation 3.5 and 3.7 is described as a relative saturation, the ratio of the actual soil moisture content over its saturated value. FC and WP will be scaled accordingly.

For a homogeneous area, the surface flux densities can be computed when the soil moisture content, the temperature of the upper soil and the meteorological conditions at the reference level are known. Therefore, first Eqs. 3.1 to 3.4 are combined with

either relation 3.5 or 3.7. Then, the resulting equation is solved for the surface temperature. Finally, the surface energy flux densities are calculated using the resulting surface temperature and Eqs. 3.2 to 3.4. In this study we adopt values for the input parameters that are typical for a site of low C_3 vegetation: $a = 0.2$, $\epsilon = 1$, $z_{0m} = 0.02$ m, $z_h = 0.002$ m, $LAI = 2$, and $\Lambda = 10 \text{ Wm}^{-2}$ (Soet et al. 2000). For the parameters of the physiological model of a C_3 plant we refer to Table 2.1.

3.3 Distributed approach versus the bulk approach

3.3.1 Variability of the relative saturation

To describe the spatial variation of the relative saturation w within the grid cell of a large-scale atmospheric model, we adopt the VIC model described by Wood et al. (1992). Within this framework, the infiltration capacity, denoted by s , is defined as the maximal volume of water that can be stored in the soil column below a surface of unit area. In areas where s is small, the soil can contain only a small volume of water before it is completely saturated. The actual volumetric content, denoted by v is defined as the volume water per unit area that is stored in the soil column. The actual volumetric soil moisture content varies between 0 when the soil column is completely dry to s when the soil column is saturated. At each point the ratio of the actual volume of water stored per unit area and the maximal volume that can be stored per unit area defines the relative saturation at each point within the grid cell: $w = \frac{v}{s}$.

In this study we assume that the grid cell can be divided in two parts. In one part the actual volumetric soil moisture content equals the maximal volume of water that can be stored per unit area. This is the saturated part where the relative saturation is 1. In the unsaturated part, the actual volume of water stored per unit area, is lower than the maximal volume of water that can be stored per unit area. This part is the unsaturated part.

In the VIC model the infiltration capacity is considered as a random variable of which the cumulative distribution, denoted by F_s , can be described using the Xinanjiang model (Zhao et al. 1990; Wood et al. 1992):

$$F_s = 1 - \left(1 - \frac{s}{s_{\max}}\right)^\beta, \quad (3.8)$$

where s_{\max} is the extremum of s within the grid cell, and β is a parameter describing the spatial heterogeneity in s .

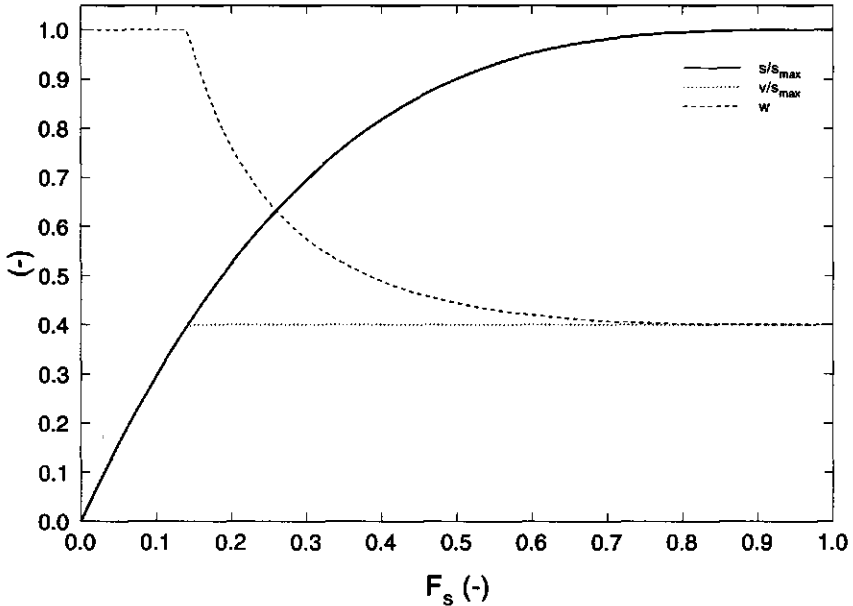


Figure 3.2: The cumulative distribution of s/s_{max} for $\beta = 0.3$ and the accompanying distribution of v/s_{max} for a value of 0.4 times s_{max} for v_{unsat} . Also shown is the distribution of the relative saturation.

Kalma et al. (1995) analyzed measurements obtained with 44 neutron moisture meter tubes which were inserted along transects located within the Lockyersleigh catchment in Australia between January 1987 and July 1990. The tubes each had a length that roughly equalled the depth of the soil between the surface and the bed rock. As an approximation to the local infiltration capacity, Kalma et al. (1995) used the difference between the maximal and the minimal volumetric moisture content obtained during the entire observational period. Indeed, they found that the distribution over the area of the calculated infiltration capacities could approximately be described by the Xinanjiang model. A confirmation of their results was given by Sivapalan and Woods (1995) who analyzed soil depths that were obtained during a drilling campaign in Western-Australia. They found that the cumulative frequency distribution of the depth of the soil that was most active in the transfer of water through the catchment, agreed well with the Xinanjiang distribution given by Eq. 3.8.

In regions where the long-term precipitation is uniform, the soil column is recharged

at the same rate throughout the grid cell. As a result, the volumetric soil moisture content is approximately uniform in the unsaturated part of the grid cell. For subareas within this part we adopt therefore a constant value for v : v_{unsat} . In the saturated areas v is bound by its maximal value and here v equals s . A schematic picture of the distribution of s and v is given Figure 3.2. It shows the cumulative distribution of s/s_{max} for $\beta = 0.3$, the distribution of v/s_{max} for a value of 0.4 times s_{max} for v_{unsat} , and the resulting distribution of the relative saturation. In the saturated areas, the relative saturation is equal to 1. When s increases, the relative saturation decreases toward a minimal value for the point where s equals s_{max} .

The assumption that the actual volume of water stored per unit area, v , is constant in the unsaturated part has been tested by Kalma et al. (1995). Using soil moisture measurement obtained in an Australian catchment, they found that the actual volume of water stored in the soil column per unit area is indeed approximately constant in the unsaturated areas. Only in very wet conditions, they found that the total volume of water in storage was somewhat higher in areas where the soil column is deeper, i.e. in areas where s is large. However, the observed variation in v was minor compared to the variation in s .

3.3.2 The distributed approach

In the distributed approach we take account of the horizontal variation of the relative saturation over the grid cell. Because the relative saturation varies over the grid cell, the soil moisture stress experienced by plants varies over the grid cell. In areas where s is small, the soil is wet and the soil moisture stress is small. In contrast, in areas where s is large, the soil is usually much drier and the plants experience a much larger stress. In the distributed approach, we appreciate the impact of the resulting differences in the relative saturation on the flux densities. Because the canopy conductance and the surface flux densities depend non-linearly on the local relative saturation, it is not possible to calculate the grid cell averaged surface flux densities analytically from the distribution of the relative saturation. We use therefore a numerical approach and impose a subgrid over our grid cell. For that purpose, we divide the values of s which range from 0 to s_{max} into a number of intervals and assign the average value of s , denoted as s_i of each interval to a subarea. Then, for each subarea we calculate the relative saturation, denoted by w_i . For the subareas located in the saturated part, the relative saturation equals 1, whereas for subareas located in the unsaturated part, it is calculated as: $w_i = v_{\text{unsat}}/s_i$. For each subarea the calculated relative saturation is

used to compute the soil moisture stress using either Eq. 3.5 or 3.7. Then, the surface energy budget is solved for each subarea separately to obtain the surface temperature and the resulting latent heat flux density and sensible heat flux density. Afterwards, the subarea flux densities, denoted by f_i are aggregated to obtain the averaged grid cell flux density, F_{dist} :

$$F_{\text{dist}} = \sum_i (F_s(s_{i,\text{max}}) - F_s(s_{i,\text{min}})) f_i, \quad (3.9)$$

where $s_{i,\text{max}}$ and $s_{i,\text{min}}$ denote respectively the maximal and the minimal value of s within the interval associated with the subarea with index i .

3.3.3 The bulk approach

Though the distributed approach is widely used to calculate the surface runoff (Dümenil and Todini 1992) most modelers adopt a bulk approach to calculate the average grid cell surface flux densities. In the bulk approach, the relative saturation is assumed to be uniform over the grid cell. The grid cell relative saturation then equals the actual total water volume stored within the entire grid cell, W , divided by the maximal volume of water that can be stored in the entire grid cell, W_{max} . The actual total water volume per unit area in the grid cell can be calculated by integrating the local volumes of water per unit area over the grid cell. The total volume of water per unit area stored in the grid cell is found by integrating separately over the saturated part of the grid cell where the volume of water stored per unit area is s and over the unsaturated part where the volume of water stored per unit areas equals v_{unsat} :

$$\begin{aligned} W &= \int_0^{v_{\text{unsat}}} \beta \frac{s}{s_{\text{max}}} \left(1 - \frac{s}{s_{\text{max}}}\right)^{\beta-1} ds + \frac{v_{\text{unsat}}}{s_{\text{max}}} \int_{v_{\text{unsat}}}^{s_{\text{max}}} \beta \left(1 - \frac{s}{s_{\text{max}}}\right)^{\beta-1} ds \\ &= \frac{s_{\text{max}}}{\beta+1} \left(1 - \left(1 - \frac{v_{\text{unsat}}}{s_{\text{max}}}\right)^{\beta+1}\right). \end{aligned} \quad (3.10)$$

The maximal volume of water than can be stored in the grid cell is obtained when the entire grid cell is saturated. It can be found by setting v_{unsat} to s_{max} , i.e. even the areas that can store the largest volume of water are saturated; the equation for W_{max} reads:

$$W_{\text{max}} = \frac{s_{\text{max}}}{\beta+1}. \quad (3.11)$$

In the bulk approach the grid cell is taken as one homogeneous patch with the relative saturation given by W/W_{max} . Consequently, the surface flux densities of the grid cell can directly be calculated when the meteorological conditions at the reference level and the temperature of the upper soil are known.

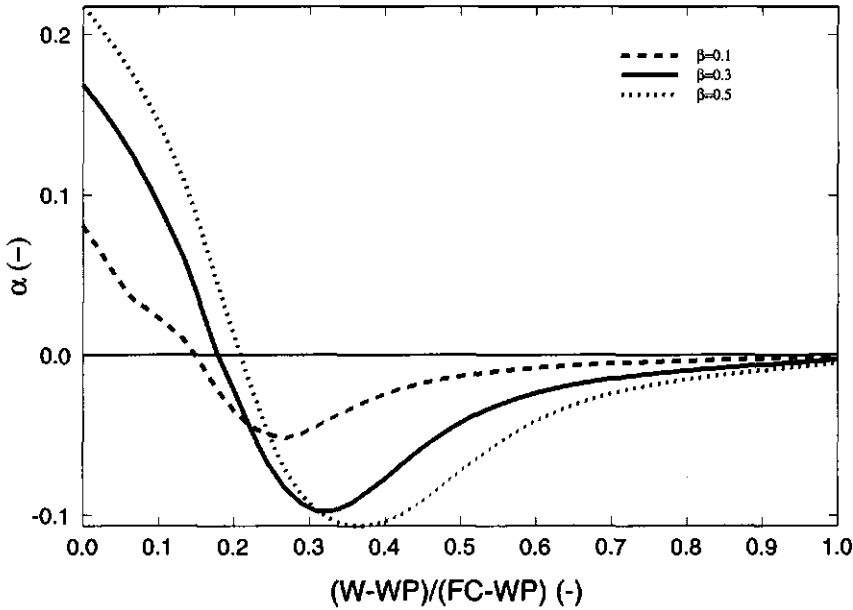


Figure 3.3: α as a function of the grid cell canopy water status for $\beta = 0.1$ (dashed), $\beta = 0.3$ (solid) and $\beta = 0.5$ (dotted).

3.3.4 Sensitivity study using fixed forcings

In this section we study the impact of the soil moisture heterogeneity on the surface heat flux densities using fixed (climatological) forcings at a reference level in the surface layer. First, we show the impact of the lateral variation in the soil moisture on the surface heat flux densities for different values for β and a medium-textured loam soil. The latter is the typical soil type for large areas in the world (Soet et al. 2000; Viterbo and Beljaars 1995). Next, we evaluate the influence of using a linear response function for the soil moisture stress rather than a quadratic one. Last, we test whether lowering the wilting point and enhancing the field capacity within the bulk approach reduces the discrepancy between the estimates of the latent heat flux density obtained by both approaches. In this section, we use the synoptic observation level of 2 m to force both the distributed and the bulk model. We adopt values that are typical for daytime conditions in a moderate climate: $K^{\downarrow} = 900 \text{ Wm}^{-2}$, $L^{\downarrow} = 300 \text{ Wm}^{-2}$, $T_a = 298 \text{ K}$, $q_a = 11.7 \text{ g kg}^{-1}$ and $T_1 = 291 \text{ K}$.

We compare both estimates of the latent heat flux density as a fraction of the available energy at the surface. Because the net radiation is dependent on the esti-

mated surface temperature, we use as a reference the isothermal net radiation. This is the net radiation that would occur if the surface layer is isothermal and the surface temperature would be equal to the air temperature (Monteith 1981). To compare both approaches we introduce a quantity called α that is defined as the ratio of the difference between both estimates of the latent heat flux density and the isothermal net radiation:

$$\alpha = \frac{\lambda E_{\text{dist}} - \lambda E_{\text{bulk}}}{(1-a)K^{\downarrow} + \epsilon L^{\downarrow} - \epsilon \sigma T_a^4} \quad (3.12)$$

For different values of β , Figure 3.3 gives α as a function of the grid cell vegetation moisture status, defined by $(W-WP)/(FC-WP)$. Here, we use a value of 0.79 for FC and a value of 0.34 for WP which refer to a medium-textured loam soil (Soet et al. 2000). For the values of the relative saturation below the wilting point, the latent heat flux density calculated using the bulk approach is minimal. In contrast, in this range the latent heat flux density calculated with the distributed approach increases approximately linearly with increasing grid cell relative saturation. In agreement with the results of Wetzel and Chang (1987, 1988), Entekhabi and Eagleson (1989), and Wood (1997) Figure 3.3 shows that the distributed approach gives larger estimates of the latent heat flux density in dry conditions, whereas it gives lower estimates of the latent heat flux density in wet conditions. The maximal difference between both approaches is about 9.0% of the isothermal net radiation (45.9 Wm^{-2}) when β equals 0.1 and the area is relatively flat. However, the maximal difference increases to about 21% of the isothermal net radiation (110 Wm^{-2}) when β equals 0.5 and the orographic variance is large.

For both the linear response function and the quadratic response function, we plot in Figure 3.4 α as a function of the grid cell canopy water status. Here, FC and WP are taken as respectively 0.79 and 0.34 and β is set at 0.3. The quadratic response function predicts less moisture stress than the linear response function, when the local soil moisture content is between the wilting point and the field capacity. As a result, the quadratic response gives larger flux densities for subareas that are above the wilting point. Consequently, the difference between the distributed and the bulk approach is larger for the quadratic response function. However, when the grid cell relative saturation is above the wilting point, the estimates of the latent heat flux obtained using the bulk approach increase rapidly with the quadratic response function. In contrast, the linear response function predicts a more gradual increase of the bulk latent heat flux density. As a result, the difference between the distributed and the bulk approach decreases more sharply with the quadratic response function (see Figure 3.4).

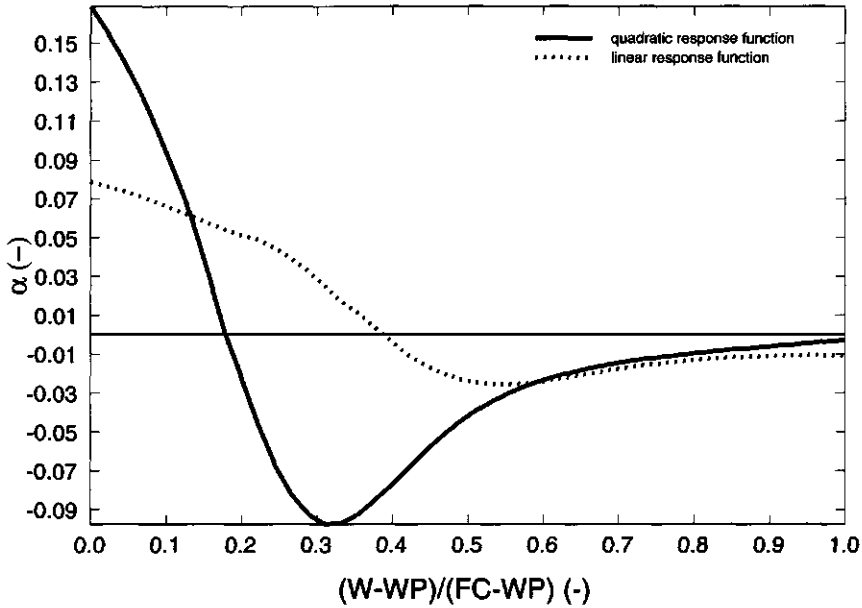


Figure 3.4: α as a function of the grid cell canopy water status for the reference quadratic response function (solid) and a popular linear response function (dotted).

Wetzel and Chang (1987) addressed the discrepancy between the horizontally averaged latent heat flux density calculated using a bulk approach and a distributed approach by lowering the wilting point and enhancing the field capacity within the bulk approach. For the normal distribution they used to prescribe the lateral variation of the soil moisture content, they found that use of these effective values for WP and FC gave estimates by the bulk approach that were in close agreement with the estimates by the distributed approach. Later, this approach was used in the PLACE model (Wetzel and Boone 1995). To test whether adopting effective values of FC and WP reduces the difference between the distributed approach and the bulk approach, we performed an extra run with the bulk where the grid cell effective wilting is set at 70 % of its original value, whereas the field capacity has been increased by 30 %. As shown in Figure 3.5 (left panel), the results obtained with the resulting effective run are globally better than the results obtained with the original model which uses the local field capacity and the wilting point. However, the difference between the latent heat flux density calculated with the distributed approach and the latent flux density calculated using the effective bulk model run, still has a maximum of about

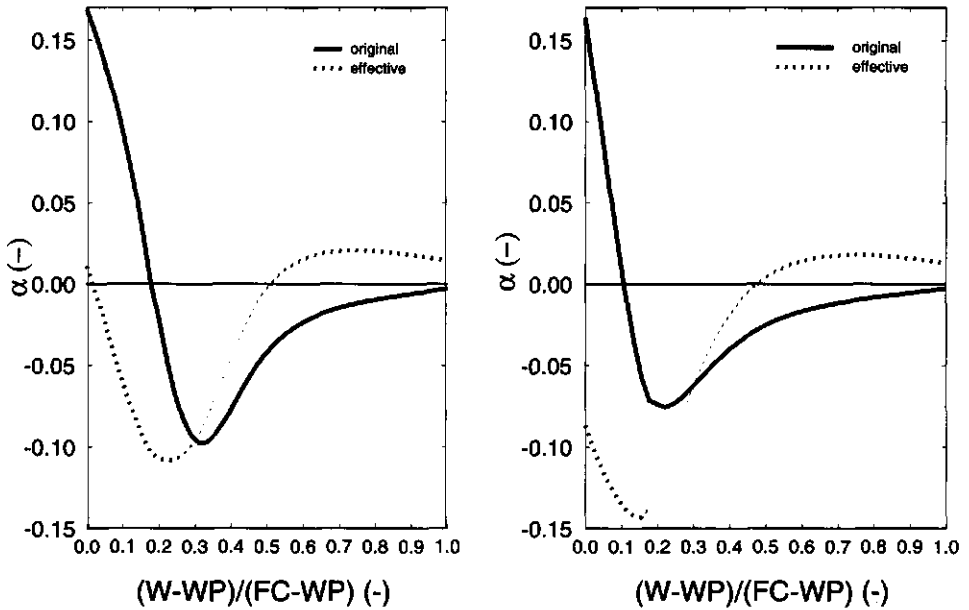


Figure 3.5: α as a function of the grid cell canopy water status for the bulk model (solid) and a model with an effective grid cell wilting point and field capacity: reference atmospheric conditions (left panel) and modified atmospheric conditions (right panel)

10% of the net radiation. Furthermore, it appears that the effective values of the wilting point and the field capacity depend on the meteorological conditions. This is shown in the right panel of Figure 3.5 which shows results of the original bulk model, the effective bulk model and the distributed approach obtained using a lower forcing temperature at 2 m of 290 K. It appears that in this run the model with modified values of the wilting point and the field capacity yields an overestimation of the latent heat flux density in dry conditions.

3.4 Impact on the seasonal cycle

In the previous section we found that introducing spatial variations in the soil moisture content typically leads to a significantly lower latent heat flux density in wet conditions. In contrast, in dry conditions, the latent heat flux density was significantly larger with the distributed approach. Here, we study whether this leads to a weaker seasonal cycle of the latent heat flux density and a resulting enhanced latent

heat flux density during the dry season.

Therefore, both the distributed and the bulk model are forced with observed data, instead of using a constant climatological forcing. In this section, we use forcings that are obtained in a dry climate and forcings obtained in a wet climate. For the dry climate we use forcings obtained in Niger during the SEBEX experiment (Gash et al. 1991). These data include hourly observations of the incoming short- and long wave radiation, direct observations of the upper soil temperature (at 10 cm below the surface), the precipitation and the specific humidity. The wet climate forcings are collected in the Hupsel catchment, located in the Netherlands (Soet et al. 2000). The data set was collected during 1982 and consists of 20-minute averages of the incoming short- and long wave radiation flux densities, the precipitation, the specific humidity and the air temperature. The temperature of the upper soil is estimated following De Rooy and Holtslag (1999). To be concise, we only show results for the typical loam soil, a value of 0.3 for β and the reference, quadratic soil moisture stress response function.

To describe the temporal evolution of the soil moisture content we use a simple bucket method. The maximal volume of water that can be stored per unit area in the bucket equals W_{\max} , whereas W represents the actual volume of water in storage per unit area in the bucket. In this study, runoff is described for both the distributed approach and for the bulk model with the method described by Dümenil and Todini (1992). The values of the parameters are taken from Van den Hurk et al. (2001). In dry climates, the soil column is usually deep. For this run, we set W_{\max} to 0.6 m. In wet climates, the plants root undeeper and the soil column is usually shallow. For the wet climate run, we estimate the maximal volume of water that can be stored in the grid cell, W_{\max} , to be 0.3 m. The initial grid cell relative saturation is obtained by performing for both approaches a run of multiple years till an equilibrium is reached.

For the dry climate, Figure 3.6 shows a time series of the midday latent heat flux density, the latent heat flux density averaged from 12:00 UTC till 14:00 UTC. At the beginning of the wet period, from day 1 to 20 and from 320 onwards, the bulk approach gives larger estimates of the latent heat flux density than the distributed approach. At the beginning of the wet period, the midday latent heat flux density predicted by the bulk approach is higher than the latent heat flux density predicted by the distributed approach. When the grid cell relative saturation is high, from day 20 to 140, the bulk approach and the distributed approach give similar estimates of the latent heat flux density. However, as the soil dries down, from day 140 till day 320,

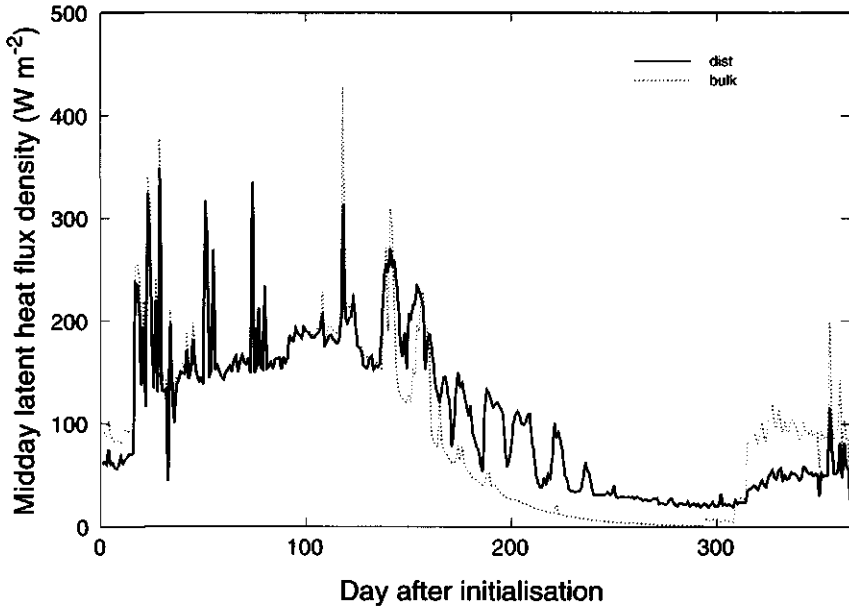


Figure 3.6: Time series of the midday latent heat flux density for the dry climate run using a distributed (solid) and a bulk approach (dotted).

the latent heat flux estimated with the bulk approach drops sharply. In contrast, the latent heat flux density predicted by the distributed approach reduces more gradually. At the beginning of the dry period, the midday latent heat flux density predicted by the distributed approach is about twice as large as the latent heat flux density predicted with the bulk model. At the end of the dry season, the bulk approach predicts, in contrast to the distributed approach, even a vanishing of the latent heat flux density, as shown in Figure 3.6. Over the dry season the difference in the cumulative evapotranspiration amounts to 72 mm, about 10 % of the annual precipitation.

For the wet climate, the difference between the seasonal cycle of the estimated latent heat flux densities is less obvious (Figure 3.7). Most of the time the soil is wet and the bulk approach and the distributed approach give similar estimates of the latent heat flux density. However, during a dry-down period, from day 210 till day 220, the bulk approach predicts significantly lower estimates of the midday latent heat flux density, as compared to the distributed approach. In contrast, from day 150 till day 160, when the soil starts to dry down, the bulk approach predicts larger estimates of the midday latent heat flux density. As a result, even in a wet moderate

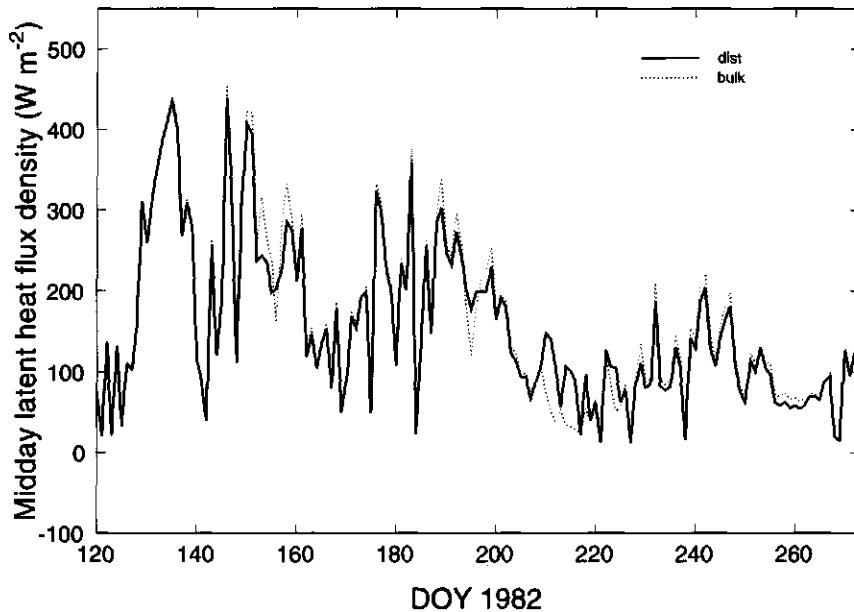


Figure 3.7: Time series of the midday latent heat flux density for the wet climate run using a distributed (solid) and a bulk (dotted) approach.

climate, estimates of the latent heat flux density obtained using the bulk approach differ from estimates obtained using a distributed approach.

3.5 Coupling to the Convective Boundary Layer

In this section we explore the impact of the spatial heterogeneity of the soil moisture content on the latent and sensible heat flux density when the surface is coupled to a developing convective boundary layer (CBL). Previous sensitivity studies revealed that the surface flux densities are less sensitive to surface variables when the boundary layer is allowed to feed back on the surface (Jacobs and De Bruin 1992). A larger latent heat flux density leads to a more moist convective boundary layer. As a result, the specific humidity difference over the surface layer is reduced. Consequently, the initially larger latent heat flux density is, at its turn, suppressed. Also, we study in this section the impact of the spatial variation in the soil moisture content on the temperature and specific humidity in the boundary layer and at 2 m.

To estimate the impact of the boundary layer feedback, we couple the model for

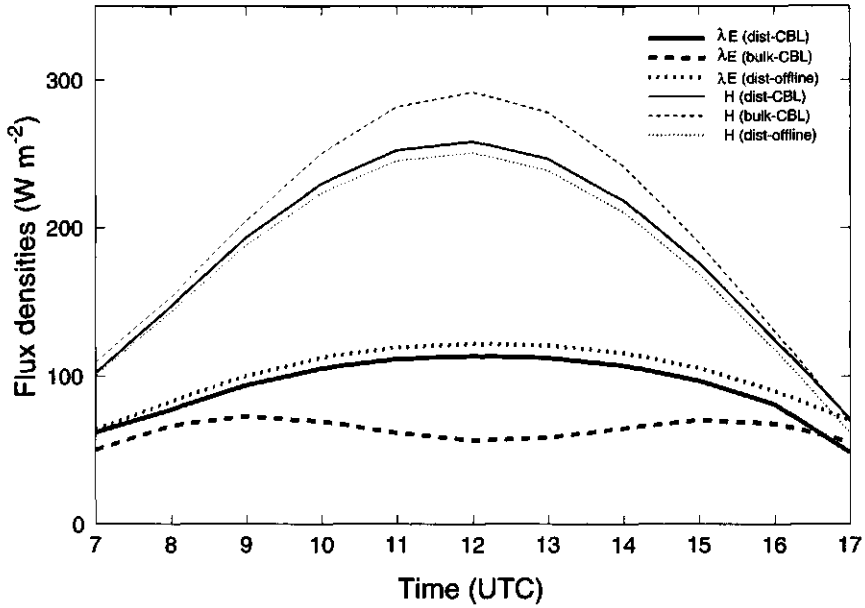


Figure 3.8: Diurnal variation of the sensible heat flux density (thin) and the latent heat flux density (thick) as calculated using the distributed approach (solid), the bulk approach (dashed) and the distributed approach forced in the surface layer (dotted): results are given for a grid cell relative saturation of 0.37.

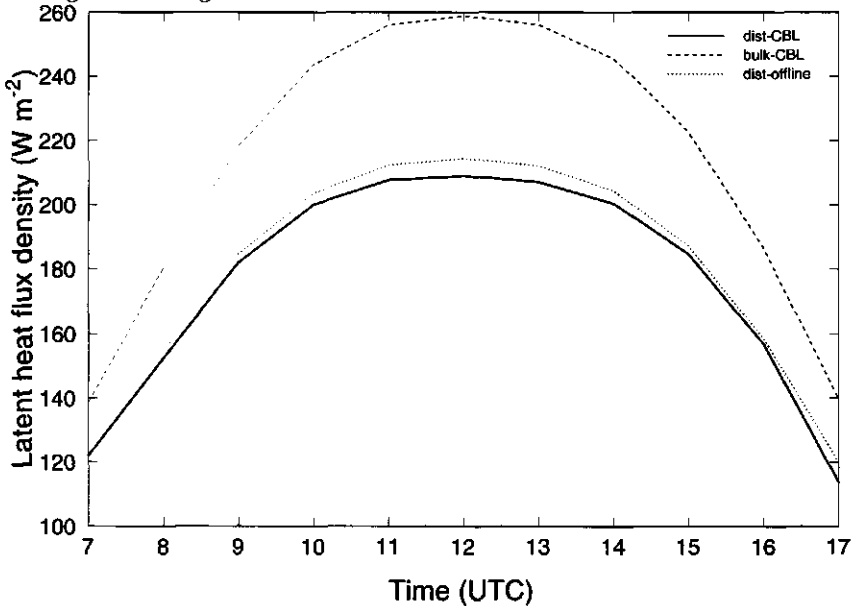


Figure 3.9: Diurnal variation of the latent heat flux density as calculated using the distributed approach (solid), the bulk approach (dashed) and the distributed approach forced in the surface layer (dotted) for a grid cell relative saturation of 0.45.

the averaged surface flux densities to a convective boundary layer model (Tennekes 1973). The reference level which is used to calculate the flux densities at each subgrid is taken as the top of the surface layer, one tenth of the height of the convective boundary layer, denoted as h . At the reference level, the wind speed and the specific humidity and the potential temperature are taken to be constant over the entire grid cell. These are used to compute the resulting areally averaged surface flux densities which force the thermal growth of the boundary layer. We perform two coupled runs, one for each approach to obtain the areally averaged surface flux densities. Additionally, we perform a run where the impact of spatial variations in the soil moisture content is studied without boundary layer feedback. In this run, we estimate the flux densities with the distributed approach using forcings that are prescribed at 2 m, obtained by extrapolating the boundary layer temperature, specific humidity and the wind speed obtained using flux densities and gradients from the coupled bulk model towards 2 m.

To estimate the meteorological conditions in the free troposphere and to initialize the boundary layer model, we use radiosoundings launched at 0:00 UTC and 12:00 UTC on August 1 1995 in De Bilt, the Netherlands. We use data obtained on this day, because the tropospheric profiles of temperature and specific humidity are typical for a fine day in the summer of a moderate climate. We are primarily interested in fine days, because on these days the incoming solar radiation is largest which implies that the differences in estimated flux densities calculated using either the bulk or the distributed approach are most pronounced. The boundary layer height is initialized at 50 m, the potential temperature in the convective boundary layer, θ_{CBL} at 293.5 K and the specific humidity in the convective boundary layer, q_{CBL} at 7.6 gkg^{-1} . Using the radiosounding at 12.00 UTC we estimate the mean wind speed in the atmospheric boundary layer as 6 ms^{-1} . In this study, the subsidence velocity is simply set at 0 ms^{-1} . The temperature of the upper soil is set at its climatological value of 291 K. The entrainment heat flux density at the top of the boundary layer is taken as one fifth of the surface heat flux density. The incoming short wave radiation varies over the day is described using a simple sine function. The maximal incoming short wave radiation flux density is 900 Wm^{-2} , the sun rises at 4:00 UTC, whereas sunset is at 20:00 UTC. These values are typical for a mid-summer day in a moderate climate. For the incoming long wave radiation we adopt a constant value of 300 Wm^{-2} . We start our calculations at 7:00 UTC. To be concise, we only show results for an intermediate value for β of 0.3, the typical medium-textured loam soil and the quadratic soil moisture stress response function.

Figures 3.8 and 3.9 give the diurnal variation of the surface flux densities, calculated using both coupled runs and the run without boundary layer feedback. Figure 3.8 refers to a very low grid cell relative saturation of 0.37 which is below the inflection point in Figure 3.2. Figure 3.9 refers to a larger grid cell relative saturation of 0.45 which is above the inflection point in Figure 3.2. For the low relative saturation, it appears that the run without boundary layer feedback gives a slightly higher estimate of the latent heat flux density than the run where the boundary layer is allowed to feed back on the surface. However, even when the surface is coupled to a convective boundary layer, a bulk approach predicts a considerably lower latent heat flux density when the soil is near the wilting point. The low impact of boundary layer feedback is because in dry conditions the canopy conductance is much smaller than the aerodynamic conductance. This means that the flux densities at the land surface are relatively independent on the conditions in the boundary layer (Jacobs and De Bruin 1992). Also for the higher soil moisture content, the run without boundary layer feedback gives a higher estimate of the latent heat flux density than the run including boundary layer feedback. This is caused by the predicted stomatal closure with increasing values of the specific humidity deficit of the air (see section 2). In the run including feedback the air gets drier. As a result, in this run the canopy conductance increases and the latent heat flux density is reduced. In these conditions, inclusion of boundary layer feedback enhances the difference between the estimates obtained using the distributed approach and the bulk approach. For the grid cell relative saturation of 0.37, Figure 3.10 shows the specific humidity of the boundary layer and the averaged 2 m specific humidity (left panel). When the distributed approach is used, the boundary layer appears to be about 0.3 gkg^{-1} more moist as compared to the bulk approach. Furthermore, the averaged specific humidity near the surface is about 0.7 gkg^{-1} larger for the coupled run with the distributed approach than the run with the bulk approach. As result, in areas where our typical distribution describes the spatial variation of the soil moisture content well, using a bulk approach would give a dry bias. This is important since Viterbo (1994) typically found that the ECMWF numerical weather prediction model showed a dry bias of 0.5 to 1 gkg^{-1} during dry summer conditions. As a result, the heterogeneity of the soil moisture content may explain some of the dry bias often found in large-scale atmospheric models. For the same grid cell relative saturation of 0.37, Figure 3.10 shows for both the distributed and the bulk approach the air temperature in the boundary layer and the estimated temperature at 2 m (right panel). It appears that with the bulk approach the average 2 m temperature is slightly higher than with the distributed approach. For a grid cell

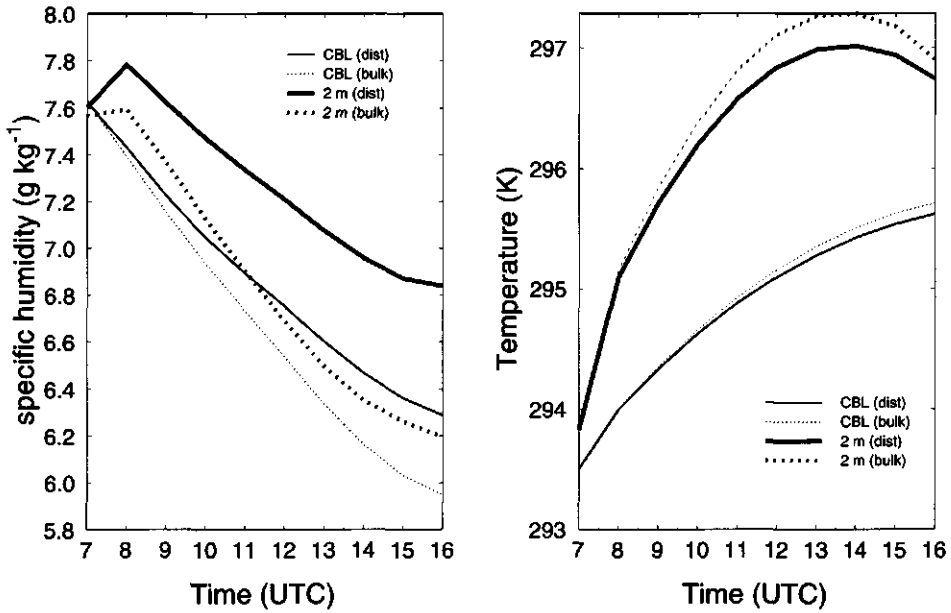


Figure 3.10: Diurnal variation of the specific humidity (left panel) and the temperature (right panel) at 2 m (thick lines) and in the convective boundary layer (thin lines), simulated using a distributed approach (solid) and a bulk approach (dotted): grid cell relative saturation is 0.37.

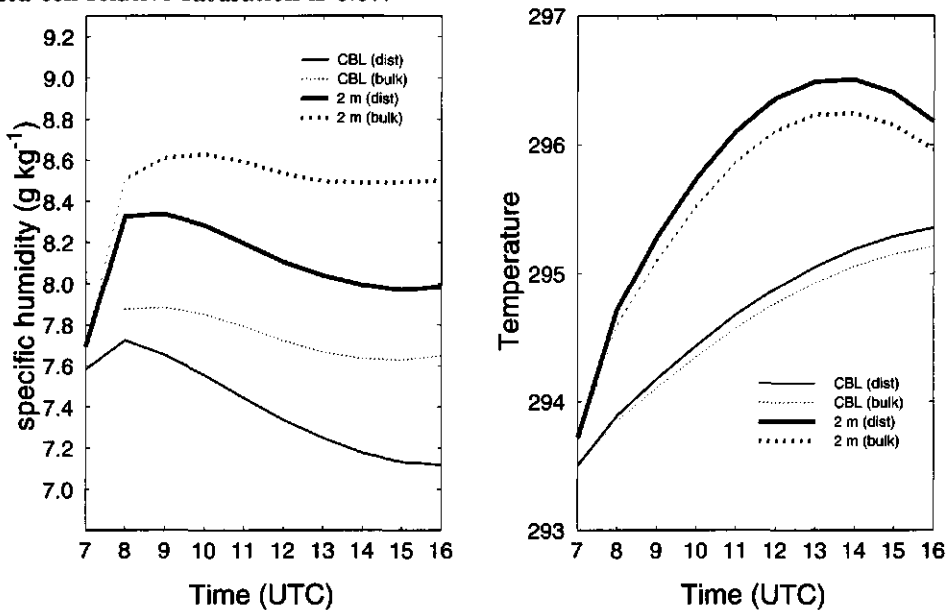


Figure 3.11: As in Figure 3.10 for a grid cell relative saturation of 0.45.

relative saturation of 0.45, Figure 3.11 (right panel) shows for both the distributed and the bulk approach the temperature in the boundary layer and the temperature at 2 m. It appears that the distributed approach predicts a slightly higher temperature at 2 m, as compared to the bulk approach. Furthermore, from Figure 3.11 (left panel) it appears that the specific humidity as estimated with the distributed approach is lower than the bulk approach.

3.6 Summary and Conclusion

The objective of this study was to investigate the spatial distribution of the soil moisture content and its impact on the surface energy flux densities and the near-surface meteorological conditions. Therefore, we performed a sensitivity study where we compared estimates of the surface flux densities obtained using two approaches: a distributed approach that takes account of spatial variations in the soil moisture content, and a bulk approach that calculates the soil moisture stress of vegetation as a function of one uniform soil moisture content.

In wet conditions, when the grid cell relative saturation is above the field capacity, both approaches give similar estimates of the latent heat flux density. However, as the soil dries down, the latent heat flux density is typically larger when a bulk approach is used. When the grid cell relative saturation becomes very low, a bulk approach gives lower estimates of the latent heat flux density. When the spatial variation in the soil moisture content is large, differences in flux densities of up to 120 Wm^{-2} can be expected.

The form of the function that describes the impact of soil moisture stress on the canopy conductance is important. Use of a quadratic response function (see the previous chapter) leads to larger maximal differences between both approaches, as compared to a linear response function (Viterbo and Beljaars 1995). However, as the soil becomes wetter, the difference between both approaches decreases sharply for the quadratic response function. In contrast, for the linear response function, the bulk approach gives smaller estimates of the latent heat flux density, even when the soil is considerably wet.

Introducing effective values for the wilting point and the field capacity slightly improves the results obtained with the bulk model. However, the effective values appear to depend on the atmospheric conditions which hampers a straightforward relation between the effective values and the parameters describing the spatial heterogeneity.

Typically, the distributed approach predicts a weaker seasonal cycle of the latent

heat flux density. Especially for drier climates, the bulk approach gives significantly lower estimates of the latent heat flux density during the dry season. Over the dry season the difference in cumulative evapotranspiration amounts to 72 mm. However, even in a wet climate a bulk approach gives smaller predictions of the latent heat flux density during dry-down.

Even when the boundary layer is allowed to feed back on the surface, a bulk approach gives significantly different estimates of the surface flux densities compared to a distributed approach. Also, the lower prediction of the evapotranspiration in dry conditions and higher prediction in wet conditions appeared to affect the near-surface meteorology. In dry conditions the bulk approach typically gives a warm and dry bias as compared to the distributed approach. In contrast, in wet conditions, the bulk approach predicts a lower temperature at 2 m and a larger specific humidity at 2 m.

It appears that the spatial variations in the soil moisture content have a large impact on the estimated surface flux densities and the near-surface meteorology. Unfortunately, for the scales considered here there are no detailed measurements of the flux densities. This prohibits a validation using observations of the important impact of the soil moisture heterogeneity on the seasonal evolution of the latent heat flux density. An important step towards observations on such scales are satellite-derived estimates of the latent heat flux density (Van den Hurk et al. 1997). However, since satellites require cloud-free meteorological conditions, only for very limited areas continuous series can be obtained.

Our study is a sensitivity study and as a result, no general conclusions about the impact of spatial heterogeneity within grid cells of large-scale atmospheric models can be drawn. However, the prescribed distribution has been successfully used to describe the impact of the spatial heterogeneity of the soil moisture content on the runoff (Dümenil and Todini 1992). Furthermore, the proposed cumulative distribution of the infiltration capacity, and the assumption that that actual volumetric soil moisture content is constant in the unsaturated part of a catchment have been tested using observations (see Kalma et al. 1995). As a result, we conclude that taking account of the horizontal heterogeneity of the soil moisture content is a prerequisite for a proper representation of the seasonal hydrological cycle within large-scale atmospheric models.

Chapter 4

The Concept of 'Effective' Bulk Exchange Coefficients for Determination of Surface Flux Densities

This chapter is based on Ronda, R.J., and H.A.R. de Bruin, 1999: A note on the concept of 'effective' bulk exchange coefficients for determination of surface flux densities. *Boundary-Layer Meteor.*, **93**(1), 155-162

abstract

Because most land surfaces are non-uniform on meteorological model scales, usually applied flux-profile relationships to obtain surface flux densities cannot be used. Therefore, some modelers assume that these relations are scale-invariant if the local bulk transfer parameters are replaced by effective parameters. This approach leads to wrong results for grid cells that contain subgrid areas that differ largely with respect to stability. Hence, in such cases, the surface energy budget needs to be solved for each subgrid separately. Therefore, to obtain the correct surface flux densities in all situations, for each grid cell in the horizontal domain of meteorological models, subgrid areas that differ with respect to stability need to be identified.

4.1 Introduction

The horizontal grid cell size of numerical weather prediction and climate models is typically 50^2 km^2 or larger. On such scales land surfaces are usually heterogeneous. Therefore, bulk transfer relations, which relate flux densities of homogeneous surfaces to vertical profiles (flux-profile relationships) can not be used.

However, above the blending height (Wieringa 1986; Mason 1988; Claussen 1991; Wood and Mason 1991) the mean quantities become uniform. Hence, by using this height as a reference level for each homogeneous subgrid area (tile or patch) the flux density can be calculated. The grid cell average flux density is then obtained by taking the linear average of these subgrid area flux densities (Koster and Suarez 1992; Claussen and Klaassen 1993; Blyth et al. 1993; Dolman 1993; Dolman and Blyth 1997). This method is used to infer surface flux densities from remote sensing images. Typically, these procedures assume that the temperature at a reference level is constant for an entire image (Bastiaanssen 1995; Van den Hurk et al. 1997). Then, for each pixel the surface skin temperature is derived and the flux densities computed.

Consistent aggregation of the remotely sensed surface flux densities and surface skin temperature towards the scales of an atmospheric model requires the partitioning of the grid cell into a number of patches equal to the number of pixels. To circumvent the calculation of flux densities for each homogeneous patch in some meteorological models it is assumed that the flux-profile relationships are scale-invariant (Hu and Islam 1997; Sellers 1995). An example is the ECMWF (European Centre for Medium-Ranged Forecasts) Numerical Weather Prediction Model (Viterbo and Beljaars 1995). Hence, by replacing local patch parameters with effective parameters heterogeneous terrain surface bulk transfer relations can be derived. Methods to obtain effective parameters have been derived by Lhomme (1992), Blyth et al. (1993), Lhomme et al. (1994), McNaughton (1994), Raupach (1991, 1993, 1995) and Raupach and Finnigan (1995).

The investigators mentioned above concentrated on grid cells consisting of subgrid areas that differ only slightly with respect to stability. In this research large stability differences are considered: the fluxes over the subgrid areas could be of opposite sign. The aim of this study is to show with three examples that in cases where large stability differences exist the use of effective parameters leads to wrong results (Mahrt 1987; Mahrt et al. 1996; Ronda and De Bruin 1999). Hence, it is required to differentiate the area into a set of tiles that are relatively homogeneous with respect to stability. For that purpose, we will consider a surface of type A according to a classification

proposed by De Bruin, (1987) (see also Shuttleworth (1988) and Dolman and Blyth (1997)) that consists of a regular mosaic of two surface components. In this study three cases are considered. Each case consists of a different mixture of surface types:

- case 1: lake and grass land
- case 2: dry grass and snow field
- case 3: dry and wet forest

The flux densities from each patch will be described with the standard Monin-Obukhov similarity theory (Garratt 1992). The calculated flux densities will be used as forcings for a simple slab model for the planetary boundary layer (PBL) (Driedonks 1981), in order to mimic the interaction between the surface flux densities and the PBL. In the convective boundary layer moisture and temperature are well-mixed. The bottom of the mixed layer acts as a blending height. The choice of using a slab model limits our study to situations where a convective boundary layer (CBL) develops. Besides, the model is one-dimensional and two- and three-dimensional processes like local advection and mesoscale circulations cannot be taken into account.

In section 4.2 a brief description of flux density upscaling techniques is given. Section 4.3 gives a description of the three cases and deals with the PBL model used in this study. The results for the three cases are shown and discussed in section 4.4. Section 4.5 provides a conclusion.

4.2 Upscaling the Surface Energy Balance

In General Circulation Models the partitioning of incoming short wave radiation and incoming long wave radiation is calculated by solving the surface energy balance (SEB). For a homogeneous patch this balance reads (Garratt 1992):

$$K^\downarrow - K^\uparrow + \epsilon L^\downarrow - L^\uparrow = H + \lambda E + G, \quad (4.1)$$

In this equation K^\downarrow is the incoming short wave radiation flux density, K^\uparrow is the outgoing short wave radiation flux density, L^\downarrow is the incoming long wave radiation flux density and L^\uparrow is the outgoing long wave radiation flux density, H is the sensible heat flux density, λE is the latent heat flux density and G is the ground heat flux density (neglected in this study). λ is the latent heat of vaporization and E the evapotranspiration. ϵ is the emissivity of the earth's surface.

The sensible heat flux density and latent heat flux density are calculated by means

of bulk exchange relations relating the scalar flux density to scalar profiles in the surface layer (Viterbo and Beljaars 1995):

$$H = \rho_a c_p g_a (T_{sk} - T_a), \quad (4.2)$$

$$\lambda E = \rho_a \lambda g_a \frac{q^*(T_{sk}) - q_a}{1 + g_a r_{c,w}}. \quad (4.3)$$

where ρ_a is the air density, c_p is the isobaric specific heat, g_a is the aerodynamic conductance and $r_{c,w}$ is the canopy resistance to water vapor flow (the reciprocal of the conductance to water vapor flow). T_{sk} is the surface temperature and T_a is the temperature at a reference level, z_r , $q^*(T_{sk})$ is the saturated specific humidity at the surface and q_a is the specific humidity at the reference level. In atmospheric models, g_a is calculated using Monin-Obukhov similarity theory. It is calculated as a function of $|u|$, the horizontal velocity at the reference level, the roughness length for heat, z_h , the roughness length for momentum, z_{0m} , the height of the reference level and $(T_s - T_a)$ (Appendix C).

Combining Eqs. 4.1, 4.2 and 4.3 with the formulations for the outgoing short wave and long wave radiation (Garratt 1992) leads to the following equation for the SEB:

$$(1 - a) K^\downarrow + \epsilon L^\downarrow - \epsilon \sigma T_{sk}^4 = \rho_a c_p g_a (T_{sk} - T_a) + \rho_a \lambda g_a \frac{q^*(T_{sk}) - q_a}{1 + g_a r_{c,w}}. \quad (4.4)$$

In this equation is a the albedo.

Assuming that the incoming short and long wave radiation flux densities are uniform over the grid cell, the SEB for the grid cell reads:

$$(1 - \bar{a}) K^\downarrow + \bar{\epsilon} L^\downarrow - \sigma \overline{\epsilon T_{sk}^4} = \rho_a c_p g_a \overline{(T_{sk} - T_a)} + g_a \frac{\overline{q^*(T_{sk}) - q_a}}{1 + g_a r_{c,w}} \quad (4.5)$$

In this equation overbars denote linear spatial averages:

$$\bar{x} = \sum_{i=1}^M x_i f_i, \quad (4.6)$$

with f_i the fraction covered by patch number i and M the number of patches in the grid cell. In this study only cases where $M = 2$ and $f_1 = f_2 = 0.5$ are considered.

Blyth et al. (1993) and Dolman and Blyth (1997) show that when the transfer coefficient, g_a is not an explicit function of the surface temperature (the aerodynamic conductances are assumed to adopt their neutral values), Eq. 4.5 can be solved analytically to obtain the grid cell averaged surface temperature. However, either the flux density or the surface temperature has to be constant over the grid cell. Raupach

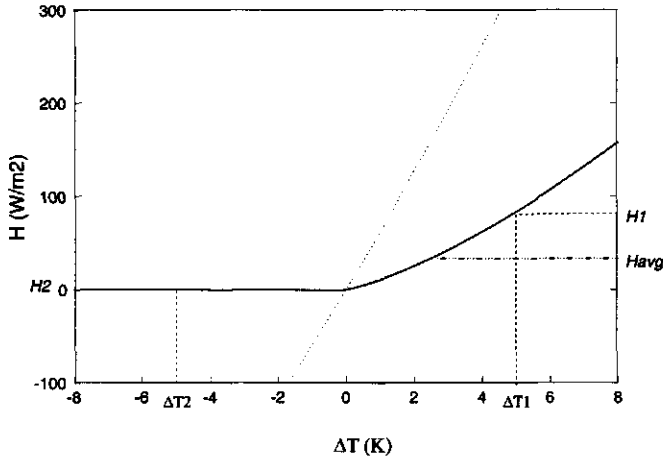


Figure 4.1: The sensible heat flux, H , as a function of ΔT for $|u| = 1\text{ms}^{-1}$ (solid), $|u| = 10\text{ms}^{-1}$ (dotted), also shown the surface temperature deficit and sensible heat flux density of a stable patch, the surface temperature deficit and sensible heat flux density of an unstable patch and the average sensible heat flux density

(1991, 1993, 1995) and Raupach and Finnigan (1995) derived estimates of the grid cell averaged flux densities by eliminating the surface temperature and linearly averaging the resulting combination equation. The differences between the radiation balance (left hand side of equation 4.1) evaluated at reference level and at the surface were accounted for by a radiative resistance.

Generally, in the atmosphere the aerodynamic conductances are functions of stability (Appendix C). These functions are non-linear and therefore analytic solutions for the grid cell average surface balance cannot be obtained. In Figure 4.1 H is shown as a function of ΔT for different horizontal wind velocities and a specified height geometry ($z_r = 10\text{m}$, $z_{0m} = 0.1\text{m}$ and $z_h = 0.01\text{m}$). It can be seen that especially for low wind speeds this relation is highly non-linear. If both patches differ largely with respect to stability the average sensible heat flux density (H_{avg}) is larger than the sensible heat flux density evaluated at the averaged temperature difference: in the example given in Figure 4.1 the averaged temperature difference and hence the sensible heat flux density evaluated at the averaged temperature both equal 0. In the unstable region and when the wind speed is high in the stable region H is approximately a linear function of ΔT . Here, estimation of the average sensible heat flux density using the averaged surface temperature is accurate.

Table 4.1: Initial Conditions

Quantity	Case lake/grass	Case snow/grass	Case wet/dry forest
$\theta_{CBL}(K)$	275.9	283.3	292.0
q_{CBL}	3.0E-3	3.0E-3	7.1E-4
Δq_h	3.0E-3	3.0E-3	7.1E-4
$h(m)$	248.3	276.4	436.0

4.3 Setup of evaluation study

The incoming short wave radiation varies over the day. Here, we describe the diurnal evolution using a simple sinus function:

$$K^\downarrow = K_m \sin\left(\frac{2\pi(t - t_{sr})}{t_{st} - t_{sr}}\right), \quad (4.7)$$

where K_m is the maximal incoming short wave radiation, t local time, t_{sr} the local time of sunrise and t_{st} the local time of sunset. The incoming long wave radiation is evaluated from the temperature of the CBL:

$$L^\downarrow = \epsilon_a \sigma T_a^4, \quad (4.8)$$

where ϵ_a is the effective emissivity of the atmosphere ($\epsilon_a = 0.8$).

The aerodynamic conductance, g_a is calculated as described in the appendix C. The reference level is the top of the surface layer given as one tenth of the height of the convective boundary layer denoted as h . In this study the patches represent subareas within the grid cell of a large-scale atmospheric model. Therefore, we assume that they are so small that the reference height temperature is constant over the grid cell. However, they are large enough to neglect the effects of local advection.

Case 1 refers to mixture of cold lake next to a grass land. Due to the large heat capacity of water, the lake surface temperature is taken as constant during the day ($T_{sk, lake} = 275K$). Therefore, the sensible and latent heat flux densities of the lake patch are directly computed with Eqs. 4.2 and 4.3. $r_{c,w}$ is 0 for the lake patch. For the grass patches the surface energy balance is solved directly. The albedo is 0.2, the $r_{c,w}$ is 60 sm^{-1} , the emissivity is 0.996, the roughness length for momentum (z_{0m}) is 0.1 m and the roughness length of heat (z_h) is 0.01 m. The wind speed in the convective boundary layer is 1 ms^{-1} . For this case the incoming short wave radiation is taken as typical for a spring day at high latitudes: K_m is 500 Wm^{-2} , t_{sr} is 5:00 UTC and t_{st} is 19:00 UTC.

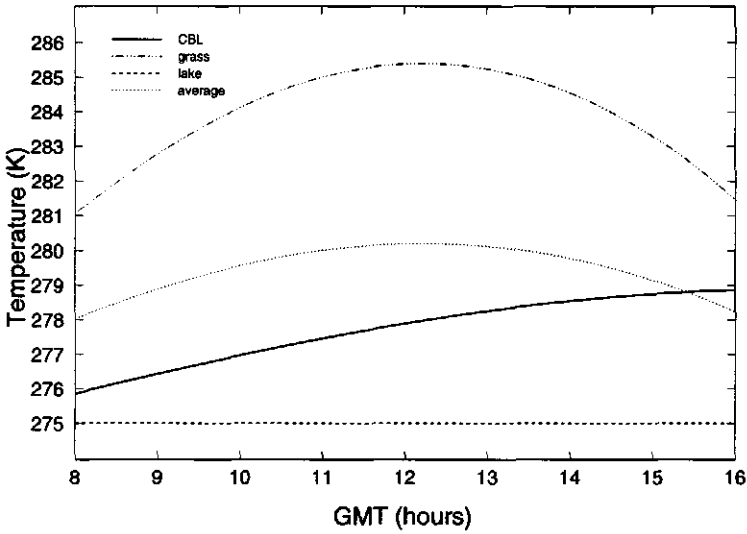


Figure 4.2: Diurnal variation of the CBL potential temperature (solid), the grass patch surface temperature (dash-dotted), the lake patch surface temperature (dashed) and the averaged surface temperature (dotted).

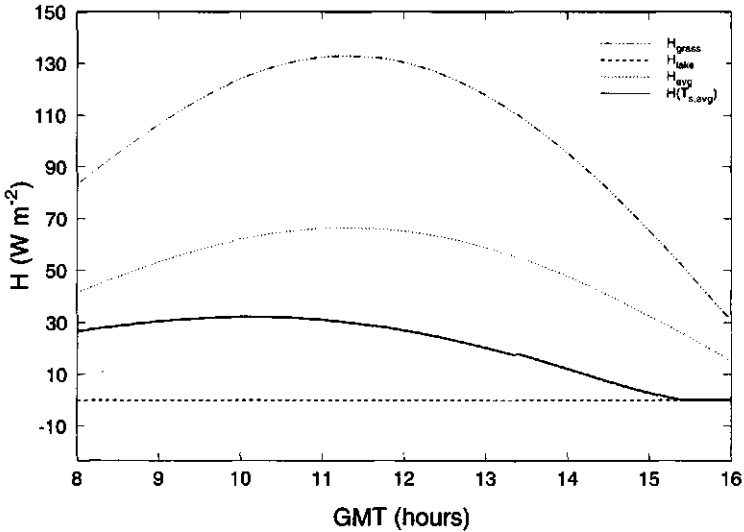


Figure 4.3: The sensible heat flux density of the cold lake patch (dashed), the sensible heat flux density of the grass patch (dash-dotted), the average sensible heat flux density (solid) and the sensible heat flux density evaluated at the averaged surface temperature deficit (solid)

Case 2 refers to mixture of melting snow next to dry grass. Due to melting, the snow surface temperature is taken as constant during the day ($T_{sk,snow} = 273K$). Therefore, the surface energy flux densities of the snow patch are directly computed with Eqs. 4.2 and 4.3. $r_{c,w}$ is 0 for the snow patch. For the grass patches the surface energy balance is solved. The albedo is 0.2, the emissivity is 0.996, the roughness length for momentum (z_{0m}) is 0.1 m and the roughness length of heat (z_h) is 0.01 m. Because of permafrost, boreal grass lands are usually very dry. Here, we set $\lambda E = 0$ for the grass patch. The wind speed in the convective boundary layer is 1 ms^{-1} . K_m , t_{sr} and t_{st} are the same as for case 1.

Case 3 refers to mixture of wet and dry forest. For both patches the surface energy balance is solved directly; the albedo is 0.2, the emissivity 0.996, the roughness length for momentum (z_{0m}) is 0.1 m and the roughness length of heat (z_h) is 0.01 m. For the wet forest patch $r_{c,w}$ is 0, whereas we set $\lambda E = 0$ for the dry forest patch. The wind speed in the convective boundary layer is 1 ms^{-1} . For this case K_m is 900 Wm^{-2} , t_{sr} is 4:00 UTC and t_{st} is 20:00 UTC. These values are typical for a summer day in mid-latitude regions.

To update the CBL temperature and humidity the subgrid area flux densities are linearly averaged and a grid cell flux density is calculated. The updated quantities are used to calculate the new values for the flux densities of the patches. The parameters of the CBL model (Appendix C) are $w_h = 0 \text{ ms}^{-1}$, $\gamma_\theta = 0.0073 \text{ Km}^{-1}$ and $\gamma_q = 0 \text{ m}^{-1}$.

The CBL model forced by the averaged surface flux densities consists of a set of ordinary differential equations which can be integrated. Table 4.1 gives for each case the initial values of the prognostic quantities (θ_{CBL} , h , q_{CBL} and Δq) of the model.

4.4 Results

Figure 4.2 refers to the first case where a lake patch is located next to a grass patch. It shows the CBL potential temperature, the lake patch surface temperature, the grass patch surface temperature and the averaged surface temperature as a function of time. It can be seen that during the whole day the surface layer above the lake patch is stable, whereas it is unstable above the grass patch. Bulk transfer relations predict a downward directed sensible heat flux density over the lake. In contrast, an upward directed sensible heat flux density is predicted over the grass patch (Figure 4.3). The grid cell averaged surface temperature is only slightly larger than the CBL potential temperature (Figure 4.2). As a result, the use of the grid cell averaged tem-

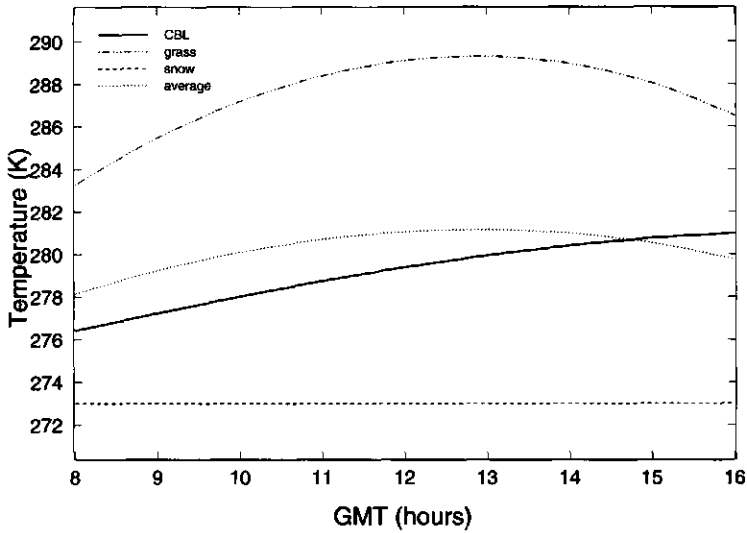


Figure 4.4: Diurnal variation of the CBL potential temperature (solid), the grass patch surface temperature (dash-dotted), the snow patch surface temperature (dashed) and the averaged surface temperature (dotted).

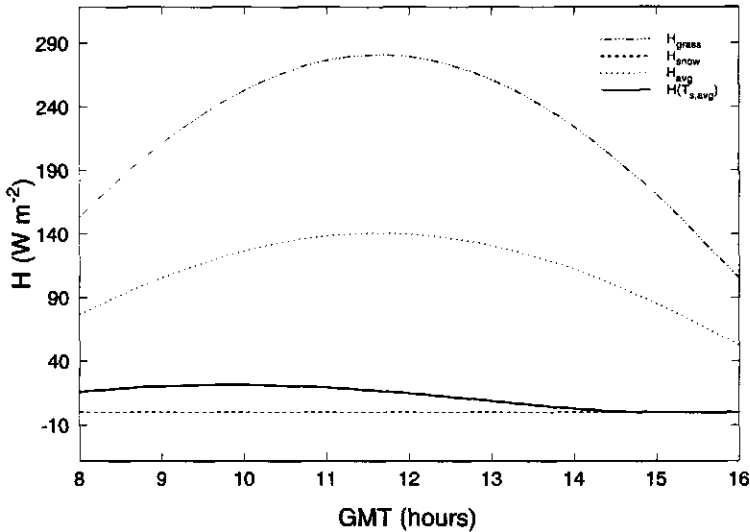


Figure 4.5: The sensible heat flux density of the snow patch (dashed), the sensible heat flux density of the grass patch (dash-dotted), the average sensible heat flux density (dotted) and the sensible heat flux density evaluated at the averaged surface temperature deficit (solid)

perature difference to obtain the grid cell sensible heat flux density, leads to a small upward directed sensible heat flux density (maximum 30 Wm^{-2} as is shown in Figure 4.3. However, the average sensible heat flux density is much larger (maximum of 60 Wm^{-2}) (Figure 4.3). Therefore, using one uniform temperature for the entire grid cell leads to an underestimation of the grid cell sensible heat flux density of about 50 % in this case. Our calculations are confirmed by the results of Frech and Jochum (1999). Using aircraft observations of the sensible heat flux density above a heterogeneous area, these authors found that, particularly for low wind speeds, the effective exchange coefficient depends on the averaging scale. When they removed the stably stratified lake from the analysis, the mean sensible heat flux density could be better described using the mean surface temperature.

The results of case 2, the melting snow patch next to the dry grass patch, are similar to the results of case 1. Figure 4.4 shows the diurnal cycle of the potential temperature, the snow patch surface temperature, the grass patch surface temperature and the averaged surface temperature. It appears that the surface layer above the snow patch is stable. In contrast, it is unstable above the grass patch. Bulk transfer relations predict a downward directed sensible heat flux density over the snow. An upward directed sensible heat flux density is predicted over the grass patch (Figure 4.5). The difference between the averaged surface temperature and the CBL potential temperature is small (Figure 4.4). Thus, using this temperature to calculate the average sensible heat flux density leads to an underprediction of the sensible heat flux density, as is shown in Figure 4.5. The underprediction in this case is much larger than in case 1. The cause is the larger stability difference between both patches in this case. This is caused by the smaller surface temperature of the snow patch as compared to the lake patch. Furthermore, since the latent heat flux density is absent, the grass patch becomes much warmer in this case (compare Figure 4.2 and Figure 4.4). This is reflected in the sensible heat flux density which is much larger over the grass patch located next to the snow area than over the grass patch next to the lake.

Case 3 is the wet forest next to a dry forest. For this case Figure 4.6 shows the CBL the diurnal cycle of the potential temperature, the wet forest patch surface temperature, the dry forest patch surface temperature and the averaged surface temperature. The surface layer above the dry forest is very unstable. The temperature difference between the dry forest surface temperature and the CBL temperature is large. In contrast, the surface layer above the wet forest is only slightly unstable. This surface loses most of its energy due to the latent heat flux density. The difference between the averaged surface temperature and the CBL potential temperature is small (Figure

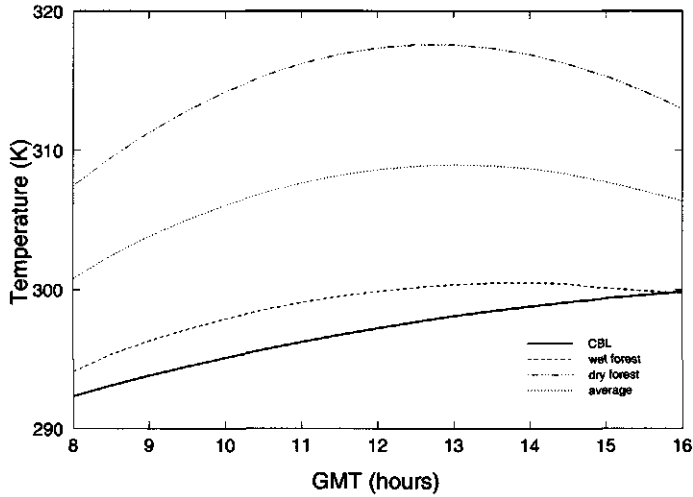


Figure 4.6: Diurnal variation of the CBL potential temperature (solid), the dry forest patch surface temperature (dash-dotted), the wet forest patch surface temperature (dashed) and the average surface temperature (dotted).

4.6). Also in this case, using this temperature to calculate the average sensible heat flux density leads to an underprediction of the sensible heat flux density, as is shown in Figure 4.7. However, since the stability difference is much smaller in this case, the underprediction is smaller than in the previous cases: about 20 %. Even when the cover of the patches is the same, non-uniformity in the grid cell distribution of for example soil moisture and rainfall can lead to differences in stability and hence to a need to distinguish between different subgrid areas. Vermeulen (2001) performs a similar study for a site in the Fochteloerveen area in the Netherlands. Here, an agricultural area is located next to a forest and a wet bog. When the agricultural area is wet, typically effective exchange coefficients can be obtained. However, when the agricultural became dry, a patch-by-patch approach gives better estimates of the averaged sensible heat flux density.

4.5 Conclusion

In the previous sections it has been shown that if a grid cell consists of subgrid areas (patches) that differ largely with respect to stability, the average sensible heat flux density cannot be related to the averaged temperature difference over the surface

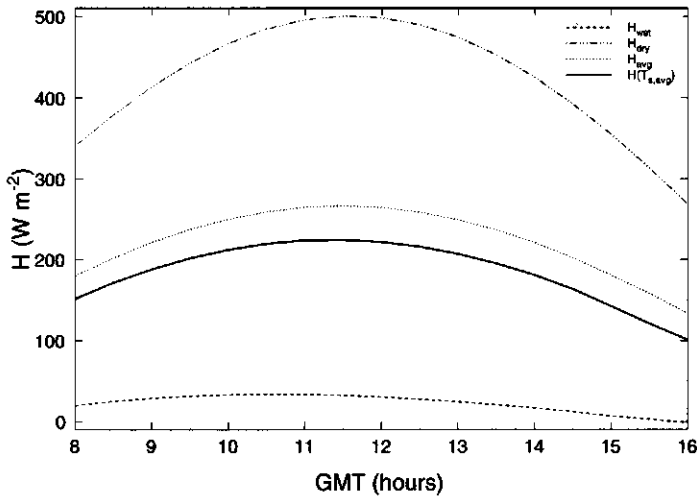


Figure 4.7: The sensible heat flux density of the wet forest patch (dashed), the sensible heat flux density of the dry forest patch (dash-dotted), the average sensible heat flux density (dotted) and the sensible heat flux density evaluated at the averaged surface temperature deficit (solid)

layer. Thus, the surface energy balance has to be solved for each patch separately. Furthermore, the use of one averaged surface temperature for deriving grid cell average surface flux densities leads to wrong results for such grid cells. This is caused by the non-linear relation between stability and flux density. As a result, consistent aggregation of remotely sensed surface energy flux densities and surface temperatures requires the definition of patches that differ with respect to stability.

This behaviour has been illustrated with three cases which occur frequently in nature. Especially for areas where vegetated patches occur next to cold surfaces, the flux densities should be calculated for each patch separately. However, even the cover of a grid cell is the same, differences in wetness can lead to differences in stability. Therefore, to obtain the correct flux densities combined with accurate estimates of the surface temperature, for each grid cell in the horizontal domain of meteorological models patches that differ with respect to stability need to be identified.

Chapter 5

Conclusion and perspective

5.1 Summary

This thesis deals with the modeling of the surface energy budget and the atmospheric boundary layer over natural surfaces. Its central aim is to elucidate how to describe this exchange in large-scale atmospheric models appreciating that the parameter values of these models should be obtained from coarse land surface maps, and that the land surface within grid cells of such models is usually heterogeneous. In this thesis we focus on scales of the grid cells of large-scale atmospheric model, typically 10-100 km. This thesis deals with three main items:

- the representation of the canopy conductance for low vegetation,
- the impact of spatial variation in the soil moisture content on the surface flux densities and the near-surface meteorology, and
- the impact of spatial variations of the surface temperature on the areally averaged sensible heat flux density.

In chapter 2 we develop a model for the canopy conductance of low vegetation. Therefore, we simplify and extend the approach of Jacobs (1994). This approach calculates the canopy conductance of low vegetation as a function of environmental variables evaluated at the canopy level. The environmental variables consist of the canopy temperature, the specific humidity inside the plant canopy, the carbon dioxide concentration inside the canopy and the incoming photosynthetically active radiation. Also, we develop a new formulation to account for the effect of the soil moisture stress on the canopy conductance of low vegetation. Our approach is simple and does not require iterations or numerical integration. However, it describes the major processes, including the exponential decay of the photosynthetically active radiation as a function of leaf area index. As a result, it can successfully be implemented in a large-scale atmospheric model.

The parameter values of our approach are retained from plant physiological theory. They appear to be robust and general formulations for biomes could be obtained. In this study, a distinction in C_3 and C_4 plants appears to be sufficient. We validate our approach using observations of the canopy conductance and the surface flux densities obtained at different sites with low vegetation. Here, we use measurements taken in a C_3 soybean crop in southern France, a C_4 prairie grass site in Kansas, U.S.A. and a C_3 grass land site in Cabauw in the Netherlands. We compare results obtained using our approach with results obtained with an empirical-statistical approach (Jarvis 1976;

Stewart 1988). In the empirical-statistical approach the canopy conductance is statistically related to environmental conditions at a reference level in the surface layer. The empirical-statistical approach was originally developed for micro-meteorological and hydrological applications. In these applications the environmental variables at a reference level in the surface layer are typically forcing variables. However, its use is often extended to large-scale atmospheric models. For vegetation at various experimental sites, the parameters of the empirical-statistical have been valued by fitting the calculated canopy conductance to the measured canopy conductance. By combining different local optimizations parameter values have been classified as a function of vegetation type or biome (Kelliher et al. 1993, 1995). Here, we use the values given by Van den Hurk et al. (2000).

For the tall C_4 prairie grass, the plant physiological approach gives better predictions of the canopy conductance than the traditional empirical-statistical approach. For the C_3 soybean crop, the plant physiological approach performs better. Overestimations in the latent heat flux density can be explained by overestimations in the net radiation that are relatively insensitive to the canopy conductance parameterization. For the C_3 short grass in the Cabauw area both approaches give similar results. Overall, our plant physiological approach with the proposed soil moisture response function, provides satisfactory estimates of the surface flux densities. Because the plant physiological approach is physically based and it relates the canopy conductance to environmental variables evaluated at canopy level, it can successfully be implemented in prognostic atmospheric models and in models used for climate impact studies.

In chapter 3 we show that land surface models of large-scale atmospheric models should take account of the spatial variation of the soil moisture content within the grid cell. Usually, modelers assume that the soil moisture content is horizontally homogeneous within the grid cell of a large-scale atmospheric model. As a result, all vegetation in the grid cell experiences the same soil moisture stress. The resulting soil moisture stress can then directly be used to obtain the surface temperature and to calculate the grid cell surface flux densities. This approach is called the bulk approach. In contrast, in a distributed approach we take account of spatial variations in the soil moisture content within the grid cell. In the distributed approach, we calculate the surface flux densities separately for a number of subareas with different values for the soil moisture content. The grid cell surface flux densities are then calculated by linearly averaging the subarea surface flux densities. Averaging weights are obtained from a distribution of the soil moisture content. Here, we describe the cumulative

distribution of the soil moisture content using the Xianjiang model (Sivapalan and Woods 1995). This cumulative distribution appears to be typical for scales of the grid cell of large-scale atmospheric models (Dümenil and Todini 1992). In this thesis, we compare estimates of the surface flux densities obtained using the distributed approach with estimates obtained using a bulk approach.

The distributed approach predicts a much weaker variation of the average latent heat flux density as a function of the grid cell relative saturation. When the soil is nearly-saturated, both methods give similar estimates of the surface flux densities. As the grid cell relative saturation drops below the field capacity, the soil moisture stress increases in the driest subareas. This increased moisture stress leads to a reduction of the average latent heat flux density. When the grid cell is only slightly below the field capacity, the bulk approach typically gives larger estimates of the latent heat flux density than the distributed approach, because the bulk approach ignores the reduction of the latent heat flux density in the driest areas. As the soil in the grid cell becomes even drier (near or even drops below the wilting point), the bulk approach gives minimal estimates of the latent heat flux density. In contrast, the distributed approach allows for considerable latent heat flux densities within the wetter subareas. Thus, in dry conditions the average latent heat flux density estimated using the bulk approach is much smaller than the estimate obtained using the distributed approach.

Lowering the wilting point within the bulk approach enhances the latent heat flux density in dry conditions. Increasing the field capacity leads to a reduction of the latent heat flux density predicted by the bulk approach when the soil moisture content is high. This suggests that discrepancies between the distributed and the bulk approach could be addressed by adopting effective values for the wilting point and the field capacity within the bulk approach (Wetzel and Chang 1987). However, in this thesis it is shown that even with effective values for the wilting point and the field capacity, the bulk approach gives considerable different estimates of the latent heat flux density in both wet and dry conditions compared to the distributed approach. Moreover, the optimal values for the effective wilting point and the effective field capacity appear to be sensitive to the atmospheric conditions at the reference level.

In chapter 3 we also study the impact of spatial variations of the soil moisture content on the seasonal cycle of the latent heat flux density. The bulk approach gives larger estimates of the latent heat flux density during the beginning of the dry season which leads to a more rapid depletion of the soil moisture reservoir. As a result, less water is available for transpiration later in the dry season (Dolman et al. 2002). Furthermore, the bulk approach gives much lower predictions of the latent heat flux

density when the soil is very dry. Therefore, the bulk approach gives much lower estimates of the latent heat flux density than the distributed approach during the dry season of a dry Sahelian climate. In a wet climate, the difference between the seasonal cycle as predicted by the bulk approach and the distributed approach is less obvious. However, even in this climate the bulk approach gives lower estimates of the latent heat flux density during a dry-down event.

Finally, in chapter 3, we couple both approaches to a model for a developing convective boundary layer (Tennekes 1973). It appears that the distributed approach gives lower estimates of the latent heat flux density when the soil is wetter, even when the land surface is coupled to a developing boundary layer. As a result, the distributed approach predicts a significantly drier and warmer atmospheric boundary layer in these conditions. Also, it gives a significantly smaller value for the specific humidity at 2 m and a slightly higher temperature at 2 m. When the soil is very dry, the distributed approach gives larger estimates of the latent heat flux density, even when coupled to a developing convective boundary layer. The result is that the distributed approach predicts a significantly moister and cooler boundary layer in such conditions. As a result, it gives a significantly larger value of the specific humidity at 2 m and a slightly lower temperature at 2 m. Thus, spatial variations in the soil moisture content have a significant impact on the surface flux densities and the specific humidity and the temperature near the surface. Therefore, we recommend that a next generation of land surface model takes account of the spatial variations in the soil moisture content.

In Chapter 4 we show with three cases that occur frequently in nature, that only a tiling approach can provide estimates of the averaged surface flux densities that are consistent with the averaged temperature difference over the surface layer in all situations (Mahrt 1987; Ronda and De Bruin 1999; Vermeulen 2001). Often, during daytime in convective conditions, the entire area is unstable. In such conditions the average sensible heat flux density can directly be computed as a function of the average surface temperature. However, if one or more patches are only slightly unstable or even stable, the direct relationship between the average sensible heat flux density and the averaged surface temperature breaks down. In such conditions, use of the averaged surface layer temperature difference leads to severe underestimation of average sensible heat flux density over the area. The underestimation of the sensible heat flux density then results in a too shallow and generally too wet and too cool boundary layer. Sometimes, even a stable boundary is predicted, whereas the actual average sensible heat flux density forces the development of a convective boundary

layer. In this chapter we show that situations as described above occur frequently in nature. Using a simple model, we show that when a grass field is located next to a melting snow field, the average sensible heat flux density is not directly related to the averaged temperature difference over the surface layer. Also, we show this for a situation where a grass field that is located next to a lake (Frech and Jochum 1999). Furthermore, it appears that when a wet forest is located adjacent to a dry forest, using the averaged surface temperature leads to an underestimation of the average sensible heat flux density (Vermeulen 2001).

The results in this thesis contributed to a better representation of the hydrological balance in large-scale atmospheric models. Ideas presented have been implemented and tested in large-scale atmospheric models (Dolman et al. 2002). In the next section we will summarize some main results. Furthermore, we will discuss some of the methods presented in this thesis and suggest possible routes for further research.

5.2 Perspective

An obvious route for further research is the implementation of the ideas presented in this thesis in a large-scale atmospheric models. Indeed, the proposed plant physiological model for the canopy conductance has been implemented in the Regional atmospheric climate model (RACMO). RACMO (Christensen et al. 1996) is a regional climate model that combines the dynamical package of the limited area NWPM HIRLAM (High resolution limited area model) with physical parameterization from the ECHAM4 climate model (Roeckner et al. 1996). RACMO is operated at KNMI, the Dutch meteorological office, and is used to perform climate studies over Europe. In a study reported by Van de Kastele (2001) (see also Van den Hurk 2001a) the traditional scheme where the canopy conductance is calculated using the empirical-statistical functions was replaced with the proposed plant physiological method. For low vegetation, it was found that the transpiration over Europe increased, compared to the traditional approach. The larger transpiration leads to a direct increase in the simulated specific humidity at 2 m, and as an increase in the transpiration leads to a reduction of the sensible heat flux density, a reduction of the temperature at 2 m. Furthermore, implementation of the plant physiological approach gave an increase of the (convective) precipitation over large parts of Europe. Comparing both methods using SYNOPS observations of the 2 m temperature and the 2 m specific humidity revealed that the plant physiological approach predicts too high values of the 2 m specific humidity during summer. However, this is partly because of uncertainties in

the initialisation of the soil moisture content and the underlying (prescribed) vegetation map. Both the control model and the plant physiological model were initialised using one-year equilibrium values from the control model allowing no soil moisture feedback on a seasonal scale in the run where the canopy conductance is calculated using the plant physiological approach. The root mean square error of the latent heat flux density improved when the plant physiological approach was used.

The study of Van de Kasstele revealed that the method in this paper can successfully be modified to predict the flux densities over forests. Improvement of the scheme for forest vegetation should be focus of future research. For broad-leaf forests, the plant physiological approach slightly overestimates the transpiration (Van den Hurk et al. 2001a). However, for needle-leaf forest large overestimations of the transpiration have been found. The stomata of forest react more strongly in dry conditions. Laboratory experiments suggest that the conductance of needle-leaf forests is affected by a wax layer in which the stomata are embedded. It would be interesting to see whether this could explain the low transpiration rates typically observed in pine forests (Bosveld 1999). Also, it appears that forests usually adapt to local soil and climate conditions. As a result, the parameter values of the plant physiological approach show a broad band (Calvet 2000). This suggests that the parameters of the physiological approach are less robust for forests which implies that results obtained using simulations with large-scale atmospheric models are sensitive to the specification of the vegetation distribution in forested areas (Van den Hurk et al. 2001b). Moreover, the processes within the canopy interior generate profiles of both moisture, leaf temperature, carbon dioxide and photosynthetically active radiation, which means that a simple big leaf model fails to describe the conductance of a forest canopy adequately (Denmead and Bradley 1985; Bosveld 1999).

Another focus of further research is the representation of the canopy conductance for low vegetation that are rooted in very poor soils. Using observations over a true raised bog in the Netherlands Jacobs et al. (2001) found that owing to limitations in the nitrogen and phosphate content of the soil, the assimilation was suppressed. This implies that less carbon dioxide was needed for the photosynthesis. Plant therefore need a smaller stomatal aperture to maintain the photosynthesis. As a result, even in wet areas low values for canopy conductance and consequently of the latent heat flux density have been observed (Nieveen 1999).

Cox et al. (1999b) implemented a plant physiological approach to calculate the canopy conductance in a climate model. They could successfully study the effects of doubling atmospheric carbon dioxide concentrations on the climate. They found

that higher environmental CO_2 concentrations allowed plants to reduce the stomatal closure while maintaining their assimilation. The thus induced reduction of the latent heat flux density gave a significant warming over tropical forests. In a study reported by Haarsma et al. (2002) the plant physiological approach was implemented in a climate model of intermediate complexity. It appeared that the approach gave reasonable estimates of the current climate and could successfully be used to assess the impact of different land use and greenhouse gas emission scenarios on the climate (Leemans et al. 2002).

Most large-scale atmospheric models nowadays adopt a 'tiling' approach to calculate the surface flux densities over heterogeneous terrain. In the numerical weather prediction model of the ECMWF the surface energy budget is now solved separately for eight tiles (Van den Hurk et al. 2000). These tiles include a separate tile for a snow surface, for a lake surface and for the interception reservoir. Validation using forcings at a reference level in the surface layer revealed major improvements in the simulated seasonal cycle of the surface flux densities, especially of boreal forests (Van den Hurk et al. 2001a). The introduction of a completely distributed approach to account for the variation of the soil moisture content is very rare. An important step, however, has been set by Koster et al. (2000b) who divided the North-American continent into a number of catchment areas, the principal hydrological units. Each of the catchment areas is partitioned into a saturated part, an unsaturated part and a wilting part. These are then used as tiles of an atmospheric model and the resulting flux densities are aggregated towards the grid cell of a climate model. The procedure led to major improvements in the simulated runoff. It would be interesting to investigate whether their approach also gives better results of the grid cell flux densities and the estimated atmospheric profiles of temperature and specific humidity, as suggested in this thesis.

Appendix A

The plant physiological model.

In the plant physiological model, the gross primary productivity, is a function of PAR , T_{sk} and the internal CO_2 concentration C_i :

$$A_g = f(PAR, T_{sk}, C_i). \quad (A.1)$$

Here, we adopt the formulations of Jacobs (1994):

$$A_g = (A_m + R_d) \left(1 - e^{-\frac{\mu PAR}{A_m + R_d}} \right), \quad (A.2)$$

with:

$$\begin{aligned} A_m &= A_{m,max} \left(1 - e^{-\frac{g_m(C_i - \Gamma)}{A_{m,max}}} \right), \\ \mu &= \mu_0 \frac{C_s - \Gamma}{C_s + 2\Gamma}. \end{aligned} \quad (A.3)$$

Here, μ is the light use efficiency, μ_0 the initial (at low light conditions) light use efficiency, g_m the mesophyll conductance, $A_{m,max}$ the maximal primary productivity under high light conditions and high CO_2 concentrations and Γ the CO_2 compensation point.

The parameter values for μ_0 have been derived by Collatz et al. (1991, 1992). The values for C_3 and C_4 plants respectively are given in Table 2.1 The parameters g_m , $A_{m,max}$ and Γ are functions of the leaf temperature (Jacobs 1994):

$$\Gamma(T_{sk}) = \Gamma(T_{sk} = 298) Q_{10}^{\frac{T_{sk} - 298}{10}}. \quad (A.4)$$

Γ ($T_{sk} = 298\text{K}$) and Q_{10} are parameters which values are for C_3 and C_4 plants given in Table 2.1. g_m and $A_{m,max}$ are computed as (Jacobs 1994; Collatz et al. 1991, 1992):

$$X(T_{sk}) = \frac{X(T_{sk} = 298) Q_{10}^{\frac{T_{sk}-298}{10}}}{(1 + e^{0.3(T_1 - T_{sk})}) (1 + e^{0.3(T_{sk} - T_2)})} \quad (\text{A.5})$$

In this equation X denotes g_m and $A_{m,max}$ respectively. The parameter values are for C_3 and C_4 plants given in Table 2.1.

The dark respiration R_d is calculated as:

$$R_d = 0.11A_m \quad (\text{A.6})$$

If D_s approaches D_0 equation (10) for the internal CO_2 concentration becomes:

$$(C_i)_{\min} = C_s - \frac{A_g - R_d}{\frac{g_{\min,w}}{1.6} + \frac{A_g}{C_s - \Gamma}} \quad (\text{A.7})$$

Using that if C_i is small $A_m = g_m (C_i - \Gamma)$ this equation can be rewritten as:

$$f_{\min} = 1 - \frac{0.89g_m f_{\min}}{\frac{g_{\min,w}}{1.6} + g_m f_{\min}}, \quad (\text{A.8})$$

$$f_{\min} = \frac{-\left(\frac{g_{\min,w}}{1.6} - 0.11g_m\right) + \sqrt{\left(\frac{g_{\min,w}}{1.6} - 0.11g_m\right)^2 + 4\frac{g_{\min,w}}{1.6}g_m}}{2g_m} \quad (\text{A.9})$$

In this relation f_{\min} equals $(C_i - \Gamma)/(C_s - \Gamma)$ at $D_s = D_0$.

Appendix B

Scaling the $A_g - g_{c,w}$ approach up from leaf to canopy.

In this appendix we present an analytic method to scale conductance calculated with the plant physiological approach up from leaf to canopy. To obtain $g_{c,c}$ from $g_{l,c}$, A_g must be integrated over the canopy:

$$\begin{aligned}\int_0^{LAI} A_g dL &= \int_0^{LAI} \left[(A_m + R_d) - (A_m + R_d) e^{-\frac{\mu PAR}{A_m + R_d}} \right] dL \\ &= (A_m + R_d) \left(LAI - \int_0^{LAI} e^{-\frac{\mu PAR}{A_m + R_d}} dL \right).\end{aligned}$$

It is assumed that the photosynthetically active radiation decays exponentially as a function of the leaf area index:

$$PAR = K_x PAR_t e^{-K_x L}$$

K_x is the extinction coefficient. Inserting this expression in the expression for $\int_0^{LAI} A_g dL$ yields:

$$\int_0^{LAI} A_g dL = (A_m + R_d) \left(LAI - \int_0^{LAI} e^{-oe^{-K_x L}} dL \right)$$

o is in this equation given by $o = \frac{\mu K_x PAR_t}{A_m + R_d}$. To calculate the integral the following transformation is introduced:

$$\begin{aligned}y &= be^{-K_x L} \Rightarrow \\ \frac{dy}{dL} &= -bK_x e^{-K_x L} \Rightarrow\end{aligned}$$

$$dL = -\frac{dy}{K_x b e^{-K_x L}} \Rightarrow$$

$$dL = -\frac{dy}{K_x y}$$

The integration interval boundaries become under this transformation:

$$L = 0 \Rightarrow y = b$$

$$L = LAI \Rightarrow y = b e^{-K_x LAI}$$

$\int_0^{LAI} A_g dL$ is then given by:

$$\begin{aligned} \int_0^{LAI} A_g dL &= (A_m + R_d) \left(LAI + \frac{1}{K_x} \int_b^{b e^{-K_x LAI}} \frac{e^{-y}}{y} dy \right) \\ &= (A_m + R_d) \left(LAI + \frac{1}{K_x} \left(\int_b^\infty \frac{e^{-y}}{y} dy - \int_{b e^{-K_x LAI}}^\infty \frac{e^{-y}}{y} dy \right) \right) \\ &= (A_m + R_d) \left(LAI + \frac{1}{K_x} (E_1(b) - E_1(b e^{-K_x LAI})) \right) \\ &= (A_m + R_d) \left(LAI - \frac{1}{K_x} \left(E_1 \left(\frac{\mu K_x PAR_t}{A_m + R_d} e^{-K_x LAI} \right) - E_1 \left(\frac{\mu K_x PAR_t}{A_m + R_d} \right) \right) \right) \end{aligned}$$

In these equations $E_1(x)$ is the exponential integral with argument x . The resulting expression for $g_{c,c}$ is then:

$$\begin{aligned} g_{c,c} &= \int_0^{LAI} \left(\frac{g_{min,w}}{1.6} + \frac{a_1 A_g}{(C_s - \Gamma) \left(1 + \frac{D_s}{D_*} \right)} \right) dL \\ &= \frac{g_{min,w}}{1.6} LAI + \frac{a_1 \int_0^{LAI} A_g dL}{(C_s - \Gamma) \left(1 + \frac{D_s}{D_*} \right)} \\ &= \frac{g_{min,w}}{1.6} LAI \\ &+ \frac{a_1 (A_m + R_d)}{(C_s - \Gamma) \left(1 + \frac{D_s}{D_*} \right)} \left[LAI - \frac{1}{K_x} \left(E_1 \left(\frac{\mu K_x PAR_t}{A_m + R_d} e^{-K_x LAI} \right) - E_1 \left(\frac{\mu K_x PAR_t}{A_m + R_d} \right) \right) \right] \end{aligned}$$

Appendix C

The aerodynamic conductance

The aerodynamic conductance is given by:

$$g_a = \frac{k^2|u|}{\left(\ln\left(\frac{z_r}{z_{0m}}\right) - \Psi_M\left(\frac{z_r}{L}\right) + \Psi_M\left(\frac{z_{0m}}{L}\right)\right)\left(\ln\left(\frac{z_r}{z_h}\right) - \Psi_H\left(\frac{z_r}{L}\right) + \Psi_H\left(\frac{z_h}{L}\right)\right)}. \quad (\text{C.1})$$

In this equation is k the Von Karman constant equal to 0.4. L is the Monin-Obukhov length defined as:

$$L = \frac{u_{*0}^3}{T_r} kgH, \quad (\text{C.2})$$

where T_r is a reference temperature calculated as: $T_r = \frac{1}{2}(T_a + T_{sk})$. u_{*0} is the friction velocity which is given by:

$$u_{*0} = \frac{k|u|}{\ln\left(\frac{z_r}{z_{0m}}\right) - \Psi_M\left(\frac{z_r}{L}\right) + \Psi_M\left(\frac{z_{0m}}{L}\right)}. \quad (\text{C.3})$$

The stability functions are experimentally determined. For unstable cases the functions given by Businger et al. (1971) with the coefficient given by Beljaars and Holtslag (1991) have been used:

$$\Psi_U\left(\frac{z_r}{L}\right) = \ln\frac{(1+x^2)(1+x)^2}{8} - 2\arctan(x) + \frac{\pi}{2}, \quad (\text{C.4})$$

$$\Psi_H\left(\frac{z}{L}\right) = 2\ln\left(\frac{1+y}{2}\right). \quad (\text{C.5})$$

with $x = (1 - 16\frac{z_r}{L})^{\frac{1}{4}}$ and $y = (1 - 16\frac{z_r}{L})^{\frac{1}{2}}$

For stable case the functions of Beljaars and Holtslag (1991) have been used:

$$\Psi_U\left(\frac{z_r}{L}\right) = -\left(a\frac{z}{L} + b\left(\frac{z}{L} - \frac{c}{d}\right)\exp\left(-d\frac{z}{L}\right) - \frac{bc}{d}\right), \quad (\text{C.6})$$

$$\Psi_H\left(\frac{z}{L}\right) = -\left(\left(1 + \frac{2}{3}a\frac{z}{L}\right)^{\frac{3}{2}} + b\left(\frac{z}{L} - \frac{c}{d}\right)\exp\left(-d\frac{z}{L}\right) - \left(\frac{bc}{d} + 1\right)\right), (\text{C.7})$$

with $a = 1$, $b = 0.667$, $c = 5$ and $d = 0.35$.

Appendix D

The boundary layer model

Processes in the convective boundary layer have in the past frequently been calculated using a slab model (Tennekes 1973; Driedonks 1981; McNaughton and Spriggs 1986). It considers the mixed layer as a fully mixed layer with one uniform temperature and specific humidity. At the top of the boundary layer the profiles of temperature and the specific humidity are described by jumps. Above the mixed layer by the free troposphere profile. For this mixed layer budgets can be obtained:

$$\frac{\partial c_a}{\partial t} = \frac{F_0 - F_h}{h} \quad (\text{D.1})$$

In this equation is c_a the value of a scalar quantity (temperature and specific humidity) in the convective boundary layer (CBL). F_0 is the flux density at the bottom of the mixed layer. The entrainment flux density, the flux density through the top of the mixed layer (F_h) is given by the following expression (Driedonks 1981; Garratt 1992):

$$F_h = -\Delta c_h \left(\frac{\partial h}{\partial t} - w_h \right) \quad (\text{D.2})$$

In this equation Δc_h denotes the scalar jump at the boundary layer top and w_h the subsidence velocity, a downward velocity because of large scale weather systems.

An evolution equation for the jump in concentration can be obtained by budgeting the thin layer at the top of the boundary layer:

$$\frac{\partial \Delta c_h}{\partial t} = \gamma_c \left(\frac{\partial h}{\partial t} - w_h \right) - \frac{\partial c_a}{\partial t} \quad (\text{D.3})$$

In this equation γ_c is the concentration gradient in the free atmosphere. The set of three equations contains four unknowns: c_a , h , Δc_h and F_h . Hence, the set has to be

closed.

Since this study seeks to study effects of using one temperature for a grid cell and does not focus on PBL modeling or budgeting a simple entrainment scheme is adopted (Driedonks 1981):

$$F_h = -0.2F_0, \quad (\text{D.4})$$

Bibliography

- Ball, F.K., 1960: Control of inversion height by surface heating. *Quart. J. Roy. Meteor. Soc.*, **86**, 483-494
- Ball, J.T., I.E. Woodrow, and J.A. Berry, 1987: A model predicting stomatal conductance and its contribution to the control of photosynthesis under different environmental conditions. *Progress in photosynthetic research: Proceedings of the seventh international congress on photosynthesis, Providence, Rhode Island, U.S.A., August 10-15, 1986*, J. Biggins, Ed., Vol. 4, Martinus Nijhoff Publishers, Dordrecht, 221-224
- Bastiaanssen, W.G.M., 1995: Regionalization of surface flux densities and moisture indicators in composite terrain, Report 109, DLO-Winand Staring Centre, Wageningen, the Netherlands
- Beljaars, A.C.M., and A.A.M. Holtslag, 1991: Flux parameterization over land surfaces for atmospheric models. *J. Appl. Meteor.*, **30**, 327-341
- Beljaars, A.C.M., and F.C. Bosveld, 1997: Cabauw data for the validation of land surface parameterization schemes. *J. Climate*, **10**, 1172-1193
- Betts, A.K., and J.H. Ball, 1992: The FIFE-1987 mean surface time series Data Diskette. Atmospheric research data diskette.
- Betts, A.K., and A.C.M. Beljaars, 1993: Estimation of roughness length for heat and momentum from FIFE data. *Atmos. Res.*, **30**, 251-261
- Blyth, E.M., A.J. Dolman, and N. Wood, 1993: Effective resistances to sensible and latent heat flux in heterogeneous terrain. *Quart. J. Roy. Meteor. Soc.*, **119**, 423-442

- Bonan, G.B., D. Pollard, and S.L. Thompson, 1992: Effects of boreal forests vegetation and global climate. *Nature*, **359**, 716-718
- Bosveld, F.C., 1999: Exchange processes between a coniferous forest and the atmosphere., PhD thesis Wageningen University, Wageningen, 184 pp
- Braud, I., J. Noilhan, P. Bessemoulin, P. Mascart, R. Haverkamp, and M. Vauclin, 1993: Bare-ground surface heat and water exchanges under dry conditions: observations and parameterization. *Boundary-Layer Meteor.*, **66**, 173-200
- Calvet, J.-C., J. Noilhan, J.-L. Roujean, P. Bessemoulin, M. Cabelguenne, A. Olioso, and J.-P. Wigneron., 1998: An interactive vegetation SVAT model tested against data from six contrasting sites. *Agric. For. Meteor.*, **92**, 73-95
- Calvet, J.-C., 2000: Investigating soil and atmospheric plant water stress using physiological and micrometeorological data. *Agric. For. Meteor.*, **103(3)**, 229-247
- Charney, J.G., 1975: Dynamics of deserts and drought in the Sahel. *Quart. J. Roy. Meteor. Soc.*, **101**, 192-202
- Christensen, J.H., O.B. Christensen, P. Lopez, E. van Meijgaard, and M. Botzet, 1996: The HIRHAM4 Regional atmospheric climate model. Danish Meteor. Institute, Copenhagen, Sci. Rep. 96-4, 51 pp.
- Claussen, M., 1991: Estimation of areally-averaged surface fluxes. *Boundary-Layer Meteor.*, **54**, 387-410
- Claussen, M., and W. Klaassen, 1993: On regional surface fluxes over partly forested areas. *Beitrag Phys. Atmos.*, **65**, 243-248
- Collatz, G.J., J.T. Ball, C. Grivet, and J.A. Berry, 1991: Physiological and environmental regulation of stomatal conductance, photosynthesis and transpiration: a model that includes a laminar boundary layer. *Agric. For. Meteor.*, **54**, 107-136
- Collatz, G.J., M. Ribas-Carbo, and J.A. Berry, 1992: Coupled photosynthesis-stomatal conductance model for leaves of C₄ plants. *Aust. J. Plant Physiol.*, **19**, 519-538
- Cox, P.M., C. Huntingford, and R.J. Harding, 1999a: A canopy conductance and photosynthesis model for use in a GCM land surface scheme. *J. Hydrol.*, **212-213**, 79-94

- Cox, P.M., R.A. Betts, C.B. Bunton, R.L.H. Essery, P.R. Rowntree, and J. Smith, 1999b: The impact of new land surface physics on the GCM simulation of climate and climate sensitivity. *Clim. Dyn.*, **15**, 183-203
- Delage, Y., and D. Verseghy, 1995: Testing the effects of a new land surface scheme and of initial soil moisture conditions in the Canadian global forecast model. *Mon. Wea. Rev.*, **123**, 3305-3317
- De Bruin, H.A.R., 1987: Physical aspects of the planetary boundary layer with special reference to regional evapotranspiration. *Estimation of Areal Evapotranspiration*. Black, D.L., D.L. Spittlehouse, M.D. Novak, and D.T. Price, Eds., IAHS, Wallingford, UK
- De Bruin, H.A.R., and J.Q. Keijman, 1979: The priestley-Taylor evaporation model applied to a large, shallow lake in the Netherlands. *J. Appl. Meteor.*, **18**, 893-903
- Denmead, O.T., and E.F. Bradley, 1985: Flux-gradient relationships in a forest canopy. *The forest-atmosphere interaction*, B.A. Hutchinson, and B.B. Hicks, Eds., 421-442
- De Ridder, K., 1998: The impact of vegetation cover on sahelian drought persistence. *Boundary-Layer Meteor.*, **88**, 307-321
- De Rooy, W.C., and A.A.M. Holtslag, 1999: Estimation of surface radiation and energy flux densities from single-level weather data. *J. Appl. Meteor.*, **38**, 526-540
- Dickinson, R.E., and A. Henderson-Sellers, 1988: Modelling tropical deforestation: A study of GCM land-surface parameterizations. *Quart. J. Roy. Meteor. Soc.*, **114**, 439-462
- Dickinson, R.E., A. Henderson-Sellers, C. Rosenzweig, and P.J. Sellers, 1991: Evapotranspiration models with canopy resistance for use in climate models, a review. *Agric. For. Meteor.*, **54**, 373-388
- Dolman, A.J., 1993: A multiple source energy balance model for use in general circulation models. *Agric. For. Meteor.*, **65**, 21-45
- Dolman, A.J., and Blyth, E.M., 1997: Patch scale aggregation of heterogeneous land surface cover for mesoscale meteorological models. *J. Hydrol.*, **190**, 252-268

- Dolman, A.J., M. Soet, R.J. Ronda, and B.J.J.M. van den Hurk, 2002: Representation of the seasonal hydrological cycle in climate and weather prediction models in West Europe. Final report NRP project 951246, 125 pp.
- Dorman, J.L., and P.J. Sellers, 1989 : A global climatology of albedo, roughness length and stomatal resistance for atmospheric general circulation models as represented by the simple biosphere model (SIB). *J. Appl. Meteor.*, **28**, 833-855
- Driedonks, A.G.M., 1981: Dynamics of the Well-Mixed Atmospheric Boundary Layer, Scientific Report W.R. 81-2, KNMI, De Bilt, the Netherlands, 189 pp.
- Ducharne, A., K. Laval, and J. Polcher, 1998: Sensitivity of the hydrological cycle to the parameterization of soil hydrology in a GCM. *Clim. Dyn.*, **14**, 307-327
- Ducharne, A., R.D. Koster, M.J. Suarez, M. Stieglitz, and P. Kumar, 2000: A catchment-based approach to modelling land surface processes in a general circulation model; 2. Parameter estimation and model demonstration. *J. Geophys. Res.*, **105**, 24,823-24,838
- Dümenil, L., and E. Todini, 1992: A rainfall-runoff scheme for use in the Hamburg climate model. *Adv. Theor. Hydrology*, J.P. O Kane, Ed., European Geophys. Soc. Series on Hydrological Sciences, Vol. 1, Elsevier Science Publishers, Amsterdam, 129-157
- Ek, M.B., and A.A.M. Holtslag 2002a: Interactions of the land-surface with the atmospheric boundary layer, Part 1: Evaluation of a land-surface scheme at Cabauw. submitted to *J. Hydrometeor.*
- Ek, M.B., and A.A.M. Holtslag 2002b: Interactions of the land-surface with the atmospheric boundary layer, Part 2: Coupled model evaluation and impact of soil moisture on cumulus initiation. submitted to *J. Hydrometeor.*
- Ek, M., and L. Mahrt, 1991: A formulation for boundary-layer cloud cover. *Annal. Geophys.*, **9**, 716-724
- Entekhabi, D., and P.S. Eagleson, 1989: Land surface hydrology parameterization for atmospheric general circulation models including subgrid scale spatial variability. *J. Climate*, **2**, 816-831

- Famiglietti, J.S., E.F. Wood, M. Sivapalan, and D.J. Thongs, 1992: A catchment scale water balance model for FIFE. *J. Geophys. Res.*, **97**, 18,997-19,007
- Feddes, R.A., P.J. Kowalik, and H. Zaradny, 1978: A Simulation of field water use and crop yield. *Simulation Monogr.*, No. 9, Pudoc, 189 pp.
- Fraedrich, K., A. Kleidon, and F. Lunkeit, 1999: A green planet versus a desert world: estimating the effect of vegetation extremes on the atmosphere. *J. Climate*, **12**, 3156-3163
- Frech, M., and A. Jochum, 1999: The evaluation of flux aggregation methods using aircraft measurements in the surface layer. *Agric. For. Meteor.*, **98-99**, 121-143
- Ganzeveld, L.N., 1991: Surface-Atmosphere trace gas and aerosol exchanges on the global scale. Ph.D. thesis Utrecht University, Utrecht, 140 pp.
- Garratt, J.R., 1992: The atmospheric boundary layer. Cambridge University Press., Cambridge, 316 pp.
- Garratt, J.R., 1993: Sensitivity of climate simulations to land-surface and atmospheric boundary layer treatments. A review. *J. Climate*, **6**, 419-449
- Gash, J.H.C., J.S. Wallace, C.R. Lloyd, A.J. Dolman, M.V.K. Sivakumar, and C. Renard, 1991: Measurements of evaporation from fallow Sahelian savannah at the start of the dry season. *Quart. J. Roy. Meteor. Soc.*, **117**, 749-760
- Gollan, T., J.B. Passioura, and R. Munns, 1986: Soil water status affects the stomatal conductance of fully turgid wheat and sunflower leaves. *Aust. J. Plant Physiol.*, **13**, 459-464
- Goudriaan, J., and H.H. van Laar, 1978: Relations between leaf resistance, CO₂-concentration and CO₂-assimilation in maize, beans, lalang grass and sunflowers. *Photosynthetica*, **12**, 155-169
- Goutorbe, J.-P., 1991: A critical assessment of the SAMER network accuracy. *Land Surface Evaporation*, T.J. Schmugge, and J.-C. André . Eds., Springer, 171-182
- Haarsma, R.J., R.J. Ronda, M. Schaeffer, A.A.M. Holtslag, and J.D. Opsteegh, 2002: Feedback land surface with atmosphere at global scales. *Land Use, Climate*

- and biogeochemical cycles: feedbacks and options for emission reduction*, A.J. Dolman, Ed., 137-165
- Henderson-Seller, A., and V. Gornitz, 1984: Possible climatic impacts of land cover transformations with particular emphasis on tropical deforestation. *Clim. Change*, **6**, 231-357
- Henderson-Seller, A., K. McGuffie, and A. Pitman, 1996: The project for inter-comparison of land-surface parameterization schemes (PILPS). *Clim. Dyn.*, **12(12)**, 849-859
- Holtslag, A.A.M., and M. Ek, 1996: Simulation of surface fluxes and boundary-layer development over the pine forest in HAPEX-Mobilhy. *J. Appl. Meteor.*, **35**, 202-213
- Hu, Z., and S. Islam, 1997: Effects of spatial variability on the scaling of land surface parameterizations. *Boundary-Layer Meteor.*, **83**, 441-461
- Jacobs, A.F.G., R.J. Ronda, and A.A.M. Holtslag, 2001: Observations and model results for water vapor and carbon dioxide fluxes above a bog vegetation. submitted to *Agric. For. Meteor.*
- Jacobs, C.M.J., and H.A.R. de Bruin, 1992: The sensitivity of regional transpiration to land-surface characteristics: significance of feedback. *J. Climate*, **5**, 683-698
- Jacobs, C.M.J., 1994: Direct impact of atmospheric CO₂ enrichment on regional transpiration. Ph.D. thesis Wageningen Agricultural University, Wageningen, 179 pp.
- Jarvis, P.G., 1976: The Interpretation of the variations in leaf water potential and stomatal conductance found in canopies in the field. *Phil. Trans. Roy. Soc. London*, **273B**, 593-610
- Kalma, J.D., B.C. Bates, and R.A. Woods, 1995: Predicting catchment-scale soil moisture status with limited field measurements. *Scale issues in hydrological modelling*, J.D. Kalma, and M. Sivapalan, Eds., 203-226
- Kelliher, F.M., R. Leuning, and E.-D. Schulze, 1993: Evaporation and canopy characteristics of coniferous forests and grasslands. *Oecologia*, **95**, 153-163

- Kelliher, F.M., R. Leuning, M.R. Raupach, and E.-D. Schulze, 1995: Maximum conductances for evaporation from global vegetation types. *Agric. For. Meteorol.*, **73**, 1-16
- Kim, C.P., 1995: The water budget of heterogeneous areas. Ph.D. thesis Wageningen Agricultural University, Wageningen, 184 pp.
- Köppen, W., 1936: Das geographische system der klimate. *Handbuch der klimatologie*, **5(C)**, W. Köppen, and R. Geiger, Eds., Gebrüder Bornträger, Berlin
- Koster, R.D., and M.J. Suarez, 1992: Modelling the land surface boundary in climate models as a composite of independent vegetation stands. *J. Geophys. Res.*, **97(D3)**, 2697-2718
- Koster, R.D., and P.C.D. Milly, 1997: The interplay between transpiration and runoff formulations in land surface schemes with atmospheric models. *J. Climate*, **10**, 1578-1591
- Koster, R.D., M.J. Suarez, and M. Heiser, 2000a: Variance and predictability of precipitation at seasonal-to-interannual timescales. *J. Hydrometeorol.*, **1**, 26-46
- Koster, R.D., M.J. Suarez, A. Ducharne, M. Stieglitz, and P. Kumar, 2000b: A catchment based approach to modeling land surface processes in a general circulation model; 1. Model structure. *J. Geophys. Res.*, **105**, 24,809-24,822
- La Rivière, J.W.M., 1989: Threats to the world's water. *Scient. Amer.*, **261(3)**, 80-94
- Laval, K., and L. Picon, 1986: Effect of a change of the surface albedo of the Sahel on climate. *J. Atmos. Sci.*, **43**, 2418-2429
- Leemans, R., L. Bouwman, G. Busch, B. Eickhout, E. Kreileman, M. Schaeffer, B. Strengers, and B. de Vries, 2002: Integrated assessment with IMAGE 5. *Land Use, Climate and biogeochemical cycles: feedbacks and options for emission reduction*, A.J. Dolman, Ed., 194-239
- Leuning, R., 1990: Modelling stomatal behaviour and photosynthesis of *Eucalyptus grandis*. *Aust. J. Plant Physiol.*, **17**, 150-175
- Leuning, R., 1995: A critical appraisal of a combined stomatal-photosynthesis model for C₃ plants. *Plant Cell Environ.*, **18**, 357-364

- Lhomme, J.-P., 1992: Energy Balance of heterogeneous terrain: averaging the controlling parameter. *Agric. For. Meteor.*, **61**, 11-21
- Lhomme, J.-P., A. Chehbouni, and B. Monteny, 1994: Effective Parameters of Surface Energy Balance in Heterogeneous Landscape. *Boundary-Layer Meteor.*, **71**, 297-309
- Mahfouf, J.-F., A.O. Manzi, J. Noilhan, H. Giordani, and M. Deque, 1995: The land surface scheme ISBA within the Meteo-France climate model ARPEGE. Part I: Implementation and Preliminary results. *J. Climate*, **8**, 2039-2057
- Mahrt, L., 1987: Grid averaged surface fluxes. *Mon. Wea. Rev.*, **115**, 1550-1560
- Mahrt, L., 1996: The bulk aerodynamic formulation over heterogeneous surfaces. *Boundary-Layer Meteor.*, **78**, 87-119
- Manabe, S., 1969: Climate and ocean circulation I. The atmospheric circulation and the hydrology of the earth's surface. *Mon. Wea. Rev.*, **93**, 739-774
- Mason, P., 1988: The formation of areally averaged roughness lengths. *Quart. J. Roy. Meteor. Soc.*, **114**, 399-420
- McNaughton, K.G., 1994: Effective stomatal and boundary-layer resistances of heterogeneous surfaces. *Plant, Cell Environ.*, **17**, 1061-1068
- McNaughton, K.G., and T.W. Spriggs, 1985: A mixed-layer model for regional evaporation. *Boundary-Layer Meteor.*, **34**, 243-262
- Milly, P.C.D., and K.A. Dunne, 1994: Sensitivity of the global water cycle to the water holding capacity of land. *J. Climate*, **7**, 505-526
- Monteith, J.L., 1965: Evaporation and the environment. *Symp. Soc. Exp. Biol.*, **19**, 205-234
- Monteith J. L., 1981: Evaporation and surface temperature. *Quart. J. Roy. Meteor. Soc.*, **107**, 1-27
- Nieveen, J.P., 1999: Eddy covariance and scintillation measurements of atmospheric exchange processes over different types of vegetation. Ph.D. thesis Wageningen Agricultural University, Wageningen, 122 pp.
- Niyogi, D.S., and S. Raman, 1997: Comparison of four different resistance schemes using FIFE observations. *J. Appl. Meteor.*, **36**, 903-917

- Noilhan, J., and S. Planton, 1989: A simple parameterization of land surface processes for meteorological models. *Mon. Wea. Rev.*, **117**, 536-549
- Owe, M., E.B. Jones, and T.J. Schmugge, 1982: Soil moisture variation patterns observed in Hand County, South Dakota. *Water Res. Bull.*, **18(6)**, 949-954
- Raupach, M.R., 1991: Vegetation-atmosphere interaction in homogeneous and heterogeneous terrain: some implications of mixed-layer dynamics. *Vegetatio*, **91**, 105-120
- Raupach, M.R., 1993: The averaging of surface flux densities in heterogeneous landscapes. *Exchange Processes at the Land Surface for a range of Space and Time Scales, Proc. Symp. J3.1. Joint Scientific Assembly of IAMAP and IAHS, Yokohama, Japan, 11-23 July 1993, IAHS Publ.*, **212**, H.-J. Bolle, R.A. Feddes, and J.D. Kalma, Eds., 343-355
- Raupach, M.R., 1995: Vegetation-atmosphere interaction and surface conductance at leaf, canopy and regional scales. *Agric. For. Meteorol.*, **73**, 151-179
- Raupach, M.R., and J.J. Finnigan, 1995: Scale issues in boundary-layer meteorology: surface energy balances in heterogeneous terrain. *Hydrol. Proc.*, **9**, 589-612
- Roeckner, E., K. Arpe, L. Bengtsson, M. Christoph, M. Claussen, L. Dümenil, M. Esch, M. Giogetta, U. Schlese, and U. Schulzweida, 1996: The atmospheric general circulation model ECHAM-4: Model description and simulation of the Present-day climate. *Report No. 218*, Max-Planck-Institut für Meteorologie, Hamburg
- Ronda, R.J., and H.A.R. De Bruin, 1999: A note on the concept of 'effective' bulk exchange coefficients for determination of surface flux densities. *Boundary-Layer Meteorol.*, **93**, 155-162
- Ronda, R.J., H.A.R. de Bruin, and A.A.M. Holtslag, 2001: Representation of the Canopy Conductance in Modeling the Surface Energy Budget for Low Vegetation. *J. Appl. Meteorol.*, **40**, 1431-1444
- Ronda, R.J., B.J.J.M. van den Hurk, and A.A.M. Holtslag, 2002: Spatial heterogeneity of the soil moisture content and its impact on the surface flux densities and near-surface meteorology. under review for *J. Hydrometeorol.*

- Rowntree, P.R., 1995: The water budget of middle latitude continental regions-a modelling and observational study. Hadley Centre CRTN 59, Bracknell, UK
- Rutter, A.J., K.A. Kershaw, P.C. Robins, and A.J. Morton, 1972: A predictive model of rainfall interception in forests. Part I: Derivation of the model from observations in a plantation of Corsican pine. *Agric. Meteor.*, **9**, 367-384
- Sellers, P.J. ., F.G. Hall, G. Asrar, D.E. Strebel, and R.E. Murphy, 1988: The First ISLSCP Field Experiment (FIFE). *Bull. Amer. Meteor. Soc.*, **69**(1), 22-27
- Sellers, P.J., M. Heiser, and F.G. Hall, 1992: Relations between Surface Conductance and Spectral Vegetation Indices and Intermediate ($100m^2$ to $15 km^2$) Length Scales. *J. Geophys. Res.*, **97**, 19,033-19,059
- Sellers, P.J., D.A. Randall, G.J. Collatz, J.A. Berry, C.B. Field, D.A. Dazlich, C. Zhang, G.D. Collelo, and L. Bounoua, 1996: A Revised land surface parameterization (SIB2) for Atmospheric GCMs. Part I: model formulation. *J. Climate*, **9**, 676-705
- Shao, Y., and A. Henderson-Sellers, 1996: Validation of soil moisture simulation in landsurface parameterisation schemes with HAPEX data. *Global Planet. Change*, **13**, 11-46
- Shuttleworth, W.J., 1988: Macrohydrology - the new challenge for process hydrology. *J. Hydrol.*, **100**, 31-56
- Shuttleworth, W.J., 1989: Micrometeorology of forests. *Phil. Trans. Roy. Soc. Lond.*, **B 324**, 299-334
- Sivapalan, M., and R.A. Woods, 1995: Evaluation of the effects of general circulation models' subgrid variability and patchiness of rainfall and soil moisture on land surface water balance fluxes. *Hydrol. Proc.*, **9**, 697-717
- Soet, M., R.J. Ronda, J.N.M. Stricker, and A.J. Dolman, 2000: Land surface scheme conceptualisation and parameter values for three sites with contrasting soils and climate. *Hydrol. Earth Syst. Sc.*, **4**, 283-294
- Song, J., C.J. Willmott, and B. Hanson, 1997: Influence of heterogeneous land surfaces on surface energy and mass fluxes. *Theor. Appl. Climatol.*, **58**, 175-188
- Stewart, J.B., and A.S. Thom, 1973: Energy budgets in pine forest. *Quart. J. Roy. Meteor. Soc.*, **99**, 134-170

- Stewart, J.B., 1988: Modelling surface conductance of pine forest. *Agric. For. Meteorol.*, **30**, 111-127
- Stewart, J.B., and S.B. Verma, 1992: Comparison of Surface Fluxes and Conductances at Two contrasting Sites Within the FIFE Area. *J. Geophys. Res.*, **97**, 18,623-18,628
- Stricker, J.N.M., and W. Brutsaert, 1978: Actual evapotranspiration over a summer period in the "Hupsel Catchment". *J. Hydrol.*, **39**, 139-157
- Stull, R.B., 2000: Meteorology for scientists and engineers. Brooks/Cole, Pacific Grove, USA, 502 pp.
- Tennekes, H., 1973: A model for the dynamics of the inversion above a convective boundary layer. *J. Atmos. Sci.*, **30**, 558-567
- Van den Hurk, B.J.J.M., 1995: Sparse canopy parameterizations for meteorological models. Ph.D. thesis Wageningen Agricultural University, Wageningen, 273 pp.
- Van den Hurk, B.J.J.M., W.G.M. Bastiaanssen, H. Pelgrum, and E. Van Meijgaard, 1997: A new methodology for assimilation of initial soil moisture fields in weather prediction models using meteosat and NOAA data. *J. Appl. Meteorol.*, **36**, 1271-1283
- Van den Hurk, B.J.J.M., P. Viterbo, A.C.M. Beljaars, and A.K. Betts, 2000: Offline validation of the ERA40 surface scheme. ECMWF Tech. Memo 295, 42 pp.
- Van den Hurk, B.J.J.M., A.J. Dolman, A.A.M. Holtslag, R. Hutjes, J. van de Kassteele, R.J. Ronda, and R.J.M. Ijpelaar, 2001a: The land-component in the climate system. *The climate system*, J.J.M. Berdowski, R. Guicherit, and B.-J. Heij, Eds., A.A. Balkema publishers, Lisse, 79-104
- Van den Hurk, B.J.J.M., P. Graham, and P. Viterbo, 2001b: Comparison of land surface hydrology in regional climate simulations of the Baltic Sea catchment. *J. Hydrol.*, **255**, 169-193
- Van de Kassteele, J., 2001: Evaluation of a plant physiological canopy conductance model in the ECMWF land surface scheme. KNMI technical report 234, 55 pp.

- Verhoef, A., 1995: Surface energy balance of shrub vegetation in the Sahel. Ph.D. thesis Wageningen Agricultural University, Wageningen, 248 pp.
- Vermeulen, J.P.L., 2001: The atmospheric boundary layer over a heterogeneous vegetated landscape. Ph.D. thesis Vrije Universiteit Amsterdam, 164 pp.
- Viterbo, P., 1994: The representation of surface processes in general circulation models. Ph.D. thesis, University of Lisbon, Lisbon, Portugal, 202 pp.
- Viterbo, P., and A.C.M. Beljaars, 1995: An improved Land Surface Parameterization Scheme in the ECMWF Model and its validation. *J. Climate*, **8**, 2716-2748
- Wang, Y.P., and R. Leuning, 1998: A two-leaf model for canopy conductance. *Agric. For. Meteorol.*, **91**, 89-111
- Wetzel, P.J., and J.-T. Chang, 1987: Concerning the relationship between evapotranspiration and soil moisture. *J. Climate Appl. Meteorol.*, **26**, 18-27
- Wetzel, P.J., and J.-T. Chang, 1988: Evapotranspiration from non-uniform surfaces: A first approach for short-term numerical weather prediction. *Mon. Wea. Rev.*, **116**, 600-621
- Wetzel, P.J., and A. Boone: A parameterization for land-atmosphere-cloud exchange (PLACE): documentation and testing of a detailed process model of the partly cloudy boundary layer over heterogeneous land. *J. Climate*, **8**, 1810-1837
- Wieringa, J., 1986: Roughness dependent geographical interpolation of surface wind speed averages. *Quart. J. Roy. Meteor. Soc.*, **112**, 867-889
- Wood, N., and P. Mason, 1991: The influence of static stability on the effective roughness lengths for momentum and temperature. *Quart. J. Roy. Meteor. Soc.*, **117**, 1025-1056
- Wood, E.F., D.P. Lettenmaier, and V.G. Zartarian, 1992: A land-surface hydrology parameterization with subgrid variability for general circulation models. *J. Geophys. Res.*, **97**, 2717-2728
- Wood, E.F., 1997: Effects of soil moisture aggregation on surface evaporative fluxes. *J. Hydrol.*, **190**, 397-412

- Woodward, F.I., 1987: Climate and plant distribution. Cambridge studies in ecology. Cambridge University press, Cambridge, UK, 174 pp.
- Wösten, J.H.M., A. Lilly, A. Nemes, and C. Le Bas, 1998: Using existing soil data to derive hydraulic parameters for simulation models in environmental studies and in land use planning. DLO-Staring Centre report 156, 106 pp.
- Zhang, H., and P.S. Nobel, 1996: Dependency of c_i/c_a and leaf transpiration efficiency on the vapor pressure deficit. *Aust. J. Plant Physiol.*, **232**, 561-568
- Zhao, R.J., Y.L. Zhang, L.R. Fang, X.R. Liu, and Q.S. Zhang, 1980: The Xinanjiang model. *Hydrol. forecasting proceedings of the Oxford Symposium, IAHS Publ.*, **129**, 351-356

Samenvatting

Dit proefschrift gaat over het modelleren van de oppervlakte-energiebalans en de atmosferische grenslaag over natuurlijke landoppervlakken. Daarbij richten we ons met name op schalen in de orde van 10-1000 km, de typische roosterpuntsafstand in moderne atmosferische modellen. Het doel van dit onderzoek is om inzicht te krijgen in de manier waarop de processen die bepalen hoe de atmosfeer warmte and massa uitwisselt met het onderliggende landoppervlak, moeten worden beschreven in grootschalige atmosferische modellen.

In hoofdstuk 2 ontwikkelen we een methode om de gewasweerstand voor lage vegetatie te beschrijven. In deze methode wordt de gewasweerstand berekend met behulp van de temperatuur van het gewas, de specifieke vochtigheid in het gewas, de concentratie van koolstofdioxide in het gewas en de geabsorbeerde kortgolvlige straling. Onze methode is simpel en er zijn geen iteraties nodig om de gewasweerstand uit te rekenen. Toch beschrijft deze methode de belangrijkste processen, waaronder de exponentiele uitdoving van de kortgolvlige straling dieper in het gewas. Zij is dus erg geschikt voor gebruik in grootschalige atmosferische modellen. Ook ontwikkelen we in hoofdstuk 2 een nieuwe formulering om het effect van watertekorten in de bodem op de gewasweerstand te beschrijven. De parameterwaarden van onze methode worden ontleend aan de plantenfysiologie. Zij blijken robuust te zijn en kunnen gemakkelijk worden gerelateerd aan vegetatietypen. In feite blijkt in onze studie een scheiding in C_3 and C_4 planten voldoende. We valideren de methode voor de gewasweerstand met waarnemingen van de gewasweerstand en de energiestromen aan het oppervlak. Deze zijn verkregen op verschillende plaatsen met een verschillende vegetatie: een C_3 sojaboongewas in Frankrijk, een C_4 prairie grasland in Kansas, in de Verenigde Staten van Amerika en een C_3 grasland in Cabauw, gelegen in Nederland. We vergelijken de resultaten die we met onze methode hebben verkregen met resultaten die zijn verkregen met behulp van een statistisch-empirische aanpak. In deze aanpak wordt

de gewasweerstand gerelateerd aan de temperatuur, de specifieke vochtigheid en de concentratie van koolstofdioxide op een referentiehoogte in de oppervlaktelaag. Ook voor deze methode hebben we de parameterwaarden geschat op basis van een vegetatieclassificatie. De methode die gebaseerd is op de plantenfysiologie blijkt betere schatting te geven van de gewasweerstand en de energiestromen aan het aardoppervlak van het C₄ grasland. Ook is deze methode beter geschikt om de energiestromen aan het aardoppervlak te schatten boven een C₃ soja gewas. De energiestromen aan het aardoppervlak van een C₃ grasland worden door beide methoden ongeveer even goed geschat. Onze conclusie is dat de methode gebaseerd op de plantenfysiologie waarbij het effect van bodemvocht door de voorgestelde formulering wordt berekend, goede resultaten geeft. Aangezien deze methode is gebaseerd op een fysiologische aanpak, raden wij deze aan om in atmosferische modellen te gebruiken.

In hoofdstuk 3 onderzoeken we het effect van variaties in het bodemvocht op de gemiddelde latente warmtestroom van een heterogeen gebied. Modelleurs nemen meestal aan dat het bodemvochtgehalte binnen een roosterpunt niet varieert. De planten ervaren dan overal dezelfde druk bij watertekorten. Dit gemiddelde bodemvochtgehalte kan dan meteen worden gebruikt om de oppervlakte-energiebalans op te lossen en de latent warmtestroom uit te rekenen. Deze aanpak noemen we de uniforme aanpak. In tegenstelling tot de uniforme aanpak wordt in een gedistribueerde aanpak rekening gehouden met variaties in het bodemvocht. In deze aanpak verdelen we het roosterpunt in een aantal deelgebieden met verschillende bodemvochtgehalten. Voor ieder deelgebied apart rekenen we dan de energiebalans en de latente warmtestroom uit. De gemiddelde latente warmtestroom vinden we dan door de stromen van de deelgebieden te middelen. De factoren om de gemiddelden uit te rekenen halen we daarbij uit een verdeling van het bodemvochtgehalte die kenmerkend is voor de schaal van grootschalige atmosferische modellen. Het blijkt dat met de gedistribueerde aanpak de warmtestromen veel geleidelijker variëren met het gemiddelde bodemvochtgehalte. Als de bodem erg nat is, bijna verzadigd, berekenen beide methoden ongeveer dezelfde warmtestromen. Als het droger wordt neemt het bodemvochtgehalte in de droogste gebieden snel af. Het resultaat is dat dan de gedistribueerde aanpak lagere schattingen van de latente warmtestroom geeft. Als het de bodem in het roosterpunt erg droog wordt, voorspelt de uniforme aanpak een zeer lage latente warmtestroom. Echter, in de natste deelgebieden is de latente warmtestroom nog steeds hoog. Het gevolg is dat in erg droge omstandigheden de gedistribueerde warmtestroom een veel hogere latent warmtestroom geeft dan de uniform aanpak. Dit heeft grote gevolgen voor de seizoenscyclus van de transpiratie. Aan het begin het droge seizoen geeft

de uniforme aanpak een snellere uitdroging van het bodemvochtreservoir. Als gevolg daarvan is er in de zomer minder water beschikbaar voor verdamping. De uniforme aanpak voorspelt dus een erg kleine verdamping gedurende de zomer, ook omdat deze methode een veel lagere verdamping geeft als de bodem erg droog is. Voor een nat klimaat zijn de verschillen minder duidelijk. Toch zie je ook daar dat de uniforme aanpak een grotere verdamping geeft als de bodem relatief nat is, en een veel lagere verdamping als de bodem erg droog is. Tot slot kijken we in hoofdstuk 3 naar het effect van de verschillen in berekende warmtestromen als het landoppervlak is gekoppeld aan een zich ontwikkelende convectieve grenslaag. Het blijkt dat zelfs met grenslaagkoppeling de uniforme methode veel grotere schattingen van de verdamping geeft als de bodem relatief nat is en veel lagere schattingen als de bodem erg droog is. Bovendien blijkt dat de verschillen in geschatte energiestromen leiden tot verschillen in de specifieke vochtigheid en temperatuur in de grenslaag en op 2 m, vlak bij het oppervlak.

In hoofdstuk 4 laten we met drie voorbeelden die vaak in de natuur voorkomen zien dat alleen een opsplitsing in deelgebieden altijd leidt tot gemiddelde warmtestromen die consistent zijn met het gemiddelde temperatuurverschil over de oppervlaktelaag. Vaak is gedurende de dag het hele gebied onstabiel. In dat geval kan de voelbare warmtestroom direct worden gerelateerd aan het gemiddelde temperatuurverschil over de oppervlaktelaag. Maar soms is de stratificatie over één of meerdere gebieden stabiel, terwijl het gebied gemiddeld onstabiel is gelaagd. In die gevallen geeft gebruik van het gemiddelde temperatuurverschil over de oppervlaktelaag een te lage voelbare warmtestroom. Vervolgens resulteert deze onderschatting van de voelbare warmtestroom in een te lage en normaalgesproken te koude en te vochtige grenslaag. In hoofdstuk 4 tonen we met behulp van een simpel model aan dat als een droog grasland is gelegen naast een veld met gesmolten sneeuw, de voelbare warmtestroom niet direct kan worden gerelateerd aan het gemiddelde temperatuurverschil over de oppervlaktelaag. Hetzelfde laten we zien voor een grasland dat ligt naast een koud meer. Het blijkt zelfs dat als nat bos is gelegen naast een droog bos, de verschillen in stratificatie zo groot zijn, dat de gemiddelde voelbare warmtestroom niet direct kan worden gerelateerd aan het gemiddelde temperatuurverschil over de oppervlaktelaag. De gestoorde relatie tussen de gemiddelde voelbare warmtestroom en het gemiddelde temperatuurverschil over de oppervlaktelaag heeft niet alleen gevolgen voor de representatie van de oppervlakte-energiebalans in grootschalige modellen, maar ook voor het gebruik van technieken uit de remote sensing om grootschalige modellen te valideren.

In hoofdstuk 5 vatten we de resultaten uit de voorgaande hoofdstukken nog eens

samen. Bovendien laten we dit hoofdstuk zien hoe de verdere ontwikkelingen van de ideeën in dit proefschrift zijn gegaan. Ook geven we in dit hoofdstuk suggesties voor verder onderzoek.

Curriculum vitae

Ik, Reinder Jan Ronda, ben geboren op 20 juni 1973 te Westernieland in de gemeente Eenrum (nu gemeente De Marne). Op driejarige leeftijd verhuisde ik naar Sleen (nu in de gemeente Coevorden) waar ik tot mijn achttiende zou wonen. In 1991 behaalde ik het VWO-diploma aan de Gemeentelijke Scholengemeenschap te Emmen, waarna ik in 1992 begon met de studie Bodem, Water en Atmosfeer aan de Landbouwniversiteit Wageningen. Mijn eerste afstudeervak bracht mij naar Lyon in Frankrijk waar ik de ruimtelijke verdeling van Rhôneafvoeren heb bestudeerd. Daarna heb ik op de vakgroep waterhuishouding gekeken naar de toepassing van de gemengde eindige-elementenmethode voor de modellering van grondwaterstroming. Aan het eind van mijn studie ben ik nog een zomer aan de Zeeuwse kust geweest waar ik bij het Rijksinstituut voor Kust en Zee in Middelburg de stroming in en rond een haven heb gemeten en gemodelleerd. In 1996 studeerde ik af, waarna ik in 1997 begon aan een promotie-onderzoek aan de vakgroep meteorologie (nu leerstoelgroep meteorologie en luchtkwaliteit) van de Landbouwniversiteit. Het onderwerp was het modelleren van de oppervlakte-energiebalans en de atmosferische grenslaag boven grote, heterogene gebieden. Een van de resultaten van mijn onderzoek is dit proefschrift. Intussen heb ik van de zomer van 2000 tot de zomer van 2001 in totaal zes maanden voor het KNMI gewerkt. Daar heb ik een grenslaagschema voor het klimaatmodel ECBilt ontwikkeld. Per 1 maart werk ik als post-doc bij de afdeling geo-milieuwetenschappen van de faculteit der aard- en levenswetenschappen van de Vrije Universiteit Amsterdam.

List of publications by the author

Peer-reviewed articles

Ronda, R.J., and H.A.R. De Bruin, 1999: A note on the concept of 'effective' bulk exchange coefficients for determination of surface flux densities. *Boundary-Layer Meteor.*, **93**, 155-162

Ronda, R.J., H.A.R. de Bruin, and A.A.M. Holtslag, 2001: Representation of the Canopy Conductance in Modeling the Surface Energy Budget for Low Vegetation. *J. Appl. Meteor.*, **40**, 1431-1444

Ronda, R.J., B.J.J.M. van den Hurk, and A.A.M. Holtslag, 2002: Spatial heterogeneity of the soil moisture content and its impact on the surface flux densities and near-surface meteorology. *accepted for J. Hydrometeor.*

Soet, M., R.J. Ronda, J.N.M. Stricker, and A.J. Dolman, 2000: Land surface scheme conceptualisation and parameter values for three sites with contrasting soils and climate. *Hydrol. Earth Syst. Sc.*, **4**, 283-294

De Bruin, H.A.R., R.J. Ronda, and B.J.H. van de Wiel, 2000: Approximate solutions for the Obukhov length and the surface fluxes in terms of bulk Richardson numbers. *Boundary-Layer Meteor.*, **95**, 145 - 157

Van de Wiel, B.J.H., R.J. Ronda, A.F. Moene, H.A.R. de Bruin, and A.A.M. Holtslag, 2002: Intermittent Turbulence and oscillations in the stable boundary layer over

land. Part I: A bulk approach. *J. Atmos. Sc.*, **59**, 942-958

Van de Wiel, B.J.H., A.F. Moene, R.J. Ronda, H.A.R. de Bruin, and A.A.M. Holtslag, 2002: Intermittent Turbulence and oscillations in the stable boundary layer over land. Part II: A system dynamics approach. accepted for *J. Atmos. Sc.*

Books and reports

Dolman, A.J., M. Soet, R.J. Ronda, and B.J.J.M. van den Hurk, 2002: Representation of the seasonal hydrological cycle in climate and weather prediction models in West Europe. Final report NRP project 951246, 125 pp.

Van den Hurk, B.J.J.M., A.J. Dolman, A.A.M. Holtslag, R. Hutjes, J. van de Kasstelee, R.J. Ronda, and R.J.M. IJpelaar, 2001: The land-component in the climate system. *The climate system*, J.J.M. Berdowski, R. Guicherit, and B.-J. Heij, Eds., A.A. Balkema publishers, Lisse, 79-104

Haarsma, R.J., R.J. Ronda, and M. Schaeffer, 2002: Feedback land surface with atmosphere at global scales. *Land Use, Climate and biogeochemical cycles: feedbacks and options for emission reduction*, A.J. Dolman, Ed., 137-165

Conference papers

Ronda, R.J., and M. Soet, 1999: Intercomparison of the racmo svat scheme with swaps. *Proceedings of the 11th conference on applied climatology, 10-15 Januari Dallas TX*, 133-134

Ronda, R.J., and M. Soet, 1999: Comparison of two methods to calculate the canopy conductance to transpiration. *24th General Assembly Hydrology, Oceans and Atmosphere : 24th General Assembly Hydrology, Oceans and Atmosphere. - Den Haag, Nederland : European Geophysical Society, 1999*, 470

Ronda, R.J., A.A.M. Holtslag, and H.A.R. de Bruin, 2000: Representation of the Canopy Conductance in Modelling the Surface Energy Balance. *Proceedings 14 Symposium on Boundary Layer and Turbulence : 14 Symposium on Boundary Layer and Turbulence, Aspen, 2000*, 314-318

Soet, M., and R.J. Ronda, 1999: Comparing SVAT schemes for different soil, vegetation and climate regimes. *24th General Assembly Hydrology, Oceans and Atmosphere : 24th General Assembly Hydrology, Oceans and Atmosphere. - Den Haag, Nederland : European Geophysical Society, 1999, 470*

This study was carried out at the department of Meteorology and Air Quality of Wageningen University. Financial support was provided by the Netherlands Organisation of Scientific Research (NWO) within the framework of the Dutch National Research Programme on Global Air Pollution and Climate Change: the project number was 951246 and it was entitled 'Representation of the seasonal hydrological cycle in climate and weather prediction models in West-Europe.

Printed by Ponsen & Looijen, Wageningen